

DOCTORAL THESIS

STANDARDIZED TESTING CONDITIONS
FOR SATELLITE COMMUNICATIONS
ON-THE-MOVE (SOTM) TERMINALS

Mostafa ALAZAB ELKHOULY

*Dissertation zur Erlangung des
akademischen Grades Doktor-Ingenieur (Dr.-Ing.)*

Anfertigung im: Fachgebiet Elektronische Messtechnik & Signal Verarbeitung
Institut für Informationstechnik
Fakultät für Elektrotechnik und Informationstechnik

Gutachter: Univ.-Prof. Dr.-Ing. Giovanni Del Galdo
Univ.-Prof. Dr.-Ing. Albert Heuberger
Univ.-Prof. Dr.-Ing. Andreas Knopp

Vorgelegt am: 02. Juli 2018

Verteidigt am: 20. November 2018

Abstract

Satellites have proven their success in providing communication services especially between distant locations. For Satellite Communication On-The-Move (SOTM) applications, accurate satellite tracking algorithms must be applied in order to ensure the highest possible throughput and also to avoid harmful interference to adjacent satellites. Performance validation of SOTM terminals is becoming more important as the satellite operators recognize the negative influence of suboptimal terminals on their satellite networks. Traditionally, SOTM testing is performed with actual operational satellites in field tests, which lack repeatability. The capability to repeat the conditions in which SOTM terminals are tested is important, especially when the performance of multiple terminals is compared.

This contribution is dedicated to study how to conduct a comprehensive qualification test of SOTM terminals in a laboratory environment so that repeatability can be ensured. A major advantage of a laboratory environment is the ability to test the complete terminal as if it was in the field of operation, yet without the involvement of real satellites effectively reducing the costs of testing. This thesis presents the methodology for testing SOTM terminals at the Fraunhofer Facility for Over-the-air Research and Testing (FORTE). Important performance parameters, such as, antenna de-pointing and Adjacent Satellite Interference (ASI) can be accurately measured and evaluated. The procedure used to obtain the proposed profiles and results of testing a Ka-band SOTM terminal are also presented in this thesis.

A major contribution of this thesis is represented by the development of motion and shadowing profiles suitable for standardization of SOTM testing. Motion profiles for the land mobile and the maritime environment have been developed. For each environment two classes were defined, Class A with rough motion conditions and Class B with more relaxed motion conditions. The proposed motion profiles were added to the well-known GVF-105 standard recommendations of the Global VSAT Forum. Shadowing profiles were defined for land mobile applications in different environment types, e.g., urban, suburban, highway, etc. Standardization of such profiles is necessary to guarantee a fair comparison of the performance of different terminals and therefore leading to sort out the bad performing terminals which cause harmful interference to the existing satellite networks. This will lead to an overall improvement in the performance of the satellite industry.

Zusammenfassung

Von Beginn an haben Satelliten Kommunikationsdienste über große Distanzen bereit gestellt. Endgeräte für die mobile Satellitenkommunikation sind mit einer Nachführeinrichtung ausgestattet, um den verwendeten Satelliten bei Bewegung zu verfolgen. Für höchstmöglichen Datendurchsatz und um Störaussendungen zu benachbarten Satelliten zu vermeiden bedarf es akkurater Nachführalgorithmen. Die Prüfung solcher Satcom-On-The-Move (SOTM) Terminals wird dabei zunehmend wichtig, wie Betreiber von Satellitendiensten anhand des negativen Einflusses suboptimaler Geräte auf ihre Infrastruktur bemerken. Herkömmlich werden SOTM-Terminals im Rahmen von Feldtests mit operativen Satelliten geprüft. Solche Tests sind allerdings nicht exakt wiederholbar. Die Reproduzierbarkeit von Tests ist jedoch insbesondere beim Vergleichstest mehrerer Terminals wichtig.

Dieser Beitrag widmet sich der Untersuchung eines umfassenden Qualifikationstests von SOTM-Terminals innerhalb einer Laborumgebung, welche Reproduzierbarkeit ermöglicht. Wesentlicher Vorteil der Laborumgebung ist die Möglichkeit, Terminals unter realitätsnahen Bedingungen zu testen – ohne dass reale Satelliten benötigt werden, was die Kosten reduziert. Diese Arbeit behandelt darüber hinaus die Testmethodik in der Fraunhofer-Testanlage "Facility for Over-the-air Research and Testing (FORTE)". Wichtige Leistungsparameter wie Nachführgenauigkeit (Antenna De-pointing) und Nachbarsatellitenstörung (Adjacent Satellite Interference, ASI) können akkurat gemessen und ausgewertet werden. Die verwendete Methodik zur Gewinnung der vorgeschlagenen Profile wird in der Arbeit ebenso behandelt wie Testergebnisse von Ka-Band-SOTM-Terminals. Wesentlicher Beitrag dieser Arbeit ist die Entwicklung von Bewegungs- und Abschattungsprofilen für SOTM-Terminaltests. Bewegungsprofilen für die Landmobile und Maritime Umgebungen wurden entwickelt. Für jede Umgebung, zwei Klassen wurden definiert, Klasse A mit Profile die hohe Bewegungsdynamik haben und Klasse B mit Profile die relativ niedriger Bewegungsdynamik haben. Die vorgeschlagenen Bewegungsprofile wurden in der GVF-105 Standard des Global VSAT Forums berücksichtigt. Die Standardisierung solcher Profile ist notwendig, um einen fairen Leistungsvergleich verschiedener Terminals zu garantieren und solche Geräte sicher zu identifizieren, welche Interferenzen im Satellitennetz verursachen. Dies bedeutet im Ergebnis einen Gewinn für die gesamte Satellitenindustrie.

Acknowledgements

I would like to express my sincere gratitude to my advisor Prof. Giovanni Del Galdo for the continuous support of my Ph.D study and related research. His guidance, knowledge, and patience were important during all the time of writing this thesis, but at some milestones they were definitely crucial and remarkable.

Besides my advisor, I would like to thank the rest of my thesis committee: Prof. Albert Heuberger and Prof. Andreas Knopp for their insightful comments and encouragement. I carry a special gratitude to Prof. Albert Heuberger who was the first to help me to shape my academic path and to offer me the chance to join the Fraunhofer Institute. Through this excellent entity, I managed to build a solid scientific background and a strong practical experience.

My sincere thanks also go to Dr.-Ing. Markus Landmann who provided me the continuous support and the deep technical supervision. Without his precious support it would have not been possible to conduct this research. It was of my pleasure to have him all the time for detailed and rather sophisticated technical discussions during our extensive measurement campaigns.

I would like also to thank my colleagues Florian Raschke and Gregor Siegert for their support in the measurement campaigns and for the fruitful team work throughout the years of my work in this dissertation. A special thank to my colleague Niklas Beuster for helping with his excellent skills in software development and in graphical illustrations. A special thank goes to my colleague Jonas König who was using all the chances to motivate me to continue this long path of writing a doctoral thesis.

I would also like to thank two of our intelligent Post-doctors: Dr.-Ing. Alexander Ihlow and Dr.-Ing. Florian Römer for their continuous support and scientific consultancy. Having Dr.-Ing. Florian Römer also as an office mate was like having an always accessible scientific pool just a few meters away. He has never saved an effort to offer help.

I thank all the team members of the Electronic Measurements and Signal Processing (EMS) research group who did not save any effort to help me towards achieving this thesis in its final shape and with whom I felt almost like at home.

Last but not least, I would like to thank my family: my wife, my parents, my brother, and my sister for supporting me spiritually throughout writing this thesis and throughout my life in general. It will never be possible to express in words what they all have done for me.

Contents

Abstract	iii
Zusammenfassung	v
Acknowledgements	vii
Contents	ix
1 Introduction	1
1.1 History of Satellites	1
1.2 Regulatory Considerations	2
1.3 Satellite Applications	2
1.4 Satellite Frequencies	3
1.5 Impairments and challenges	4
1.6 Satellite Communication On-The-Move (SOTM)	4
1.7 Contributions and Outline	5
2 Fundamentals of Satellite Communications	9
2.1 The Space Segment	9
2.1.1 Kepler's Laws of Planetary Motion	9
2.1.1.1 Kepler's First Law	10
2.1.1.2 Kepler's Second Law	11
2.1.1.3 Kepler's Third Law	11
2.1.2 Satellite Orbits	12
2.1.2.1 The Low Earth Orbit (LEO)	12
2.1.2.2 The Medium Earth Orbit (MEO)	12
2.1.2.3 The Geosynchronous/Geostationary Orbit (GSO/GEO)	13
2.1.2.4 The High Earth Orbit (HEO)	13
2.1.3 Orbital Perturbations	14
2.1.4 Orbital Effects on the Communication Systems	14
2.1.4.1 Doppler Shift	14
2.1.4.2 Solar Eclipse and Sun Transit Outage	15
2.1.4.3 Range Variations	16
2.2 The Ground Segment	17
2.2.1 The Antenna Subsystem	18
2.2.1.1 Radiation Pattern	18
2.2.1.2 Antenna Types	19
2.2.1.3 Pointing Angle of a Ground Segment Antenna	20
2.2.1.4 Tracking	22
2.2.2 The Radio Frequency (RF) Subsystem	23

2.2.3	The Communication Subsystem	23
2.2.4	The Network Interface Subsystem	23
2.3	Propagation Effects	24
2.3.1	Rain Attenuation and Depolarization	24
2.3.1.1	Rain Attenuation	25
2.3.1.2	Rain Depolarization	25
2.3.2	Other Impairments	26
2.3.2.1	Attenuation by Atmospheric Gases	26
2.3.2.2	Cloud Attenuation	26
2.3.2.3	Scintillation	27
2.3.2.4	The Faraday Rotation	27
3	State Of The Art Satellite Communication Services and OTM Testing	29
3.1	Satellite Communication Services	29
3.2	Satellite Communication On-The-Move Testing	31
3.2.1	SOTM Standard Metrics	32
3.2.2	SOTM Type Approvals	33
3.2.3	SOTM Testing Procedures and Environments	34
4	Proposed Testing Methodology	39
4.1	Off-axis Emissions Measurements	40
4.2	Antenna De-pointing Measurements	40
4.2.1	Antennas with Fixed Radiation Patterns	41
4.2.1.1	Optimum Sensor Positions	42
4.2.2	Phased Arrays	46
4.3	Transmit Mute Measurements	48
4.4	Data Traffic Measurements	48
5	Proposed Motion Profiles	51
5.1	Measurement of the Motion Dynamics	52
5.2	Statistical Analysis	53
5.3	Measurement Classification	54
5.4	Profile Selection	54
5.5	Applying the Procedure for Land mobile and Maritime	55
5.5.1	Land Mobile	55
5.5.1.1	Class A Motion Profile	56
5.5.1.2	Class B Motion Profile	57
5.5.1.3	Profile Time Series	57
5.5.2	Maritime	63
5.5.2.1	Class A Motion Profile	64
5.5.2.2	Class B Motion Profile	64
5.5.2.3	Profile Time Series	65
5.6	Land mobile, Maritime, and Churchville B	69
5.7	Standard Motion Profiles in GVF-105	70
6	Proposed Shadowing Profiles	71
6.1	Image Capturing and Environment Definition	72
6.2	Image Post Processing	73
6.3	Shadowing Profile Extraction	74
6.4	Definition of Standard Shadowing Profiles	75

6.5	Combining Motion and Shadowing Profiles for Testing	78
7	Measurement Results	81
7.1	The Measurement Scenario	81
7.2	An Excerpt of the SOTM Type Approval Results	82
7.2.1	Antenna Characteristics	82
7.2.1.1	Gain Measurements	82
7.2.1.2	Radiation Pattern Measurements	83
7.2.2	Dynamic Tests	85
8	Concluding Remarks and Possible Future Extensions	91
	Appendices	93
A	Coordinate Transformations at FORTE	95
B	Analysis of the Angular Rate and Acceleration Correlations	101
C	Wave Polarization and its Measurement Methods	107
D	Satellite Communication On-The-Move (SOTM) Test Facilities	111
	Bibliography	120
	Index	121
	Erklärung	123

Chapter 1

Introduction

1.1 History of Satellites

In 1945, Arthur C. Clarke published his proposal for a practical satellite communication scenario which can provide global coverage [12]. He suggested that communication links which are able to support global coverage can be established using three satellites that are located in an equatorial circular orbit at approximately 36000 km above mean sea level. Satellites at this altitude will remain over the same relative point on the Earth's equator and will have an orbital period equal to the Earth's rotation on its axis (1 Sidereal Day=23h 56m)¹. The main challenge was that the existing rockets at that time did not have the ability to achieve such an altitude. Clarke in his article was driven by the motivation to enhance the situation of distant communications (telephony and telegraph) as well as of television services. The best television station could serve only a hundred miles area. Transcontinental television links were yet impossible. High Frequency (HF) radio was offering a chance for radio communication over long distances. However, it was not at all reliable due to ionospheric transmission impairments which might cause several days of continuous outage. Cables capable of carrying voice signals had been laid across the Atlantic and began to serve in 1953. Prior to satellite being in space, calls to Europe from the United States costed more than 1\$ per minute. According to the latest US government Customer Price Index (CPI) data, an item that costed 1\$ in 1945 will cost 14\$ with the measures of 2018 [13]. The average wage back then in 1945 was 1.5\$ per hour. A worker had to work 40 minutes in order to make a one-minute call [14].

Twenty years after Clarke's proposal, specifically on April 16, 1965, the first commercial geostationary satellite, *Early Bird* and renamed *Intelsat I*, started to provide distant telephone services over the Atlantic Ocean. The continuous development of launch vehicles made it possible to carry the approximately 40 kg satellite and locate it at the targeted orbit. *Early Bird* had a capacity of 240 circuits or one TV channel.

¹A sidereal day is defined as one complete rotation of the Earth relative to the fixed stars.

For the first time, news and live sport events could be relayed across continents. The satellite remained providing full-time service for four years. Today, approximately 450 satellites are located in the Geostationary Orbit (GEO) [15]. Geosynchronous² satellites have been continuously increasing in weight, lifetime and capacity. Call rates from the United States to Europe dropped nowadays to below 0.10\$ per minute, while an average worker earns more than 10\$ per hour. Hundreds of thousands of transcontinental television channels, video links, and telephone circuits exist today to cover live events and carry them all over the globe.

1.2 Regulatory Considerations

Satellites have proven from the first day, their success in providing communication services especially between distant locations. Due to the global scale of their applications, there is a conflict of interests. For example, countries that are located geographically close to each others or countries which are located on the same longitude but on different latitudes have a common interest in the few orbital locations covering their regions. With the continuously increasing number of satellites in space, standardization is therefore important. International regulatory bodies such as the International Telecommunications Union (ITU) and regional organizations such as the Federal Communications Commission (FCC) and the European Telecommunications Standards Institute (ETSI) assign and regulate orbital slots at which communication satellites can be located. Satellites also exist in other orbits, e.g. the Low Earth orbit (LEO) and the Medium Earth Orbit (MEO). For instance, the satellites of the well-known Global Positioning System (GPS) are located in Medium Earth Orbits. Due to their limited look angles, satellites in the geostationary orbit can not cover the poles of the Earth. For that reason, satellites are rather positioned in Low Earth Orbits to provide pole visibility. Standardization is important not only for orbital allocations of the huge amount of satellites in space, but also to coordinate frequencies used by satellite applications, to regulate satellite footprints and coverages, and other multiple operational limits for the space, as well as for the ground segments.

1.3 Satellite Applications

Satellites are launched not only for communication and navigation applications but also for other purposes such as weather forecast and Earth observation. There is a strong relationship between the application and the orbit that is chosen for each satellite. For example, GPS is very sensitive to time delay and therefore the GPS satellites were placed in an orbit which is not very high in altitude. Television and radio broadcast

²The term geosynchronous and geostationary are used interchangeably in this dissertation.

applications need a satellite to be stationary with respect to the Earth's rotation and need the satellite footprint to be wide. Therefore, the geostationary orbit is an ideal choice. New technologies are continuously emerging driven by the constant demand for higher bandwidth and data rates. At the beginning of the twenty first century, High Throughput Satellites (HTS) started to offer more capacity than that offered by conventional Fixed Service Satellites (FSS). The efficient redesign of the satellite footprint in multiple spot beams combined with frequency reuse technologies allowed for a significant increase in the offered capacity. Mobile satellite applications, e.g., Satellite Communication On-The-Move (SOTM) enable satellite communication and broadcast services for a moving platform in land mobile, maritime, aeronautical, and high speed railway environments. This application requires an earth segment which is capable of tracking the target satellite(s) in order to keep the highest possible Quality of Service (QoS) and to avoid interference with other satellite networks.

1.4 Satellite Frequencies

Most of the existing communication satellites work in frequencies ranging from 1 to 40 GHz. Generally, the higher the frequency the wider the available bandwidth, yet the more the negative effect of rain fade becomes. The L-band (1-2 GHz) with its limited bandwidth is typically used for navigation and mobile satellite applications, e.g., the Iridium system. The S-band (2-4 GHz) is used for weather radar applications and some communication applications, especially those used by the National Aeronautics and Space Administration (NASA) to communicate with the International Space Station (ISS). In the C-band (4-8 GHz), a trade off between an average available bandwidth and moderate effect of rain fade can be achieved. Therefore, it is commonly used for satellite television networks and satellite communications in tropical regions where there is high probabilities of rainfall. The X-band (8-12 GHz) is mainly used for military radar, weather monitoring, and vehicle tracking applications. The Ku-band (12-18 GHz) is used for communication services and direct Broadcast Satellite Services (BSS). Due to the congested Ku-band, new satellite services started to exploit the Ka-band (26-40 GHz). The Ka-band offers capacities suitable for the new broadband technologies and applications. Figure 1.1 depicts the frequency spectrum showing the frequencies used for satellite telecommunications.

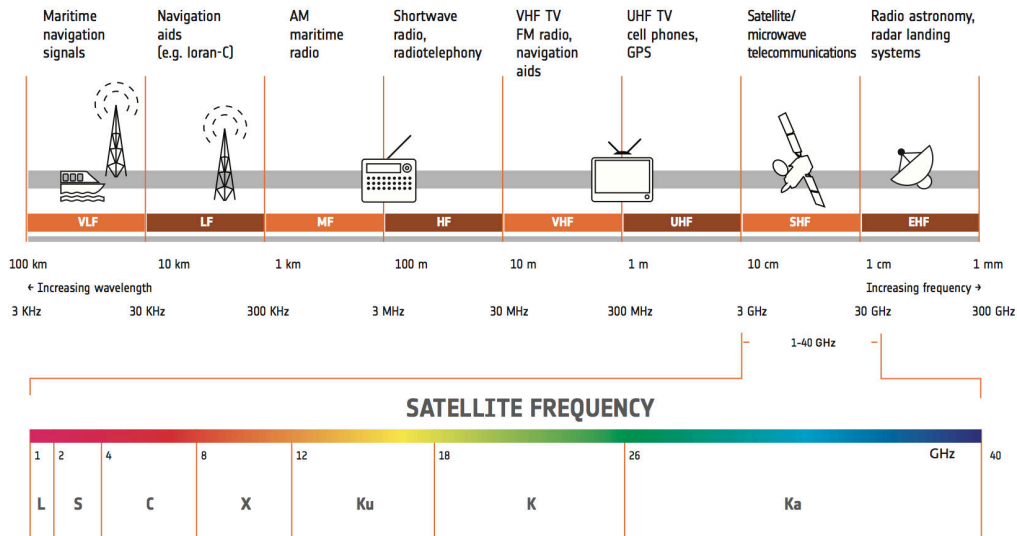


Figure 1.1: The frequency spectrum from 3 KHz up to 300 GHz along with the corresponding applications. Satellite telecommunications occupy the frequency range between 1 and 40 GHz. Figure courtesy of the European Space Agency (ESA).

1.5 Impairments and challenges

Although satellites are successful for the purposes they were invented for, scientists still research how to overcome multiple challenges and impairments of satellite communications. Atmospheric impairments including rain fade, Faraday rotation of wave polarization, the ionospheric scintillations, etc are challenging particularly at high frequencies. The Free Space Path Loss (FSPL) and the propagation delay change depending on the altitude of the satellite. Active power amplifiers are used before transmitting signals from or to the satellite. These amplifiers have nonlinear transfer functions. The amplification gain must be deliberately adjusted in order to avoid operating the amplifier in its nonlinear region while achieving the maximum possible value in the linear region.

1.6 Satellite Communication On-The-Move (SOTM)

The Satellite Communication On-The-Move (SOTM) market has experienced a rapid growth in the recent years. A study for the European Space Agency (ESA) in collaboration with the Global VSAT Forum (GVF) revealed that SOTM is seen by all members of the value chain as a primary source of new business [1]. In situations where no terrestrial communication infrastructure exists, SOTM systems represent one of the best solutions.

SOTM is a strong candidate in many other applications such as news gathering, mobile TV, public security, rescue, maritime, aeronautical, and military applications. However, SOTM systems still encounter many challenges which hinder the potential market increase. Most challenging are antenna tracking and signal shadowing. The latter is often mitigated by forward error correction schemes [16]. The former not only causes a degradation in the link quality, but is also a source of interference to adjacent satellites. Although Very Small Aperture Terminals (VSAT) are desired to be used in SOTM systems due to their directive antennas and potential to provide high data rates, many satellite operators reported to be harmfully affected by VSAT interferences, e.g., [17]. In order to limit the interference caused by VSATs, regulatory authorities such as the ITU, ETSI, and FCC define operational limits on the transmission from SOTM terminals [18], [19]. In addition, the regulations specify limits on the maximum allowable pointing error of the SOTM antenna, the so-called *antenna de-pointing*, and define a transmit cessation time if the pointing error is larger than the permitted threshold.

Testing a SOTM terminal against these standardized limits is essential for the satellite operators in order to guarantee that the terminal does not cause harmful interferences to their satellite networks. Testing, moreover, offers SOTM manufacturers the ability to demonstrate the performance of their products and to identify their strengths and weaknesses. Antenna de-pointing, transmit cessation time, and Adjacent Satellite Interference (ASI) must be measured to evaluate the tracking performance of the terminal. To evaluate the performance of the SOTM modem, channel emulators are used to generate realistic states of the communication link between the terminal and the satellite. The values of the FSPL, the signal reception states (Line of Sight or blockage), the propagation delay, and Doppler are emulated as being in a real operational scenario.

A comprehensive test which comprises all the components of the SOTM terminal, including its Outdoor Unit (ODU) and Indoor Unit (IDU), is necessary. This thesis proposes a methodology to perform comprehensive SOTM tests in controlled laboratory environment.

1.7 Contributions and Outline

The scientific contribution of this thesis is to develop a methodology to test SOTM terminals according to repeatable conditions in a laboratory environment. The development of motion and shadowing profiles suitable for standard SOTM testing is also a major contribution. The content of each chapter in this thesis is as the following:

- Chapter 2 (Fundamentals of Satellite Communications): The Fundamentals of the satellite communication systems are presented in this chapter.
 - The fundamentals of the space segment are discussed in Section 2.1. The section starts with the Kepler's Laws of planetary motion and continues with

presenting the multiple orbits which are used nowadays for satellite communications and the effects of the orbital perturbations on the communication subsystems.

- The ground segment is introduced in Section 2.2 including its multiple subsystems: the antenna, the Radio Frequency (RF), the communication, and the network interface subsystems.
 - Section 2.3 deals with the effect of the Earth-to-space channel on the propagation of the electromagnetic waves.
- Chapter 3 (State Of The Art Satellite Communication Services and On-The-Move Testing):
 - Section 3.1 summarizes the state-of-the-art satellite communication services and applications.
 - The state-of-the-art SOTM standards and recommendations are summarized and the SOTM testing approaches are presented in Section 3.2. The standards which govern the performance of SOTM terminals in the Ku-/Ka-bands are listed. The existing type approval programs and the state-of-the-art SOTM testing environments are also introduced.
 - Chapter 4 (Proposed Testing Methodology): In this chapter, the proposed methodology of testing SOTM terminals in a laboratory environment is introduced. Testing the terminal with respect to the standard SOTM performance metrics is considered. The measurement of the off-axis emissions, the antenna de-pointing, the transmit mute duration, and the data traffic is presented in Sections 4.1, 4.2, 4.3, and 4.4, respectively. The methodology was presented in multiple publications, e.g., [2,3].
 - Chapter 5 (Proposed Motion Profiles): This chapter deals with the process of developing the proposed standard motion profiles and their inclusion in the GVF-105 recommendations.
 - Section 5.1 presents the campaigns carried out to measure the motion dynamics.
 - Sections 5.2 and 5.3 discuss the analysis and classification of the measurement data.
 - In Section 5.4, the process of profile selection is introduced.
 - The complete profile definition process is applied to the measurements in the land mobile and the maritime environment and the proposed profiles are presented in Section 5.5. The developed motion profiles were published in [4].

- Section 5.7 presents the inclusion of the proposed motion profiles in the GVF-105 standard recommendations.
- Chapter 6 (Proposed Shadowing Profiles): In Chapter 6, the development process of the proposed standard shadowing profiles for the land mobile applications is presented. The proposed shadowing profiles were published in [4].
 - Section 6.1 presents the definition of the environment types and how the fish eye images, which are captured parallel to the measurement of the motion dynamics, were classified into these environment types.
 - In Section 6.2, the image post processing algorithm is introduced.
 - Sections 6.3 and 6.4 present the process of shadowing profile extraction from the image profiles. The shadowing profile is extracted from the image profile of a certain environment for a specific geographical location and for a specific satellite longitudinal position.
 - In a laboratory environment, the standard shadowing profile from any type of environment can be combined with any motion profile in order to have flexible conditions for SOTM testing. This is the scope of Section 6.5.
- Chapter 7 (Measurement Results): In this chapter, the results of the proposed testing procedures applied at the Fraunhofer Facility for Over-the-air Research and Testing (FORTE)¹ are presented.
 - Section 7.1 presents the measurement scenario and the antenna under test.
 - In Section 7.2, parts of the measurement results are introduced. The conformance of the radiation pattern with the SOTM standards, the antenna de-pointing, the adjacent satellite interference (ASI), and other parameters are measured.
- Chapter 8 (Concluding Remarks and Possible Future Extensions): This chapter concludes the contributions of this thesis and discusses the possible extensions of the work.

¹<https://www.iis.fraunhofer.de/en/profil/standorte/forte.html>

Chapter 2

Fundamentals of Satellite Communications

In this chapter, the basic fundamentals of satellite communications are presented. The structure of the space segment (the satellite), its components, and its launching process are presented in Section 2.1. Afterwards, the elements of the ground segment are explained in Section 2.2. Basic concepts such as frequency allocation, polarization, and skew are also illustrated. Finally, the challenges and impairments of satellite communication systems are discussed in Section 2.3.

An artificial satellite is an object which is placed at some altitude above the surface of the Earth and has a specific orbit. Satellites in their basic form work as signal repeaters which are used to relay signals, originally received from the Earth, to another distant location on the Earth. Figure 2.1 shows the basic components of a satellite communication scenario. The ground segment, also known as *earth station*, transmits (uplinks) a signal to the satellite which retransmits (downlinks) that signal back to the ground segments located within its footprint. A satellite footprint is the region of coverage where the signal from the satellite is considered to be interpretable.

2.1 The Space Segment

Johannes Kepler, in 1609, started to formulate his remarkable laws of planetary motion based on early observations. Kepler's laws apply generally to any two bodies in space orbiting under the effect of gravity. More specifically, these laws are used to calculate the orbit of a satellite to be located in the outer space.

2.1.1 Kepler's Laws of Planetary Motion

Although Kepler's laws were written before the satellites were sent to space and they were originally written to describe the motion of the planets around the sun, they can be easily reformulated to match the terms of communication satellites.

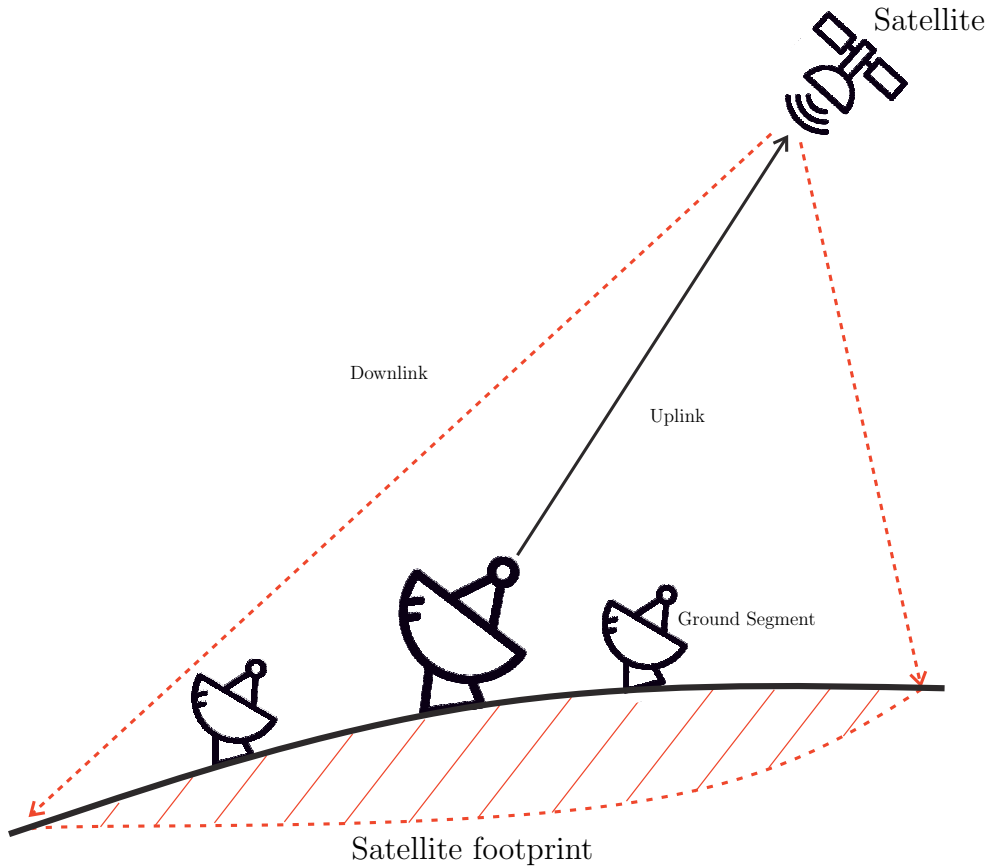


Figure 2.1: A basic satellite communications scenario. The satellite relays the received signals to the ground segments located within its footprint. Basic elements in the Figure are taken from [20].

2.1.1.1 Kepler's First Law

A two-body system comprising the Earth and the satellite can be seen in Figure 2.2. *Kepler's first law* states that the path of the satellite around the Earth is an ellipse with two focal points: F_1 and F_2 . The center of mass of the system is co-located with one focal point. Since the mass of the Earth is much bigger than that of the satellite, the center of mass of the two-body system is considered to be located at the center of Earth (F_1 in Figure 2.2). The orbit's eccentricity (e) is calculated as in Equation 2.1.

$$e = \frac{\sqrt{a^2 - b^2}}{a} \quad (2.1)$$

The eccentricity and semimajor axis are significant parameters to describe the orbit of the satellite around the Earth. If the eccentricity was *zero*, the orbit becomes circular.

In Figure 2.2, the Earth is assumed to be at the focal point F_1 . The minor and the major axes of the ellipse are also depicted.

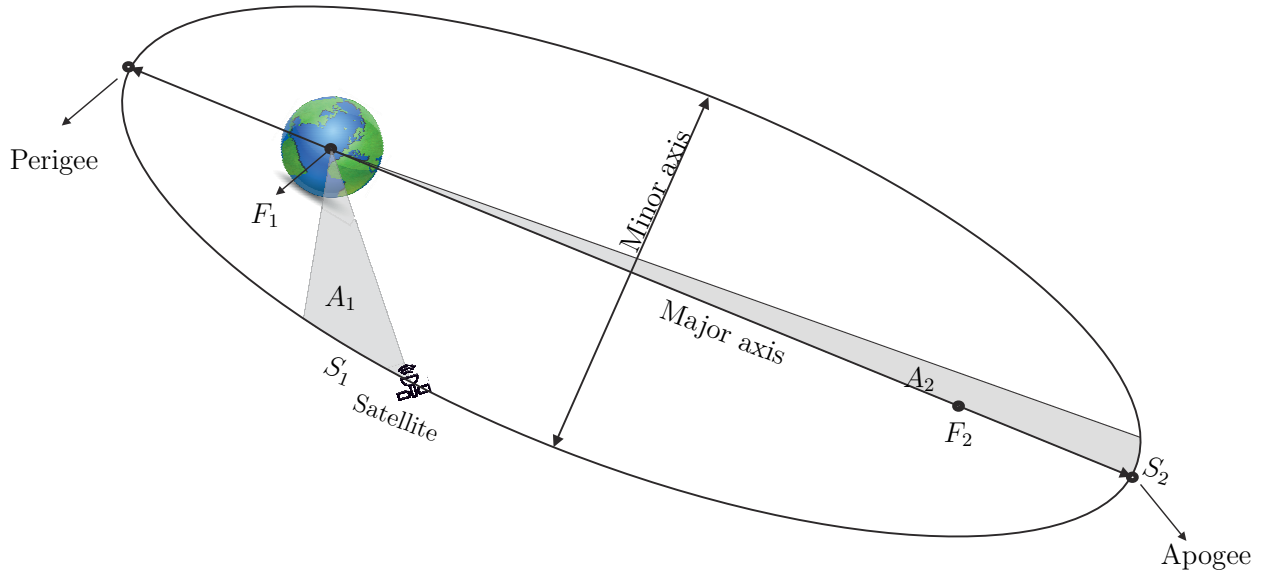


Figure 2.2: Kepler's Laws. The satellite is orbiting the Earth in an ellipse with foci F_1 and F_2 . The Earth is at the center of mass of the two-body system coinciding with F_1 . The areas A_1 and A_2 are equal if the satellite sweeps the distances S_1 and S_2 in the same time duration. Figure adapted from [21].

2.1.1.2 Kepler's Second Law

Kepler's second law states that the orbit of the satellite sweeps out equal areas in equal times. In Figure 2.2, the areas A_1 and A_2 are equal. The time period elapsed for the satellite to travel through the part of the ellipse noted S_1 is equal to that period it needs to travel through S_2 . This implies that the satellite will travel faster when it is closer to the Earth and slower when it is farther away. The satellite will be fastest at the orbit's *Perigee* and will be slowest at the *Apogee*.

2.1.1.3 Kepler's Third Law

Kepler's third law states that the square of the periodic time of the satellite orbit around the Earth equals a constant multiplied by the third power of the semimajor axis of the orbital ellipse as in Equation 2.2.

$$P^2 = \frac{4 \cdot \pi^2 \cdot a^3}{\mu} \quad (2.2)$$

where P is the orbital period in seconds, a is the semimajor axis of the orbital ellipse, and $\mu = 3.986005 \times 10^{14} \text{ m}^3/\text{s}^2$ is the Earth's geocentric gravitational constant also known as Kepler's constant. If the orbit is circular, the Earth will be located in the center of the circle and a will become the distance from the center of Earth to the satellite.

Based on the Kepler's laws, the satellites rotate around the Earth today at multiple orbits having different altitudes. For example, the altitude of the *geostationary*, theoretically circular, orbit can be calculated using Equation 2.2 where P is 1 sidereal day or 86164 seconds.

2.1.2 Satellite Orbits

There are multiple orbits designed for satellites based on the services they are launched to offer. For example, the satellites used for television broadcast are orbiting in the Geostationary orbit, whereas the satellites launched for Global Positioning (GPS) use a Medium Earth Orbit (MEO). For the satellite to keep rotating around the Earth and not to fall off, it must have a specific speed that leads to a balance between the gravity and the centrifugal force. The closer the satellite to the Earth, the stronger the gravitational pull of the Earth and the higher the required speed to balance the satellite. In this section, the characteristics of the most famous orbits are presented.

2.1.2.1 The Low Earth Orbit (LEO)

As the name implies, the LEO satellites occupy an orbit with a low altitude, between 200-1200 km above the surface of the Earth. This relatively close to Earth height leads to the following characteristics:

- A relatively less amount of energy is needed to place the satellite in orbit, less relative to that required for higher orbits.
- The satellite is generally smaller and lighter than those at higher orbits. This allows for multiple satellites per launch which reduces the average cost for systems incorporating more than one satellite.
- Satellites in this orbit travel at a speed of ≈ 8 km per second. At this speed, a satellite takes ≈ 90 minutes to orbit the Earth.
- Satellites in this orbit suffer from atmospheric drags and speed reduction due to gas frictions more than those in higher orbits.
- Free Space Path Loss (FSPL) is less than for higher orbits.
- The Round Trip Time (RTT) is less for the radio signals than that in case of higher orbits.

The satellites in LEO orbits are used for multiple applications including communications (e.g., the Iridium phone system), military purposes, remote sensing and Earth monitoring. The International Space Station is rotating around the Earth in a LEO orbit.

2.1.2.2 The Medium Earth Orbit (MEO)

Higher than the LEO satellites, the satellites occupy a Medium Earth orbit (MEO). The MEO satellites exist at altitudes between ≈ 1200 and ≈ 36000 km. In particular, two medium orbits receive most attention: the Molniya and the semi-synchronous orbits.

The Molniya orbit is an elliptical inclined orbit which was developed by the former Soviet Union to provide communication services in regions with high latitudes that are difficult to cover with geostationary satellites due to the low elevation angles. The Molniya orbit is highly eccentric ($\approx 0.722^\circ$) with its apogee located over the northern hemisphere. The angle of inclination of the orbit is 63.4° with respect to the equator. The orbital period of a satellite in the Molniya orbit is 12 hours with approximately two-thirds of the time over the northern hemisphere.

The semi-synchronous orbit is at altitude of ≈ 20000 km over the surface of the Earth. The orbital period at such an altitude is 12 hours. The semi-synchronous orbit is almost circular and therefore, a satellite in this orbit ideally crosses the same point on Earth twice per day. The main advantage of this orbit is its consistency and predictability. The satellites of the Global Positioning System (GPS) are located in semi-synchronous orbits [22].

2.1.2.3 The Geosynchronous/Geostationary Orbit (GSO/GEO)

The Geosynchronous orbit (GSO) has an altitude of ≈ 36000 km above the surface of the Earth. A particular form of the geosynchronous orbit is the geostationary orbit (GEO) in which the satellite rotates, over the equator, in the same direction as of the rotation of the Earth. A satellite in the GEO has a ≈ 24 hours orbital period and will ideally remain over the same spot of the Earth. This characteristic of the GEO satellites make it very suitable for many applications such as communications, television broadcast, and weather forecast. Although using GEO satellites for communication applications makes the design of the user terminals cheap and easy since they do not need to track the signal from the satellite, a major drawback is the relatively long RTT which leads to significant latency. A latency in the order of 250 milliseconds makes cables still preferable for long distance communications. GEO satellites can not provide polar coverage due to the limited GEO satellite visibility near the poles. Polar coverage is difficult and mostly achieved by LEO satellites.

2.1.2.4 The High Earth Orbit (HEO)

The High Earth orbit is higher than the GSO orbit in altitude at apogee. Therefore the satellite's orbital period is longer than 1 day and the satellite appears as if it orbits the Earth in a *retrograde* sense of rotation¹. The Molniya orbit is an example of HEO where its apogee is at an altitude of ≈ 40000 km over the surface of the Earth.

¹*Retrograde* rotation around the Earth is the rotation in the opposite direction to the rotation of the Earth. Whereas *Prograde*, also referred to as *Posigrade*, is the rotation in the same direction of the Earth's rotation.

2.1.3 Orbital Perturbations

Kepler's laws assume only the gravitational forces in modeling the motion of the satellite around the Earth [14]. They also assume the Earth and the satellite as point masses. In reality, the ellipsoidal orbit resulting from Kepler's laws is not constant over time. The satellite orbit is constantly changing because of many influences, including the gravitational fields of the Sun and the Moon, the asymmetry of the Earth's gravitational field, the solar pressure, and the atmospheric drag.

Together with the solar pressure, the Earth's magnetic field, which generates eddy currents in the satellite structure, cause rotation of the satellite body. If the attitude of the satellite is not corrected the satellite can spin about its central axis. The gravitational forces of the Sun and the Moon change the position of the satellite. The Moon's orbit is inclined by $\approx 5^\circ$ with respect to the equatorial plane. The plane of rotation of the Earth around the Sun is inclined by 23° with respect to the Earth's equatorial plane. These inclinations generate a force in the plane perpendicular to the satellite's orbital plane that tend to change its inclination. The yearly rate of change in orbit inclination is $\approx 0.85^\circ$ [14]. The effect of the Sun and Moon gravitational forces is higher on the satellites in the GSO orbit than on those in LEO orbits. LEO satellites are affected more by the gravitational force of the Earth and the atmospheric drag.

The Telemetry, Tracking Command and Monitoring (TTC&M) system consists of a controlling earth station and multiple sensors on the satellite. The earth station continuously measures the position of the satellite. Based on the telemetry stream received from the satellite and the orbital data, the control system sends commands to the satellite which change its position, through *thrusters*, in order to keep its nominal orbit. The satellite attitude control is important also to keep the communication antennas on-board the satellite pointing towards the Earth. Figure 2.3 shows the general structure of the TTC&M system.

2.1.4 Orbital Effects on the Communication Systems

The satellite's orbit has other effects on the performance of the communication systems. Most important to consider are the following:

2.1.4.1 Doppler Shift

In non-geostationary orbits the satellite position is not fixed relative to a stationary user on Earth. This causes Doppler shifts where the frequency received varies from the transmitted frequency depending on the velocity of the satellite. The relation between the amount of this frequency shift and the velocity is given by Equation 2.3.

$$\Delta f = \frac{V}{\lambda} \quad (2.3)$$

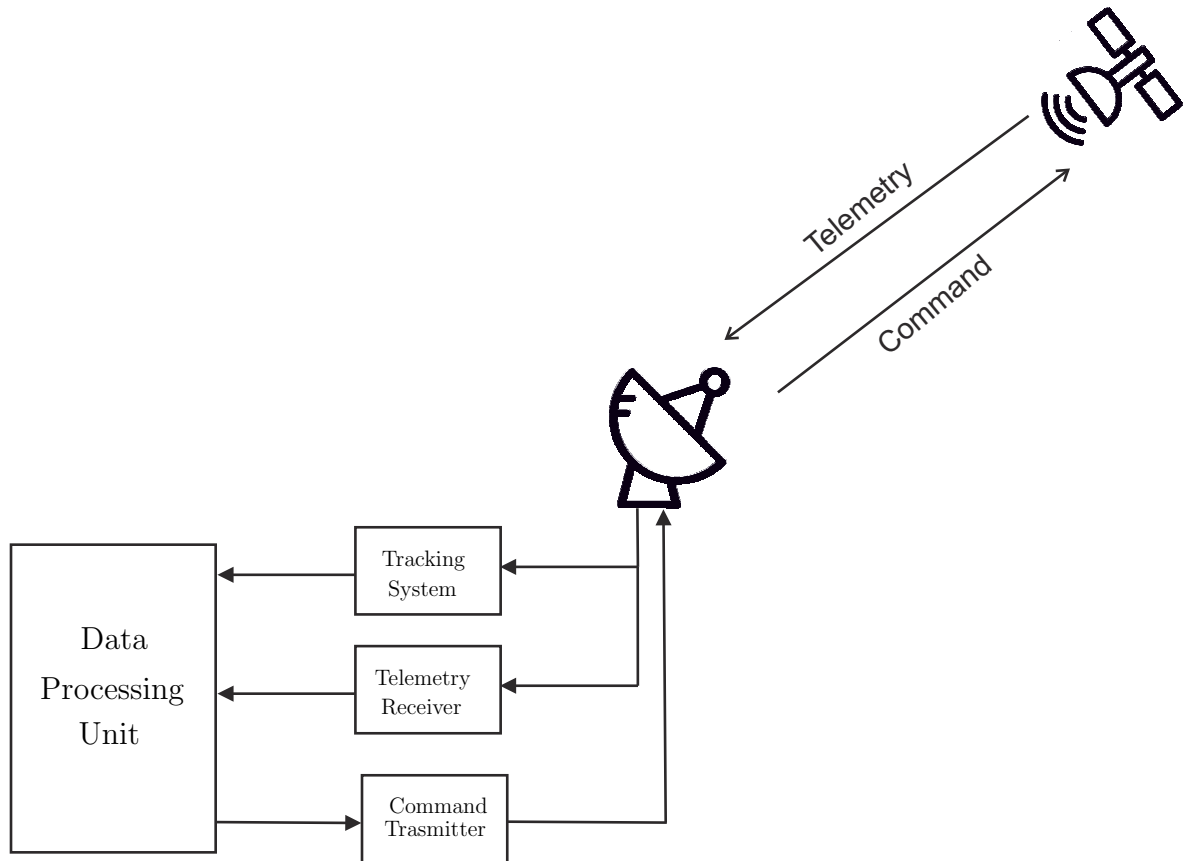


Figure 2.3: The structure of the Telemetry, Tracking Command and Monitoring (TTC&M) system. Basic idea of figure from [14].

where Δf is the Doppler shift. V is the satellite's velocity. V is positive if the satellite moves towards the receiver and negative if it moves away. λ is the wavelength of the transmitted signal.

Doppler is significant for LEO satellites and in most of the cases precise and fast frequency tracking receiver is necessary. The higher the frequency, the larger the shift in frequency and therefore at higher frequencies, e.g., Ka-band, LEO satellites are better suited for wideband applications. The effect of Doppler is negligible for the GEO satellites.

2.1.4.2 Solar Eclipse and Sun Transit Outage

Solar Eclipse: During solar eclipse, the Earth lies on the same plane between the Sun and the satellite as shown in Figure 2.4. For GEO satellites, eclipses happen close to the time of the equinoxes twice each year, around 20 March and 22-23 September. As the satellite lies in the shadow of the Earth, its solar array does not provide any energy and the satellite receives power from the batteries. The speed with which the satellite enters or exists the eclipse must be precisely monitored and controlled as these sudden temperature change phases lead to most of the satellite equipment failures.

Sun Transit Outage: This happens when the satellite lies between the Sun and the Earth on the same plane as also shown in Figure 2.4. A ground segment looking towards the satellite will also see the Sun as a *hot* microwave source in the sky. The equivalent temperature of the Sun ranges between 6000 and 10000 K. This noise temperature of the Sun will cause an outage of the reception from the satellite. However, the timings of such outages can be predicted and counter measures are usually considered, e.g., traffic offload to other satellites which are not in Sun outage.

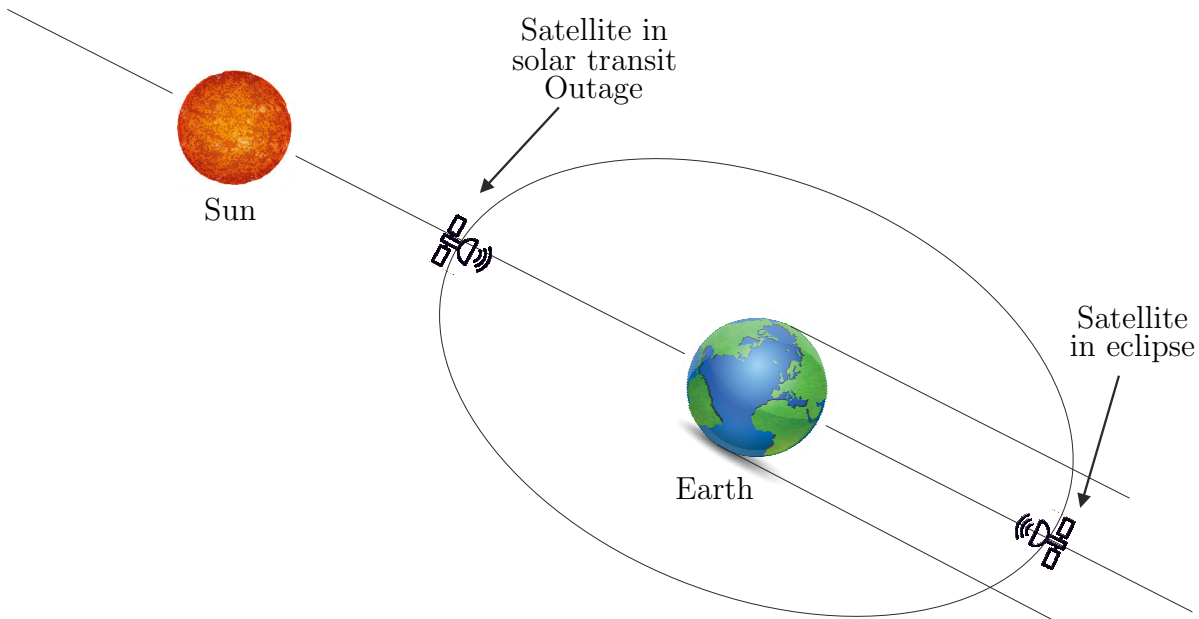


Figure 2.4: Solar Eclipse and Sun Transit Outage of a satellite. The Solar Eclipse occurs when the satellite lies in the shadow of the Earth and it receives no power from its solar arrays. The Sun Transit Outages occurs when the satellite lies in front of the Sun relative to the look angle of the ground segment. Figure abstracted from [14].

2.1.4.3 Range Variations

The satellite in orbit is subject to cyclic variations in position every day. Even with the best TTC&M stations, this variation could not be fully compensated. Consequently, a variation will occur in the time duration needed for the electromagnetic waves to travel between the satellite and the user terminals. If Time Division Multiple Access (TDMA) is used, a loss of timing synchronization may occur as the user frames can arrive in a wrong order. Time guards between the TDMA bursts can be used to ensure that synchronization is not affected, however, this will lead to loss in capacity of the satellite transponder. With modern On-board processing techniques, the effect of these variations can be minimized [14].

2.2 The Ground Segment

A ground segment, in the context of satellite communication systems, is the user terminal operating within the footprint of a space segment and is exploiting its services as shown in Figure 2.1. The ground segment can be one of the following three types [23]. The TTC&M is not included since it is considered as a part of the space segment.

Fixed Terminals: like Very Small Aperture Terminals (VSAT) used in private networks or the fixed terminal dishes that can be seen on top of the buildings to receive satellite television broadcast. These terminals access the satellite service while being fixed on Earth and not moving. For GEO satellites, once the antenna is successfully pointing towards the space segment, theoretically no tracking is needed. This facilitates the structure and the design of the terminal.

Transportable Terminals: like those used for Satellite News Gathering (SNG), are those which can be moved from one place to another but once being in location, they remain fixed and do not move during the communication activity. An initial satellite search algorithm needs to be implemented in the design of the terminal. Once the antenna points correctly towards the target satellite, no further tracking is required.

Mobile Terminals: such as those used for Satellite Communications On-The-Move (SOTM), are designed to maintain the communication activity with the satellite while being mobile. An online tracking algorithm is required to keep the antenna always pointing towards the desired satellite and to minimized the harmful interference to the the adjacent satellites. Mobile satellite terminals can be found nowadays in many land mobile, maritime, aeronautical and railway applications. In order to ensure that the antenna does not cause interference to adjacent satellites, testing of SOTM terminals is necessary. A main contribution of this thesis is the development of novel motion and shadowing profiles which are proposed to standardize the testing of SOTM terminals. Standardized SOTM testing will lead to a reduction of the Adjacent Satellite Interference (ASI) levels and to eventually will increase the overall efficiency of the whole satellite market.

The ground segment in it basic structure consists of the following subsystems [24]:

- The antenna subsystem.
- The Radio Frequency (RF) subsystem.
- The communication subsystem.
- The network interface subsystem.

2.2.1 The Antenna Subsystem

An antenna which is designed to be integrated in the ground segment should have some characteristics:

- The antenna should have a high directivity in the direction of the target satellite and a low directivity in other directions in particular those near the adjacent satellites.
- The antenna must provide a high isolation between orthogonal polarizations especially when frequency reuse by orthogonal polarizations is used.
- The antenna must keep continuous accurate pointing towards the desired satellite.
- The antenna noise temperature must be as low as possible.

2.2.1.1 Radiation Pattern

Satellite antennas are designed to have directive patterns. The antenna must direct the majority of the transmitted power through its main lobe towards a desired satellite. At the same time the power in the side lobes especially towards adjacent satellites must be minimized. The International Telecommunications Union (ITU) defined in one of its recommendations [25] the general reference mask as in Equation 2.4. The gain of any satellite antenna working in the range between 2 and 30 GHz must be below this mask.

$$G(\theta) = 29 - 25 \log \theta \quad [dBi] \quad (2.4)$$

Antenna spatial properties such as gain, radiation pattern and polarization are measured in either [26]:

- A far-field range, or
- A compact range, or
- A near-field range

Ground segment antennas are usually used in distant communication with a satellite laying in their far-field. In the far-field of an antenna, the radiated waves have planar fronts [26]. Equation 2.5 relates the far-field distance to the size of the antenna and the operating frequency. This far-field distance is also ensuring a phase taper angle less than 22.5° .

$$d = 2D^2/\lambda \quad (2.5)$$

Where λ is the operating wavelength.

The higher the frequency of operation, the larger the far-field distance. For very high frequencies, it becomes infeasible to measure antenna characteristics in the far-field. A compact range is offering a solution for such situations. Where a secondary

reflector or more are used between the illuminating source and the antenna under test. The secondary source(s) collimates the waves in planar fronts at the quiet zone. In a near-field range, the amplitude and phase of the radiation are measured directly in the near-field of the antenna and are then fed to a Fourier transform. This transform exploits the relationship between the antenna aperture fields and its far-field pattern. The majority of the state-of-the-art SOTM test facilities in the Ku-/Ka-band employ near-field and antenna compact ranges (c.f. Table D.1).

2.2.1.2 Antenna Types

Two types of antennas are used extensively in satellite communication ground segments, the parabolic antennas and the phased array antennas. Horn antennas were used for ground segments in the early days of satellite communications but are not anymore in use due to its high manufacturing cost [24].

Parabolic Antennas are the most used due to its simple structure and ease of production. It consists of a primary feed and a single or multiple parabolic reflectors. An important characteristic of a parabolic antenna is that it has a constant pattern which does not change with respect to the pointing direction. Parabolic antennas can have a symmetrical mounting, an offset mounting, or a Cassegrain mounting. In symmetrical mounting, shown in Figure 2.5(a), the reflector has symmetry of rotation with respect to the principle axis on which the primary feed is mounted at the focus. This structure has some disadvantages. The primary feed blocks part of the reflector leading to a reduction in the antenna efficiency due to aperture masking. Moreover, the primary feed in this mounting is directly facing the Earth and is collecting noise temperature from the ground leading to a reduction of the overall *gain over temperature* (G/T) figure of merit. The offset mounting, shown in Figure 2.5(b), solves the problem of aperture masking, however the primary source is also directed towards the Earth leading to a high antenna noise temperature. In [5], an investigation of the amount of the noise temperature of an offset satellite reflector antenna at different environments has been performed. The Cassegrain mounting depends on the use of an auxiliary reflector, as shown in Figure 2.5(c), and therefore the primary feed looks towards the Sky. The overall antenna noise temperature is lower compared to the previous mounting settings. However, the auxiliary reflector masks part of the waves reflected from the primary reflector leading to a reduction in the overall efficiency of the antenna.

Phased Array Antennas, unlike parabolic antennas, have multiple pattern shapes depending on the steering angle. Due to their compact structure, unlike the bulky structure of parabolic dishes, phased arrays are preferred to be used for mobile satellite applications where the ground terminal is mounted on a moving vehicle. Moreover, satellite tracking is fast and does not need to be done with drive motors like the case in parabolic antennas. With the help of an RF combiner and a phase shifter network, the power and phase of each element in the array is adjusted in order to steer the overall

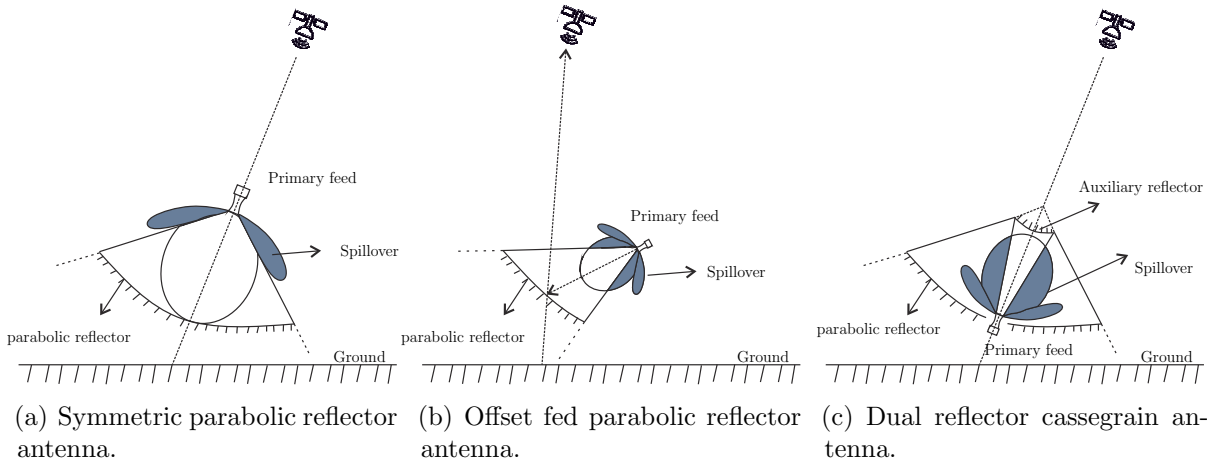


Figure 2.5: Types of parabolic reflector antennas. Figure adapted from [24].

pattern of the antenna in a specific direction. Figure 2.6 shows the structure of a phased array antenna employing a Uniform Linear Array (ULA).

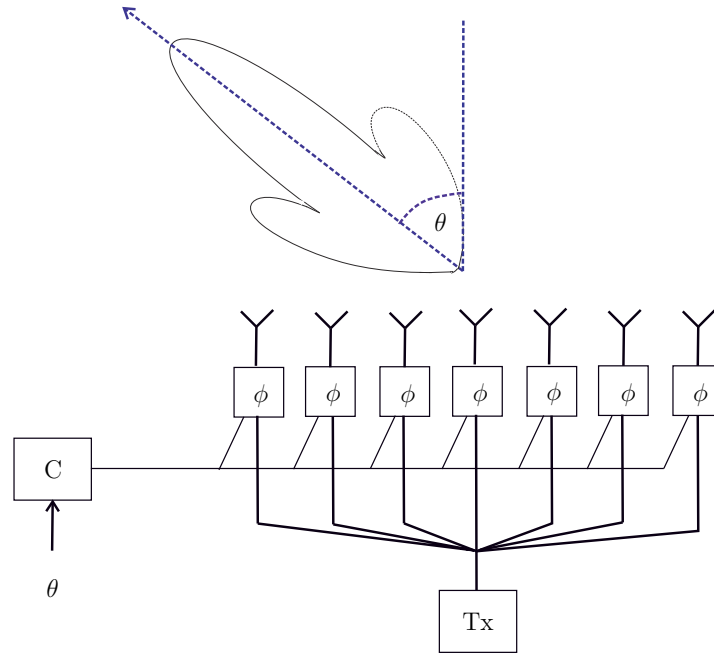


Figure 2.6: A phased array antenna with a Uniform Linear Array (ULA). The antenna steers the, e.g. transmit, beam direction using a Radio Frequency (RF) combiner and a phase shifter network.

2.2.1.3 Pointing Angle of a Ground Segment Antenna

To correctly point the antenna of an earth station towards a specific satellite, an angle pair (Azimuth and Elevation) need to be calculated. These angles are referred to as the satellite look angles. If linear polarization is used, a third angle (polarization) must be also calculated. The three pointing angles are depicted in Figure 2.7. The *azimuth angle* A is the angle through which the antenna must be turned clockwise about the

geographical north to bring its boresight into the direction of the satellite [24]. The *elevation angle* E is the angle through which the antenna must be turned from the equatorial plane upwards till its boresight is in the direction of the satellite. If the polarization of the wave is linear, an alignment of the earth station's antenna must be considered. The *polarization angle* ψ at the earth station antenna is the angle through which the antenna feed has to be turned counter-clockwise around the imaginary line connecting the antenna feed and the satellite.

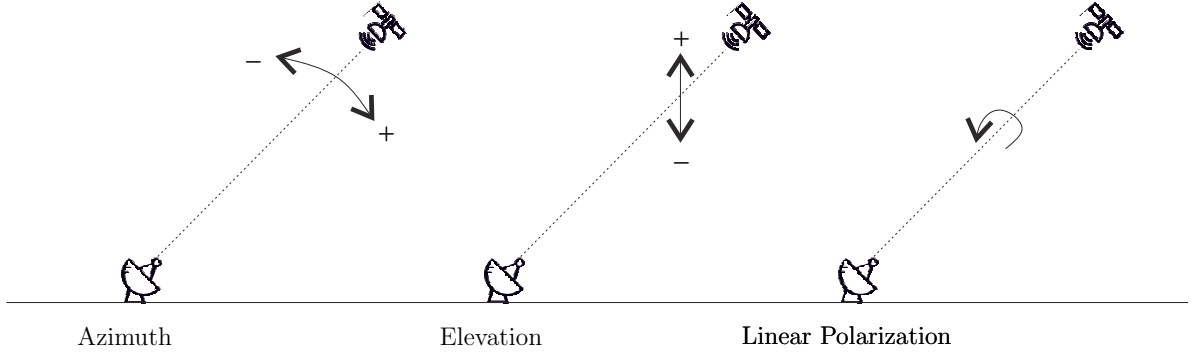


Figure 2.7: Pointing angles of an earth station antenna towards the satellite.

For the sake of simplicity, a satellite in the geostationary orbit is considered for the calculations in this section. The formulation of the look angles for satellites in general orbits can be found in multiple text books, e.g., [24,27]. The spherical coordinate system which is used to calculate the look angles is depicted in Figure 2.8.

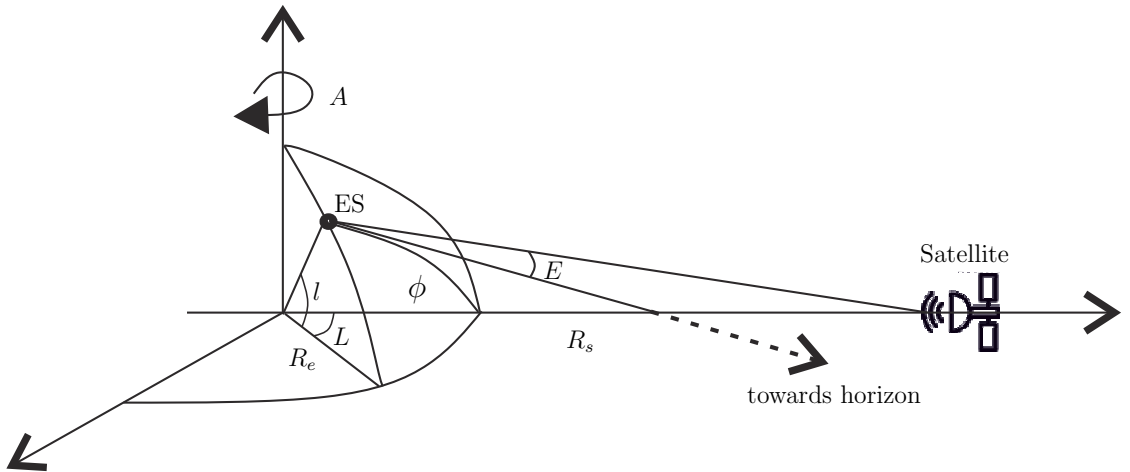


Figure 2.8: Satellite look angle calculations from an Earth Station (ES) on the surface of the Earth. Figure adapted from [24].

From Figure 2.8, the *elevation angle* E can be calculated as in Equation 2.6 [24].

$$E = \arctan \left[\frac{\cos \phi - R_e / (R_e + R_s)}{\sqrt{1 - \cos^2 \phi}} \right] \quad (2.6)$$

with:

$$\cos \phi = \cos l \cos L \quad (2.7)$$

where:

- l is the geographical latitude of the earth station.
- L is the relative geographical longitude of the earth station with respect to the longitude of the satellite. It is the absolute difference between the two longitudes.
- R_e is the radius of the Earth = 6378 km
- R_s is the altitude of the satellite above the surface of the Earth \approx 36000 km

The *azimuth angle* A has a value between 0° and 360° . A is calculated using Table 2.1.

Table 2.1: Azimuth look angle calculation.

	Satellite east of the earth station	Satellite west of the earth station
Northern hemisphere	$A = 180 - a$	$A = 180 + a$
Southern hemisphere	$A = a$	$A = 360 - a$

where:

$$a = \arctan \left(\frac{\tan L}{\sin l} \right) \quad (2.8)$$

The *polarization angle* ψ at the earth station antenna is the angle between the local vertical at the antenna and the satellite polarization plane. The satellite polarization plane is the equatorial plane for a GEO satellite emitting horizontal polarized (H) waves and the plane perpendicular to it if the waves are vertical polarized (V). In other words, $\psi = 0^\circ$ for V-polarization and $\psi = 90^\circ$ for H-polarization. ψ is generally calculated using Equation 2.9.

$$\cos \psi = \frac{\sin l \left(1 - \frac{R_e}{R_e + R_s} \cos \phi \right)}{\sqrt{1 - \cos^2 \phi} \sqrt{1 - 2 \frac{R_e}{R_e + R_s} \cos \phi + \left(\frac{R_e}{R_e + R_s} \right)^2 \cos^2 l}} \quad (2.9)$$

For GEO satellites, the satellite can be considered at infinite distance from the Earth ($R_s = \infty$). A simplified expression for the polarization angle can be obtained as in Equation 2.10.

$$\cos \psi = \frac{\sin l}{\sqrt{1 - \cos^2 \phi}} \quad (2.10)$$

Earth stations which incorporate parabolic antennas are built using specific mountings which enable the rotation of the antenna according to the previous look angles. The most famous mounting structures are: the azimuth-elevation, the polar, and the tripod mountings [24].

2.2.1.4 Tracking

Tracking is the ability of the antenna to keep the boresight of the earth terminal antenna in the direction of the desired satellite. Tracking is needed with directive antennas

when either the communication scenario includes motion of the satellite or the ground segment. There exist two main approaches to perform close loop antenna tracking: the sequential amplitude detection and the monopulse tracking. The sequential amplitude detection techniques sequentially displace the pointing direction of the antenna based on the detection of the maximum receive signal. Conical scan, step-by-step, and smoothed-step algorithms are examples of sequential amplitude detection tracking. In monopulse tracking, the correction of the antenna pointing direction is generated by a comparison of a sum signal and a difference signal. Most of the antennas which use monopulse tracking are implementing either the multiple source monopulse or the mode extraction monopulse algorithms [24].

2.2.2 The Radio Frequency (RF) Subsystem

The RF subsystem consists of a receive unit and a transmit unit. The receive unit contains a Low Noise Amplifier (LNA) and an interface to the communication subsystem. The function of the LNA is to amplify the received signal from the satellite. Since the signal received from the satellite is weak due to the long distance it travels, the noise temperature of the the LNA is critical. Modern LNAs make use of the latest transistor technologies in order to achieve low levels of noise temperature. The transmit unit of the RF subsystem consists mainly of a power amplifier and a linearizer. Tube amplifiers and transistor amplifiers are the most commonly used types. Power amplifiers are nonlinear and therefore a linearizer is used to limit the effects of the nonlinearity and help to operate the amplifier closer to the point of saturation.

2.2.3 The Communication Subsystem

On the receiving side, the communication subsystem is responsible for down-converting the signal to an Intermediate Frequency (IF) and to demodulate the IF signal. On the other hand, the transmit communication subsystem modulates the IF signal and then up-converts the modulated signal to the RF band to be ready for amplification at the RF subsystem. Multiple frequency conversion techniques exist for signal modulation and demodulation. Single frequency, dual frequency, and full band frequency conversion techniques are selected based on the system structure and the application. Frequency modulation (FM) is mostly used if the system is built for analogue transmission. With digital transmission, phase modulation is mostly used in satellite communications [24].

2.2.4 The Network Interface Subsystem

The main function of this subsystem is multiplexing or de-multiplexing the baseband channels of the terrestrial network. The most common used techniques in satellite

communications are Frequency Division Multiplexing (FDM) and Time Division Multiplexing (TDM) [24].

2.3 Propagation Effects

The electromagnetic waves bouncing between the space and the ground segments travel through the different layers of the Earth's atmosphere, including the ionosphere, and through the free space and is subject to multiple propagation effects. In order to achieve the desired level of performance, the link budget between the transmitter and the receiver must be carefully engineered. The general expression of the Earth-to-Satellite link budget is given in Equation 2.11.

$$P_r = EIRP + G_r - L_p - L_a \quad [dBW] \quad (2.11)$$

where:

- P_r is the receive power.
- $EIRP$ is the Equivalent Isotropic Radiated Power. $EIRP = 10 \log_{10}(P_t G_t)$ [dBW], where P_t is the transmit power and G_t is the gain of the transmit antenna.
- G_r is the gain of the receive antenna. $G_r = 10 \log_{10}(4\pi A_e/\lambda)$ [dBi], where A_e is the antenna effective aperture. $A_e = \eta_A A_r$, with A_r the physical receiving area and η_A the aperture efficiency. η_A is typically between 50 and 70% for parabolic reflector antennas.
- L_p is the Free Space Path Loss (FSPL). FSPL is proportionally related to the square of the distance between the satellite and the ground segment (R). $L_p = 20 \log_{10}(4\pi R/\lambda)$ [dB]. Where λ is the operating wavelength.
- L_a is the loss in the Earth's atmosphere.

In the remaining of this section, the impairments due to the propagation through the Earth's atmosphere are discussed.

2.3.1 Rain Attenuation and Depolarization

Rain attenuation is the most significant of the satellite signal propagation impairments for frequencies above 10 GHz [28]. Rain attenuation is the limiting factor in designing satellite links at Ku- and Ka-bands. Rain causes two effects, attenuation and depolarization.

2.3.1.1 Rain Attenuation

Rain attenuation depends on the frequency and the rain intensity. Rain attenuation as a function of *effective path length* through rain (L_e) is described in Equation 2.12.

$$A_{Rain} = \alpha_R L_e \quad [dB] \quad (2.12)$$

where:

- $\alpha_R = aR_p^b$ is the specific attenuation.

R_p is the rain intensity which is exceeded for an annual percentage (p [%]) in millimeter/hour (mm/h). Rain intensity is the amount of rainwater in millimeter accumulated in one hour in a rain gauge located at the position of the ground segment [21]. In Europe, a rain intensity $R_{0.01}$ ($p = 0.01\% \approx 53$ minutes per year) is around $30 mm/h$. In equatorial regions, $R_{0.01} = 120 mm/h$. a and b are constants which depend on frequency and wave polarization. Values of a and b are available in the literature, e.g., [29].

2.3.1.2 Rain Depolarization

The wave emitted by an antenna has an electric field component and a magnetic field component [30]. Wave polarization is a measure for the orientation of the electric field component relative to the direction of wave propagation. The electric field vector changes its direction with time. During one period of propagation, the electric field vector depicts an ellipse in the plane perpendicular to the direction of propagation. The polarization ellipse is shown in Figure 2.9.

Polarization is characterized by the following:

- Rotation direction of the electric field vector: clockwise or counter-clockwise.
- Axial ratio (AR): $AR = E_{co}/E_{cross}$. In the setting shown in Figure 2.9, the polarization is said to be elliptical. When $AR = 1$, the polarization is circular. When the ellipse reduces to one axis, the polarization is said to be linear and the electric field vector's direction is fixed.
- τ : the tilt angle of the semimajor axis of the polarization ellipse.

Further details on the description of the wave polarization and how polarization is measured are presented in Appendix C.

Depolarization effects originate from the non-spherical shape of raindrops. A differential attenuation and a differential phase shift occur between the two orthogonal components of the wave causing a leakage of some of the energy from the co-polarized signal component into the cross-polarized component and vice versa.

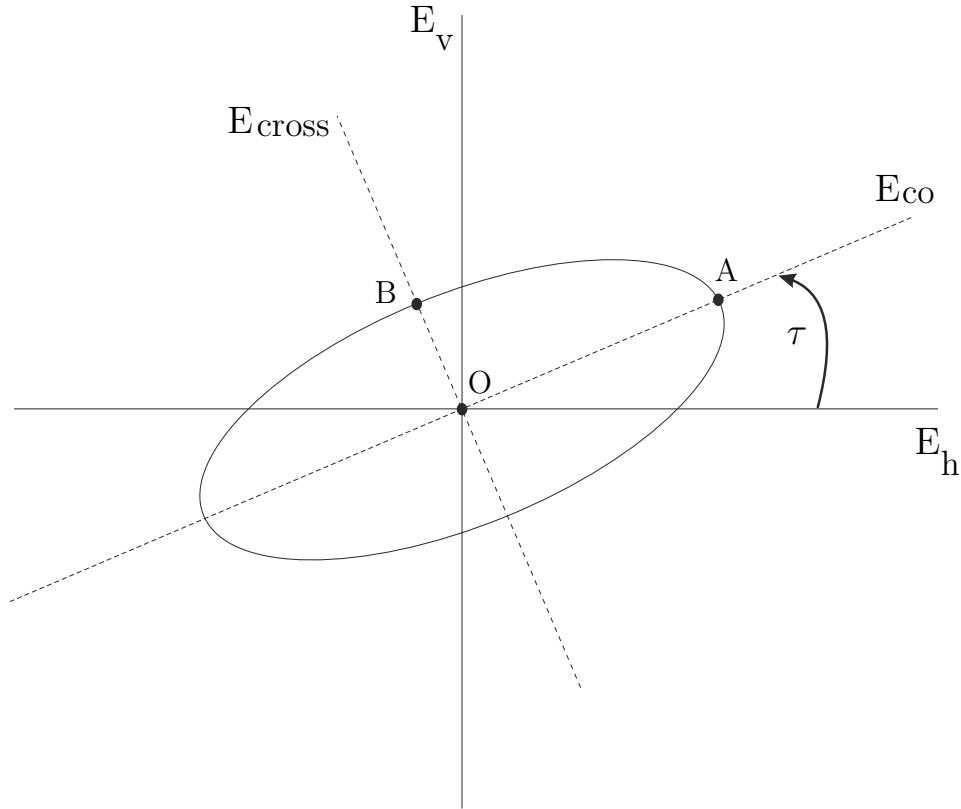


Figure 2.9: The polarization ellipse.

2.3.2 Other Impairments

2.3.2.1 Attenuation by Atmospheric Gases

The electromagnetic waves at satellite communication frequencies interact with the molecules in the atmosphere. This interaction causes signal attenuation. The attenuation depends on frequency, the elevation angle, the altitude of the ground segment, and the water vapor concentration. In the ITU Recommendation P.676-11 [31], the attenuation due to atmospheric gases has been inspected. Resonant absorption peaks exist at certain frequencies. At 22.24 GHz one of these absorption peaks is located with an attenuation of ≈ 3 dB at zenith direction [28]. At K-band, frequencies used for satellite communications are specified around this peak producing the known Ku- and Ka-bands under and above the absorption peak, respectively.

2.3.2.2 Cloud Attenuation

Cloud attenuation is significant for frequencies at Ka-band and above. Two models exist for the cloud attenuation [14]. The typical values of water-filled clouds at 30 GHz at 30° elevation are between 1 and 2 dB.

2.3.2.3 Scintillation

The variations of the refractive index of the troposphere and the ionosphere cause variations in the amplitude of the received signal. This is what is known as *scintillation*. At Ku-band, these variations can exceed 1 dB. The magnitude of the tropospheric scintillation generally increases when the frequency increases and when the elevation angle decreases [14].

2.3.2.4 The Faraday Rotation

The ionosphere introduces a rotation of the polarization of linearly polarized waves. The Faraday rotation causes a mismatch between the transmitted and the received wave polarizations. The challenge is that the rotation of the polarization plane is in the same direction for the uplink and the downlink. Therefore a simple rotation of the antenna feed can not compensate the effect of the Faraday rotation. The rotation angle of the polarization plane is inversely proportional to the square of the frequency and becomes negligible for frequencies above 10 GHz. For low frequencies, either circularly polarized signals, which do not suffer from this phenomenon, are used or accurate polarization tracking must be considered.

Chapter 3

State Of The Art Satellite Communication Services and On-The-Move Testing

This chapter presents the state-of-the-art services, applications, and component technologies that are related to satellite communications. Section 3.1 summarizes the state-of-the-art satellite communication services and applications. Since this thesis researches and introduces efficient methodologies to test Satellite Communication On-The-Move (SOTM) terminals, more focus in this chapter is given to the SOTM related state-of-the-art standards, regulations, and type approval programs. The existing methodologies to test terminals either in a laboratory or in a free field are discussed in Section 3.2. The testing methodology which is proposed as a major contribution of this thesis, is then presented in Chapter 4. The benefits of testing SOTM terminals according to the proposed standardized testing conditions are also discussed.

3.1 Satellite Communication Services

The satellite communication services, traditionally, include:

Fixed Satellite Services (FSS): These services use GEO satellites and fixed ground segments either in point-to-point or point-to-multipoint topologies. FSS are used typically for video, voice, or IP data transmission over long distances between specific ground segments at given locations. Figure 3.1(a) depicts a typical ground segment used for FSS services.

Broadcast Satellite services (BSS): These services support broadcasting satellite signals over a large area of the Earth. The most representative example is the Direct Broadcast Service (DBS) which delivers Television and Radio channels to homes. As shown in Figure 3.1(b), the dish reflector antennas mounted on the rooftops of houses to receive BSS Television signals can be seen everywhere.

Mobile Satellite Services (MSS): These services support the communication between a mobile ground segment and one or multiple space segments. Figures 3.1(c) and 3.1(d) show user terminals from EPAK GmbH [32] and Kymeta Corporation [33] developed for SOTM applications.



(a) User terminal used for FSS applications. Courtesy [34]



(b) User terminal used for BSS applications. Courtesy [35]



(c) User terminal used for MSS applications. Courtesy EPAK GmbH [32]



(d) The Kymeta mTenna U7 SOTM Antenna Subsystem Module (ASM). Courtesy Kymeta Corporation [33]

Figure 3.1: Typical types of state-of-the-art user terminals for the different satellite communication services.

The continuous demand of increased bandwidth pushes the development of both the space segment and the ground segment of the satellite communication system. In the 1980s, the move of satellite communications from the C-band to the Ku-band in order to provide larger bandwidth for satellite services represented a part of this development. Recently, High Throughput Satellites (HTS) represent a significant solution to provide higher capacity and lower cost. HTS are offering at least twice the throughput of a classic FSS satellite. For example, in 2011, the Viasat-1 satellite was launched. It was the world's highest capacity communications satellite with a total capacity of 140 Gbit/s [36].

This capacity was larger than the capacity of all the satellites covering North America combined at the time of launch. The high throughput offered by HTS is achieved by high level frequency reuse across narrowly focused spot beams [37]. The spectrum availability offered by the Ka-band makes it optimum to offer high-speed broadband internet connectivity and Direct-to-Home (DTH) High Definition Television (HD-TV) which are seen as primary applications of HTS [38]. In-mobility broadband internet services, especially in distant regions which are not covered by traditional satellites, are also amongst the applications targeted by HTS. As a leading example for an HTS comprehensive network, the alliance between Intelsat and OneWeb resulted in the first global, Pole-to-Pole HTS system. The GEO-LEO satellite network offers global high-throughput, low-latency services [39].

Along side the development of the space segment, a similar development must take place in the technology of the user terminal. The terminals developed for the Viasat-1 (*exede*), the *tooway* EUTELSAT's KA-SAT HTS, and the Advantech Wireless HTS [40], represent examples of the latest development of the fixed or On-The-Pause user terminals. For On-The-Move applications, the complexity of the tracking unit is a major factor in limiting the development of the user terminal. Recently, SOTM terminals use phased arrays instead of the bulky reflector dish antennas in order to have compact design and to facilitate the tracking. The bulky dish terminals are not suitable to be mounted, for instance, on airplanes and high speed trains. New development in the technology of phased arrays offer the ability to perform fast beam switching which is necessary for the low latency requirements of the HTS applications. The phased arrays developed by KYMETA [33] and PHASOR [41] represent the latest state-of-the-art technology. Figure 3.1(d) shows the mTenna U7 phased array antenna developed by Kymeta corporation.

3.2 Satellite Communication On-The-Move Testing

Testing the performance of SOTM terminals is the main focus of this thesis. In this Section, an overview of the existing SOTM related standards and type approvals is presented. Moreover, the state-of-the-art SOTM testing environments and procedures are presented and compared.

At a global level, the International Telecommunication Union (ITU) establishes standards which regulate the performance of all telecommunication platforms, including those relevant to Satcom On-The-Move. At the regional and the local levels, organizations such as the European Telecommunications Standards Institute (ETSI) in Europe or the Federal Communications Commission (FCC) in the United States adapt the general ITU regulations according to regional needs. Additionally, satellite operators issue type approvals to define how the SOTM terminals need to be tested.

3.2.1 SOTM Standard Metrics

The SOTM standards define operational limits with respect to the following metrics:

- Antenna absolute de-pointing,
- Off-axis emissions, and
- Transmit cessation time.

The Antenna Absolute De-pointing is a measure in degrees that specifies how far the main beam of an antenna is displaced from a target satellite. The transmit cessation time and the off-axis emission specifications depend on this metric. Antenna de-pointing is the most important parameter, as it not only directly indicates the ability of the SOTM terminal to keep a high quality of the link towards the target satellite, but also its ability to avoid Adjacent Satellite Interference (ASI). The FCC regulations state that the antenna de-pointing should not exceed 0.2° at normal operating conditions in Ku-band. This limit can be raised to 0.5° , provided that in any case the transmit power does not exceed the regulatory EIRP Spectral Density (ESD) mask and that the value of the maximum de-pointing is reported to the satellite operator. For Ka-band, FCC does not specify an absolute de-pointing threshold. The pointing requirements are defined in terms of excess power levels. The ETSI norms require, for all frequencies, that the applicant specifies the value of the maximum expected de-pointing as a function of on-axis ESD. The ESD mask must not be exceeded in any occasion. In the Satellite Operator's Minimum Antenna Performance (SOMAP) Requirements defined by the Global VSAT Forum (GVF), the de-pointing threshold is specified at 0.5° for all frequency bands [42].

The Off-axis Emissions are often parametrized by the transmit gain mask or the ESD mask. The gain/ESD mask defines the amount of gain/ESD allowed by the SOTM antenna as a function of the angular position relative the antenna boresight for co- and cross-polarized transmit components. The lower and the narrower the mask, the more challenging it is for the antenna to fulfill the off-axis emissions requirements. Different gain/ESD masks are defined by the different regulatory authorities depending on the application: commercial or military, and on the frequency of operation: Ku- or Ka-band. In general, the commercial Ka-band masks are narrower and more stringent than the commercial Ku-band masks [43]. The military Ka orbit/band is not yet crowded, the MIL-STD-188-164B Ka-band mask, defined by the Department of Defence (DOD), is therefore the most flexible amongst all. As an example for a regulatory mask specified in SOTM recommendations, the GVF-SOMAP requirements adopt the gain mask named the ' $32 - 25 \log \theta'$ ' mask for the Ku-band and the gain mask ' $29 - 25 \log(\theta)$ ' [dBi] for the Ka-band.

The Transmit Cessation Time, also referred to as the transmit mute time, is defined as the time period that the SOTM terminal stays active before it switches off its transmit activity if the antenna de-pointing is larger than a specific threshold. The

FCC Blanket Licensing Provisions 25.226 and the 25.222 define the transmit mute time to be 100 milliseconds if the antenna de-pointing exceeds 0.5° [18]. The GVF-SOMAP requirements adopt the same definition. The ETSI regulations leave the exact definition of this metric to the applicant but state that it should not exceed 2 seconds in case on Vehicle Mounted Earth Stations (VMES) [19] or 5 seconds for Earth Stations on Vessels (ESV) [44].

Table 3.1 lists the state-of-the-art SOTM standards, regulations, and norms for each environment: land mobile, maritime, airborne, and railway for the Ku and Ka frequency bands.

Table 3.1: The state-of-the-art SOTM standards, regulations, and norms listed for each environment and each frequency band.

	Land mobile		Maritime		Airborne		Railway	
	Ku	Ka	Ku	Ka	Ku	Ka	Ku	Ka
ITU	R 728-1	R S.524						
	R S580-6							
	R S.1875							
FCC	p25.226	p25.138	p25.222	p25.138	-	p25.138	-	p25.138
DoD	MIL-STD-188-164B	MIL-STD-188-164B	MIL-STD-188-164B	MIL-STD-188-164B	MIL-STD-188-164B	MIL-STD-188-164B	-	-
	Ku-Section A	Ka-Section A	Ku-Section C	Ka-Section C	Ku-Section B	Ka-Section B	-	-
ETSI	EN 302 977	EN 303 978	EN 302 340	EN 303 978	EN 302 186	EN 303 978	EN 302 448	EN 303 978
GVF	SOMAP ¹							

3.2.2 SOTM Type Approvals

As owners of the satellite network resources, satellite operators are most affected to suffer from losses caused by ASI. In the ideal case, SOTM terminals are not allowed to be deployed in a satellite network without being tested and approved according to the operator's type approval. Nowadays, the ESOG-120 from EUTELSAT, the IESS-601 from INTELSAT, and the GVF-105 from the GVF are the most known type approvals.

In [1], it is found that only about 40% of the off-the-shelf SOTM products are type approved. This low percentage is due to the high cost and the long duration of the type approvals. As a step towards reducing the effort needed for type approvals, the Mutual

¹SOMAP: Satellite Operator's Minimum Antenna Performance

Recognition Agreement (MRA) Working Group of GVF defined the GVF-101 and GVF-105 documents [45], [46]. Together the two documents specify general test guidelines and recommendations for SOTM terminals that can be used by any operator. The GVF-101 document defines a list of tests required in order to approve the performance of a terminal. In an initial phase, the manufacturer has to submit preliminary test results, especially results of the antenna pattern measurements. These results will be inspected and an initial decision in order to proceed to phase 2 will be made. In phase 2, a GVF Authorized Testing Entity (ATE) is involved. The ATE will operate the tests specified in the GVF-101 document according to the recommendations of the GVF-105 document. The GVF-105 document provides recommendations and practical guidelines how to test the SOTM terminal with respect to off-axis emissions, pattern skew, pointing error, and transmit mute functionality. The GVF-105 document does not specify any operational limits which a SOTM terminal has to meet. It is left to the satellite operator to accept the performance claimed by the manufacturer and proven by the ATE or to refuse it. The GVF-105 recommendations in addition to the GVF-SOMAP requirements offer a clear way to test the SOTM terminal with respect to a unified set of requirements following a unified set of measurements. This is beneficial for the manufacturer since the SOTM terminal will be tested once. Moreover, the profit plan of the operators are not harmed since the final decision is still taken internally by the operator after matching the test results with the relevant internal specifications.

The benefit testing SOTM terminal with respect to standardized conditions can be seen in Figure 3.2. It shows the SOTM terminal qualification flow chart starting with the terminal manufacturing and ending with the global approval of the terminal if it was tested according to a unified set of standards.

3.2.3 SOTM Testing Procedures and Environments

The testing of SOTM terminals is conducted either in the free field or in a laboratory. In a field test, the terminal is mounted on a vehicle, which drives along a certain motion track. Meanwhile, the terminal communicates via an actual real operational satellite with a master station. These tests are commonly known and are conducted at various locations, as described in [47] and [48]. Although the complete SOTM terminal is included in these tests, this approach suffers from critical drawbacks. Firstly, the environmental parameters, e.g., shadowing and motion, cannot be separated from each other and the influence of a single parameter cannot be precisely determined. Secondly, another source of uncertainty is the lack of repeatability of the same test scenario. Neither the same driving conditions, nor the weather can be exactly repeated. In order to measure the antenna de-pointing in a field test, at least two operational satellites need to be included. One satellite operates as the desired target satellite and the other as an adjacent satellite. Figure 3.3 shows how antenna de-pointing is measured in a field test using operational

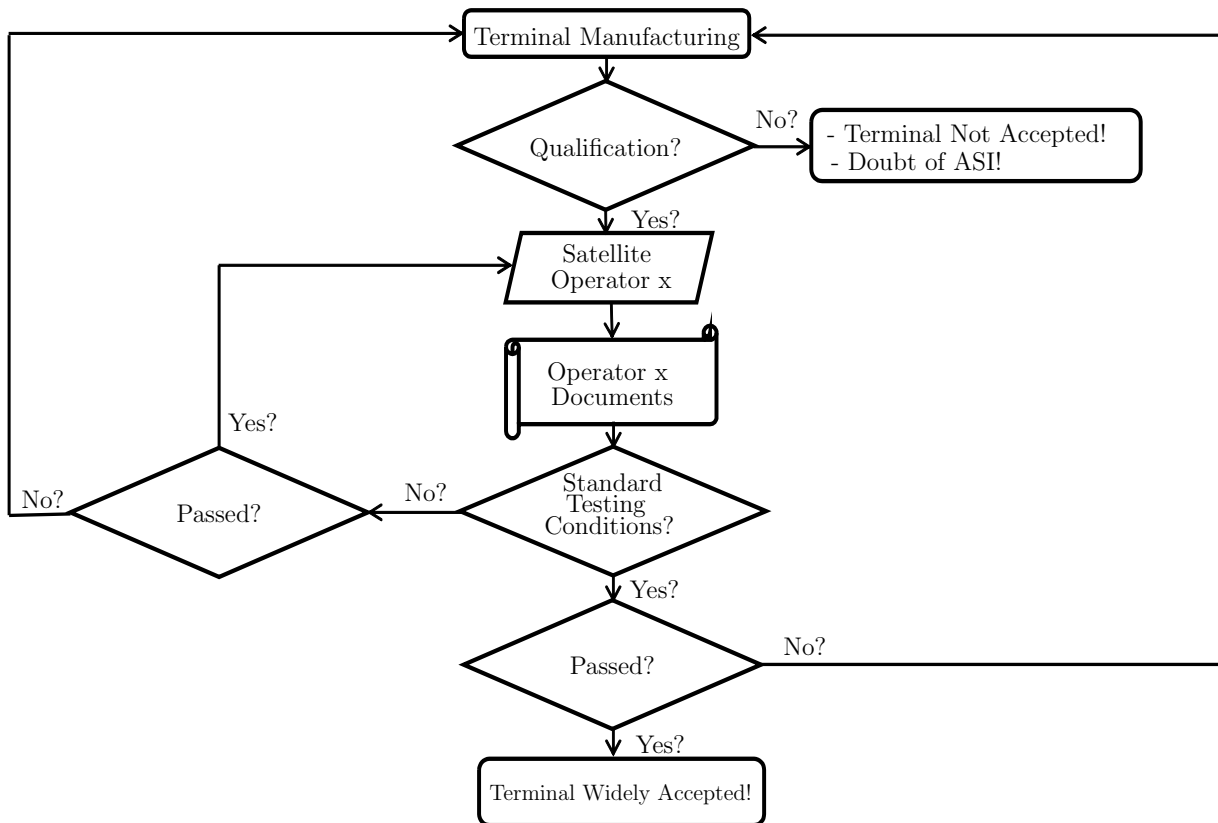


Figure 3.2: The SOTM Terminal Qualification Flow Chart.

satellites. The signals received at the desired as well as at the adjacent satellites are relayed to two fixed earth stations for monitoring.

The antenna pattern is measured along the same axis on which the de-pointing is determined, e.g., the geostationary orbit (GEO). Based on the difference between the signals received at the fixed stations, the antenna de-pointing can be determined. The slope of the antenna pattern at the position of the adjacent satellite enables detecting the signal level changes associated with the motion of the antenna.

The performance of this *Two Satellites* de-pointing estimation method is affected by the following:

- The Signal-to-Noise-Ratio (SNR) available for de-pointing measurements at the fixed earth stations is low due to the large path loss and the large distance between the terminal and the geostationary orbit.
- If the SOTM antenna beam width (w) is small with respect to the distance between the two satellites, the signal levels measured by the adjacent satellite will always be ambiguous. Thus, exact estimation of the antenna de-pointing is not possible, nevertheless, it is still possible to tell if there is harmful interference to the adjacent satellite.
- Since only two power level measurements are available, the de-pointing estimation results is ambiguous with respect to azimuth and elevation.

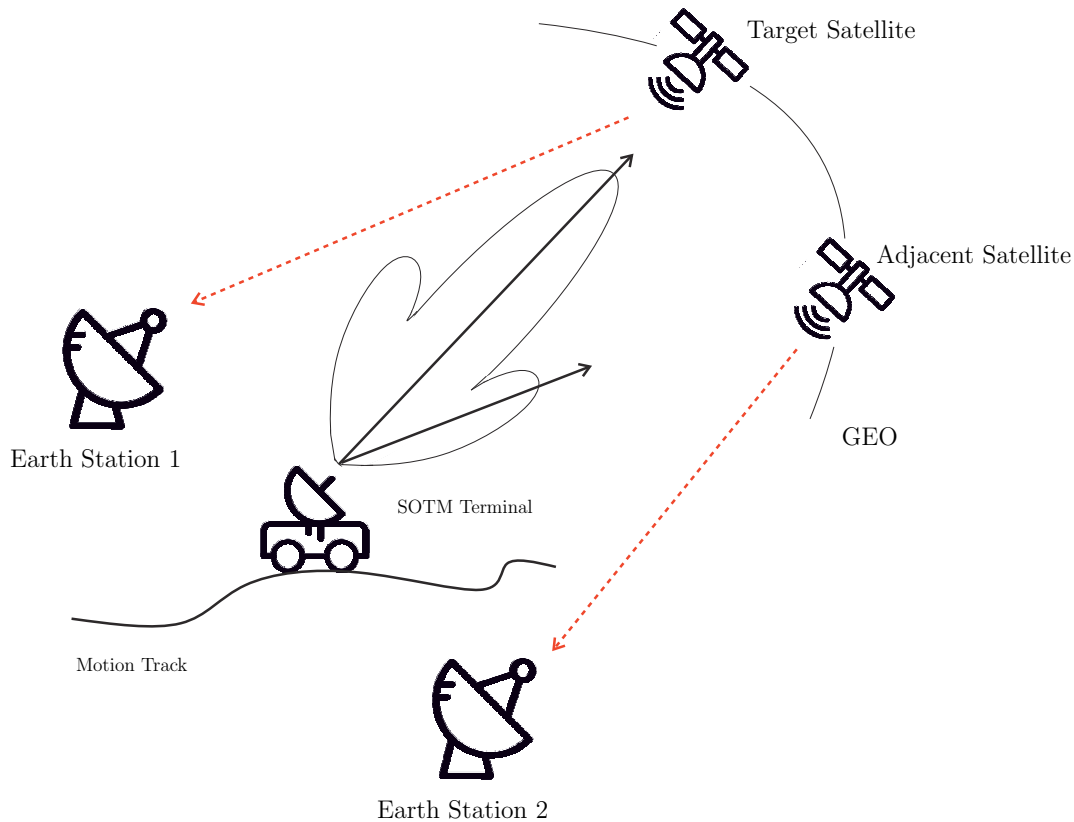


Figure 3.3: The SOTM free field test showing how antenna de-pointing is measured using two satellites in the geostationary orbit (GEO). Basic elements in the Figure are taken from [20].

- The effect of antenna de-pointing on the other adjacent satellites which are not involved in the test plan is ignored. The terminal might have some situations where it harmfully interferes to other satellites.
- Both the desired and the adjacent satellites must be accurately calibrated with respect to antennas and active elements. Furthermore, the fixed earth stations must be exactly pointing towards the satellites otherwise a link calibration for both antennas is necessary.
- A principle assumption is that the gain pattern of the antenna under test is symmetric in the azimuth-elevation plane. This assumption is necessary since the two adjacent satellites do not lie on a straight line in azimuth, but on the geostationary arc.
- Lack of repeatability is one of the main limitations of the *Two Satellites* method. Moreover, the cost of renting the operational satellites is relatively high.

The majority of the existing laboratories has the ability to test only parts of the SOTM terminal. In Appendix D, a list is presented for the major state-of-the-art environments and laboratories which have the capabilities to test either the complete SOTM terminal or only parts of it. The authors are aware of only two facilities which are built

to test the complete SOTM terminal: the Aberdeen Proving Ground (APG) in Maryland, USA and the Fraunhofer Facility for Over-the-air Research and Testing (FORTE) in Ilmenau, Germany. Due to the dimensions of the laboratory at APG, tests are performed in the near-field of the antenna [49]. The beam of the antenna will be spread depending on how far in the near-field the antenna is operating [30]. FORTE performs SOTM testing of the complete terminal in the far-field in a repeatable and controllable way. The emulation of the realistic environment, a SOTM terminal would experience, is possible by the usage of satellite payload emulators, a 3-axis motion emulator, channel, and GPS emulators. A two dimensional sensor cross mounted on an antenna tower (cf. Figure 4.2) enables the estimation of antenna de-pointing with high precision. A description of FORTE with detailed technical parameters can be found in [6–8].

A block diagram depicting the structure of FORTE is shown in Figure 3.4.

FORTE is approved as an Authorized Testing Entity (ATE) of the GVF and it combines the advantages of the laboratory and the free field environment. Table 3.2 summarizes the main advantages of FORTE compared to the field test.

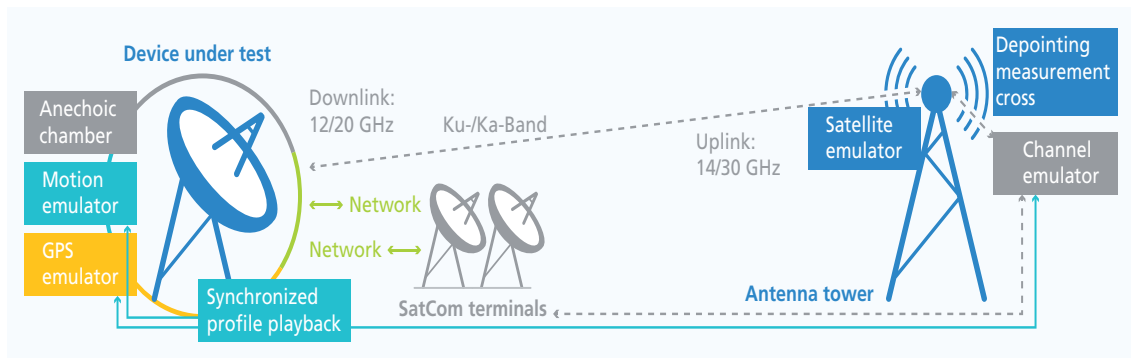


Figure 3.4: An overview of the structure of the Fraunhofer Facility for Over-the-air Research and Testing (FORTE).

Table 3.2: The advantages of SOTM testing at the Fraunhofer Facility for Over-the-air Research and Testing (FORTE) compared to testing in the field with operational satellites.

	Field Test	FORTE
Need for operational satellites	yes	no, but can be used additionally
Repeatability	challenging	guaranteed
Measurement dynamic range	10-12 dB	around 55 dB
Effect of antenna pattern shape on antenna de-pointing estimation accuracy	the measurement contrast is quite low for antennas with beam width larger than the separation between the two operational satellites	the sensor positions on the antenna tower can be adjusted and optimized with respect to the shape of the antenna pattern
Multi-dimensional de-pointing estimation	de-pointing estimation is possible along the GEO arc only	azimuth and elevation de-pointing estimation is possible due to a two dimensional sensor array

Chapter 4

Proposed Testing Methodology

This chapter presents the methodology we propose to perform qualification tests of SOTM terminals at the Fraunhofer Facility for Over-the-air Research and Testing (FORTE). A Satellite Communication On-The-Move (SOTM) terminal is tested at FORTE according to the standard performance metrics discussed in Section 3.2.1. Furthermore, we define the *data traffic throughput* as a metric to test the performance of the modem under realistic conditions. The measurement of the off-axis emissions, the antenna de-pointing, the transmit mute duration, and the data traffic is presented in Sections 4.1, 4.2, 4.3, and 4.4, respectively.

In a first step of the SOTM qualification test, the antenna pattern is measured. At FORTE, with a distance of 90 m between the terminal and the antenna tower (cf. Figure 4.2), a far-field distance for antennas with a diameter up to 90 cm in the Ku-band and up to 70 cm in the Ka-band is ensured. In the commonly used setting, the motion emulator is used to rotate the antenna for pattern measurements. The used motion emulator ensures a high degree of position accuracy (≈ 0.05 arc sec). The center sensor on the antenna tower works as a probe and is used for pattern measurements.

Due to the difference in height between the SOTM antenna and the probe on the tower, an elevation (pitch) pre-tilt is necessary in order to have the antenna looking towards the probe.

The elevation pre-tilt can be achieved either by:

1. Fixing the boresight of the antenna towards the horizon (aligned with the x-axis in Figure 4.1) and use a pre-tilt of the motion emulator.
2. Tilting the elevation of the antenna in its local frame and keeping the motion emulator's elevation at zero.

In the first setting, where the pre-tilt is achieved using the motion emulator, the coordinate frame in which the antenna pattern is defined is aligned to the coordinate frame in which the motion emulator moves its three axes. Any rotation with the motion emulator is directly mapped to the same rotation in the pattern frame. Figure 4.1 shows the trace of an azimuth cut measurement in this setting.

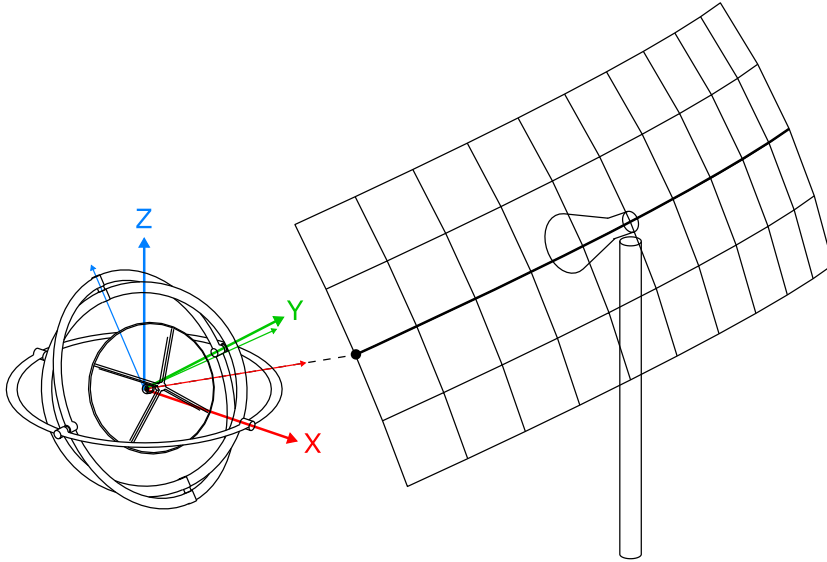


Figure 4.1: The SOTM antenna has no elevation pre-tilt in its pattern frame and therefore it matches the coordinate frame in which the motion emulator axes rotate.

Many type approvals demand the pattern to be measured at pattern elevation tilts which are not 0° . For example, the ESOG-120 type approval of EUTELSAT requires a tilt between $30^\circ - 35^\circ$ [50]. If the antenna pre-tilt angle is not zero, its pattern coordinate frame does not match that of the motion emulator and a coordinate frame transformation is required in order to correctly represent the antenna pattern in its correct local frame. The details of this coordinate transformation are presented in Appendix A.

4.1 Off-axis Emissions Measurements

The evaluation of the off-axis emissions is done by subtracting the far-field pattern from the relevant regulatory gain or EIRP Spectral Density (ESD) mask. In case there are angular positions at which the pattern exceeds the mask, they are reported together with the corresponding levels. This test evaluates the performance of the SOTM antenna and the Block Up Converter (BUC) at once. If the measured pattern violates the regulations, the manufacturer needs to redesign the antenna in order to reshape the main lobe or one of the side lobes. Alternatively, the amount of power transmitted by the BUC can be reduced to match the ESD mask. However, this leads to a degradation of the overall quality of the communication link.

4.2 Antenna De-pointing Measurements

In order to measure the antenna de-pointing, the motion emulator plays back a motion profile. Hence the SOTM antenna experiences a de-pointing which it tries to compensate using its foreseen mechanisms. The remaining de-pointing error, due to imperfect compensation is detected by a sensor array mounted on the antenna tower as shown

in Figure 4.2. Therefore, if the terminal is tested under the effect of motion only, and the effects of other impairments such as signal shadowing and Doppler are disabled, the proposed method for the antenna de-pointing measurements explicitly shows how good the tracking unit performs.

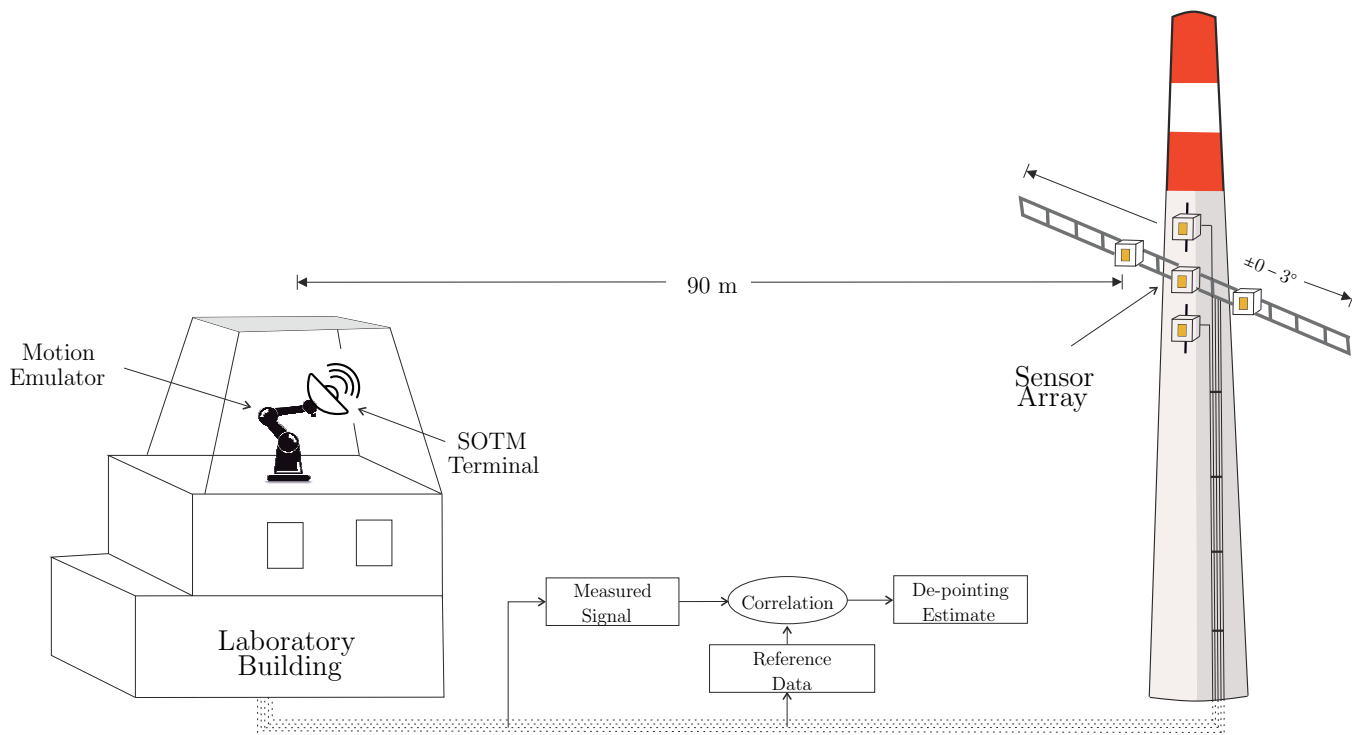


Figure 4.2: De-pointing measurements at the Fraunhofer Facility for Over-the-air Research and Testing (FORTE).

4.2.1 Antennas with Fixed Radiation Patterns

The methodology described in this section is developed to estimate the de-pointing of SOTM antennas which have fixed radiation patterns, e.g., parabolic reflector dish antennas. Section 4.2.2 deals with phased arrays and antennas which have changing radiation patterns.

A parabolic antenna has a single pattern that is the same for all pointing directions and therefore can be measured once and always used as a reference. While the antenna is being On-The-Move and transmitting, the sensor array, on the antenna tower at FORTE, is detecting the received power at five spatial points (cross-shape). The de-pointing estimation is carried out in three steps: (Figure 4.2):

1. The antenna pattern is measured in far-field with all sensors of the sensor array mounted on the antenna tower, simultaneously. This pattern manifold acts as *Reference Data*. The Reference Data holds the pattern at the center sensor and shifted versions, measured at each of the outer sensors.
2. Apply a realistic motion profile to the antenna using the motion emulator and measure the received signal at all five sensors of the sensor array on the tower.

3. Calculate the correlation between the measured signals and the Reference Data. The antenna de-pointing is indicated by the position of the peak correlation.

The azimuth sensors can be adjusted in an angular range of $\pm 0 - 3^\circ$. This enables an adaptation according to the shape of the antenna pattern, which is important to achieve the highest possible antenna de-pointing estimation accuracy that is possible for a given 3 dB beam width of the antenna [3]. The relationship between the antenna 3 dB beam width, the available Signal-to-Noise-Ratio (SNR), and the optimum sensor positions is investigated in Section 4.2.1.1.

In contrast to tests in a free field range, this framework allows to measure the antenna de-pointing both in azimuth and elevation. Furthermore, it enables a more accurate de-pointing estimation due to the relatively large number of sensors. As a part of an example type approval, the de-pointing estimation results of a SOTM dish antenna are presented in Chapter 7.

4.2.1.1 Optimum Sensor Positions

The positions of the sensors on the antenna tower at FORTE have an essential influence on the accuracy of the antenna de-pointing estimation. The optimum sensor positions that yield the best estimation accuracy are investigated in this section. The de-pointing estimation accuracy is expressed as the standard deviation calculated for a large number of estimation realizations based on simulations. The estimation accuracy depends on three parameters:

- The position of the 4 outer sensors.
- The available Signal-to-Noise-Ratio (SNR) at the sensors.
- The 3 dB beam width of the antenna under test.

The SNR and the 3 dB beam width of the antenna are fixed parameters since they result from the transmit Effective Isotropic Radiated Power (EIRP) of the antenna and the fixed beam of the antenna. Therefore, the positions of the sensors are the only variable parameters that can be adjusted to improve the de-pointing estimation accuracy. In the following, the optimum positions of the sensors are derived for the highest possible de-pointing estimation accuracy with respect to the SNR and the 3 dB beam width of the antenna. Antenna patterns with different 3 dB beam widths are simulated and the de-pointing estimation accuracy is calculated with respect to the positions of the sensors and the SNR. The simulation results lead to an empirical equation for the optimum positions of the sensors with:

$$\Delta \approx (a \cdot \rho^3 + b \cdot \rho^2 + c \cdot \rho + d) \cdot w \quad (4.1)$$

where

- Δ is the distance of the outer sensor to the centered sensor along horizontal as well as vertical axes (see Figure 4.2)
- ρ is the SNR in dB
- w is the 3 dB beam width of the antenna in degrees
- with the polynomial coefficients $a = -1.3 \cdot 10^{-06}$, $b = 1.8 \cdot 10^{-04}$, $c = -7.2 \cdot 10^{-03}$, and $d = 0.709$.

Based on Equation (4.1), the optimum sensor positions with respect to the beam widths and SNR are depicted in Figure 4.3. The different lines correspond to the optimum

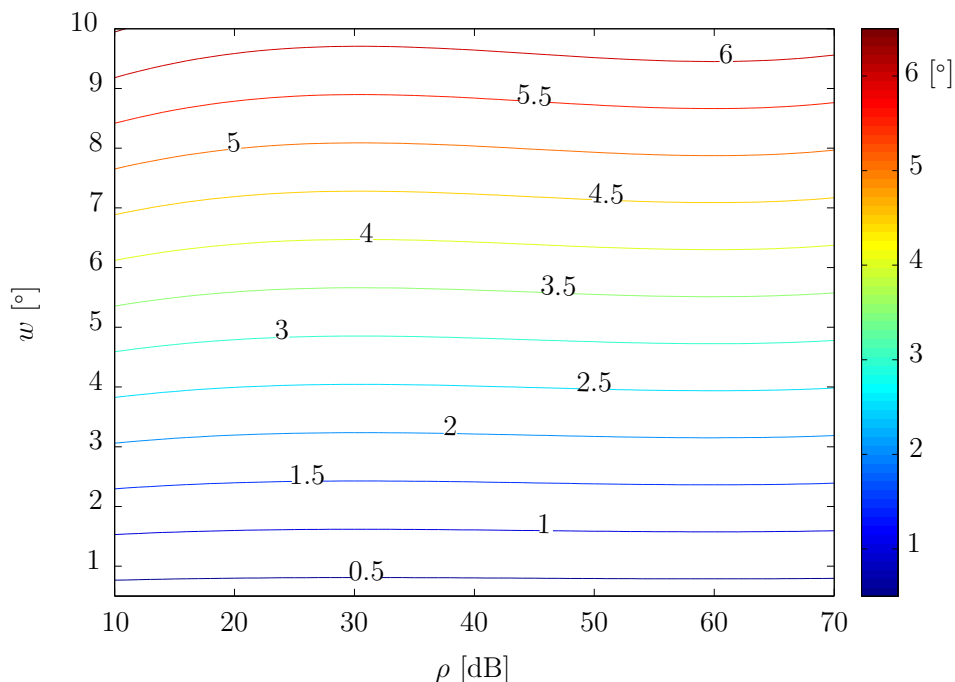


Figure 4.3: Optimum sensor positions Δ [°] with respect to antenna beam width w and SNR ρ .

sensor positions for different beam widths and SNR values. The maximum achievable estimation accuracy assuming the optimum sensor positions (c.f. Figure 4.3) are plotted in Figure 4.4. It can be seen that at a fixed antenna beam width, better estimation accuracy can be achieved by increasing the SNR. Assuming that the sensor positions can be adjusted freely, the maximum accuracy as shown in Figure 4.4 can be achieved. However, the adjustment of the sensors can be very time consuming in practice. If one wanted to test subsequently various terminals with different antenna beam widths, it would be preferable to keep the sensors at fixed positions for all tests. By defining a minimum de-pointing estimation accuracy (e.g. 0.05°) that has to be achieved in any case, a region with respect to the sensor positions and the antenna beam widths can be defined to achieve at least this accuracy at a certain SNR. As an example of

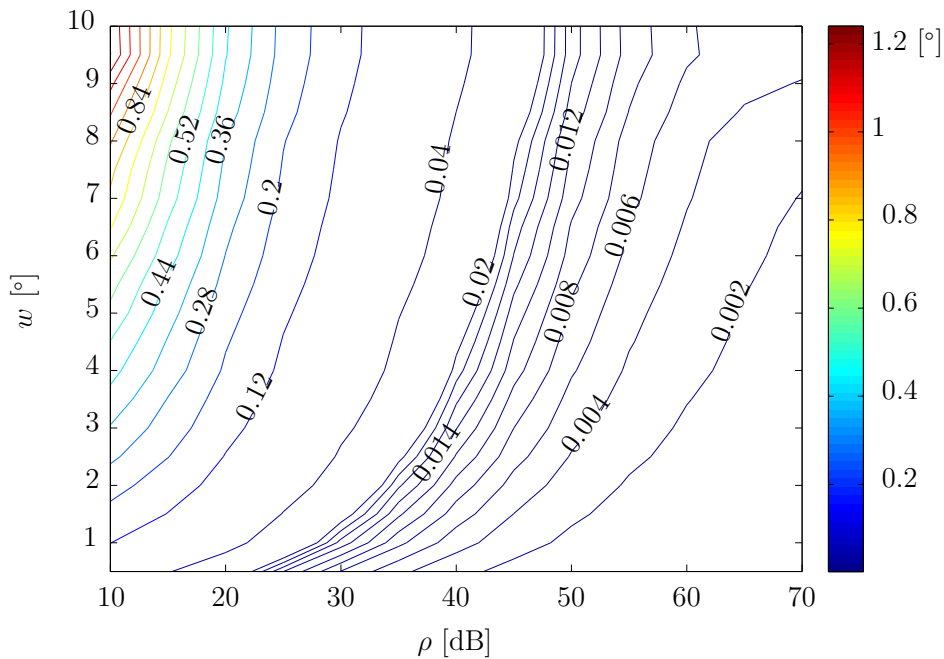


Figure 4.4: De-pointing estimation accuracy with respect to antenna beam width w and SNR ρ , assuming the sensors at the optimum positions Δ [°] calculated in Equation 4.1.

an estimation accuracy better than 0.05° , these regions are shown in Figure 4.5 for different SNR values. According to Figure 4.5, the sensor positions can be chosen in a wider range. For example, having an antenna with $w = 5^\circ$ and the sensors fixed at

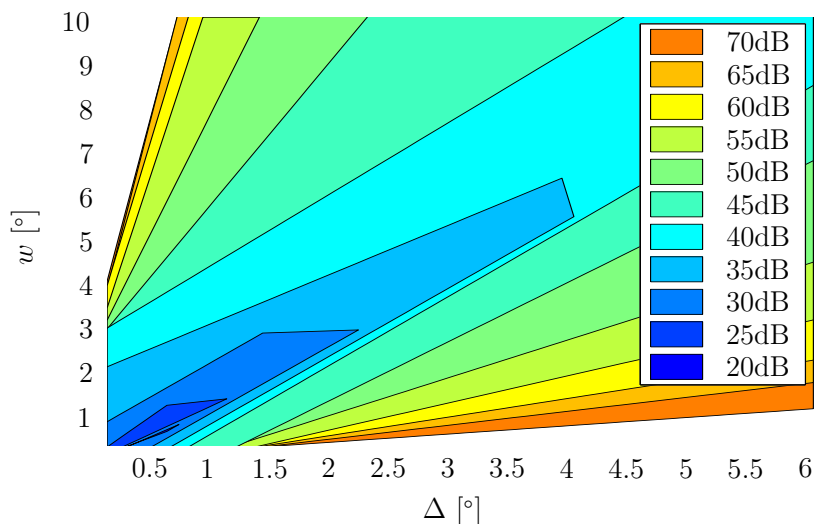


Figure 4.5: Assuming a more flexible estimation accuracy, e.g., 0.05° , wider regions of sensor positions can be considered. This facilitates mounting and de-mounting the sensors from their positions to perform several consecutive tests.

$\Delta = 3^\circ$, the following holds:

- With these sensor positions, the de-pointing estimation accuracy larger than 0.05° can be achieved if the available SNR is not below 35 dB.

- When exchanging the antenna with another antenna having 3 dB beam width of 4° , we do not need to change the position of the sensors as we can still ensure a minimum accuracy of 0.05° assuming that the SNR is not below 35 dB.
- Ensuring the same accuracy threshold of 0.05° with another antenna having a 3 dB beam width of 3° requires either:
 - Increasing the SNR to be around 10 dB larger (45 dB) while keeping the same sensor positions or,
 - Changing the sensor positions to be in the range $\in [1^\circ - 2.3^\circ]$ while keeping the SNR at 35 dB.

Similarly, in a free field test with operational satellites, the accuracy of estimating the antenna de-pointing depends on the beam width of the antenna. The satellite positions are fixed and if the antenna pattern is flat at the positions of the satellites, the accuracy of de-pointing estimation will be relatively low. In [9, 10], a comparison between the accuracy of estimation using two satellites with fixed positions and using five sensors (cf. Figure 4.2), mounted at the optimum positions with respect to the antenna under test. A Ka-band antenna with 3 dB beam width = 1° was considered. The two satellites were assumed to be fixed at $\pm 2^\circ$. The optimum sensor positions were calculated to be $\pm 0.62^\circ$. A two dimensional (2D) circular motion with radius 0.2° was assumed for the de-pointing estimation. For the *Two Satellites* method and the *Sensor Array* method, the Root Mean Squared Error (RMSE) and the confidence interval of the azimuth de-pointing estimation are depicted in Figure 4.6.

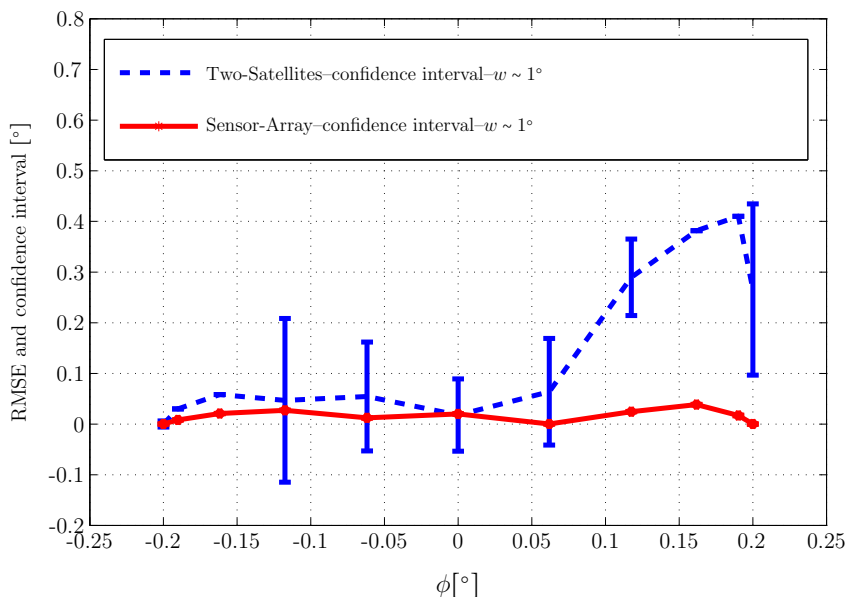


Figure 4.6: RMSE and confidence interval for the de-pointing estimation using the *Two Satellites* method and the *Sensor Array* method based on simulations using a realistic SOTM Ka-band antenna.

From the estimation results, it is evident that the *Sensor Array* method outperforms the *Two Satellites* method.

4.2.2 Phased Arrays

For phased arrays and electrically steerable antennas with beam patterns that change depending on the steering direction, it becomes practically infeasible to measure all the possible radiation patterns. Therefore, evaluating the antenna de-pointing using the methodology developed in Section 4.2.1 is difficult to be applied.

In [2], the performance of a flat panel antenna with a radiation pattern that changes with respect to the steering angle was evaluated. The effect of pattern change on the accuracy of the antenna de-pointing estimation has been investigated. The antenna was moved in a 2D diagonal track around antenna elevation steering $=37^\circ$.

To show the effect of pattern change on the de-pointing estimation performance, the following was considered:

1. The Reference Data measured for antenna elevation steering angle $= 37^\circ$ is applied for estimation to the measurement with an antenna elevation steering angle of 37°
2. The Reference Data measured for antenna elevation steering angle $= 32^\circ$ is applied for estimation to the measurement with an antenna elevation steering angle of 37°

Figure 4.7, depicts the motion excitation as well as the estimation results for the two cases.

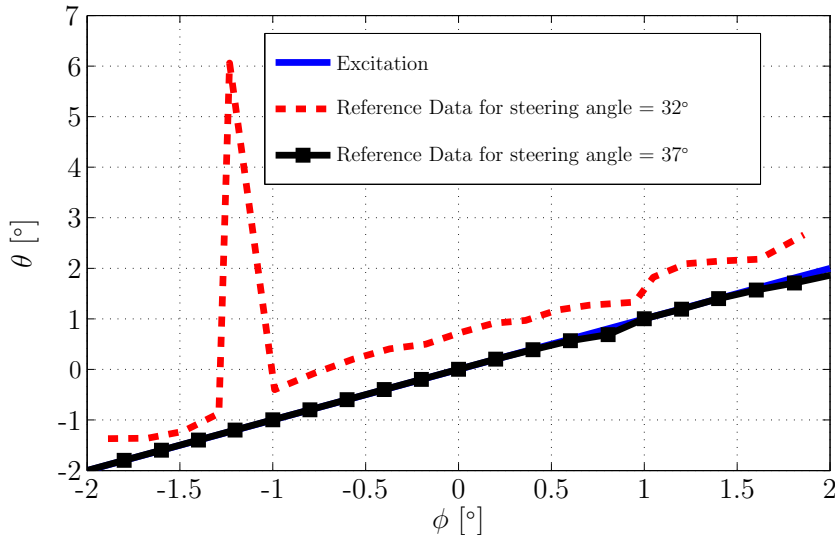
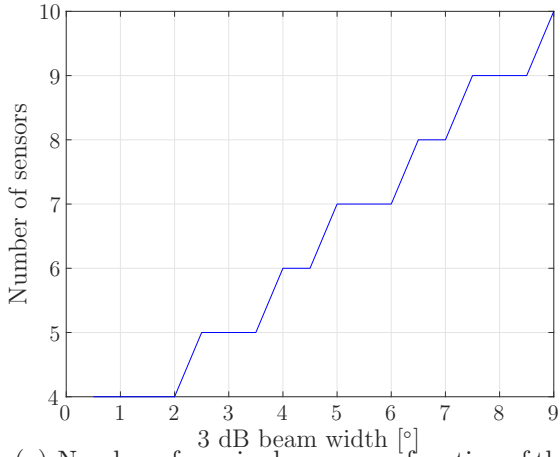


Figure 4.7: De-pointing estimation results using the Reference Data for antenna elevation steering angle $= 37^\circ$ to estimate a 2D diagonal motion centered around antenna elevation steering angle $=37^\circ$ (black line with square markers) and De-pointing estimation results using the Reference Data for antenna elevation steering angle $= 32^\circ$ to estimate the same motion excitation (red dashed line).

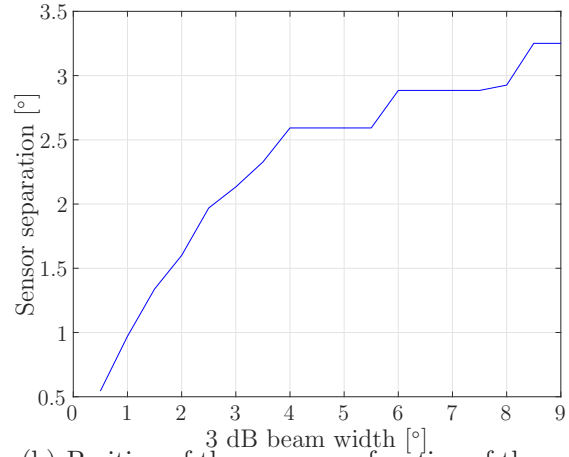
The results in Figure 4.7 show that when using the Reference Data for antenna elevation steering angle $= 37^\circ$ to estimate the motion centered around an antenna elevation

steering angle $=37^\circ$ (the black line with square markers), the proposed de-pointing estimation algorithm yields accurate results. The RMSE in azimuth is in the order of 0.002° with an accuracy of 0.001° . For elevation, the RMSE is in the order of 0.03° with an accuracy of 0.02° . When the Reference Data for a different elevation steering angle, e.g., 32° , is used to estimate the motion around antenna elevation steering angle $=37^\circ$, a biased estimation of the de-pointing (the red dashed line) is obtained. The RMSE is in the range of 0.1° with an accuracy of 0.008° for azimuth and 0.9° with an accuracy of 0.05° for elevation. The bias in the estimation violates the estimation performance requirements. Furthermore, some outliers with wrong estimation results can be observed. If a more complex motion profile is used to test the antenna, even worse results will be obtained.

For such antennas with changing patterns, Adjacent Satellite Interference (ASI) can be used instead to judge the pointing performance. ASI can be evaluated while the terminal is On-The-Move by measuring the power levels at the adjacent satellites and comparing these levels to standard regulations. At FORTE, ASI can be measured by adjusting the positions of the outer azimuth sensors on the antenna tower at the places where the adjacent satellites are located (typical values range between 2° and 3°). Another extension of the sensor array which is based on increasing the number of sensors will allow to estimate the main beam and the first side lobes of the phased array while the terminal is On-The-Move. The number of sensors and their positions, i.e. the resolution of the sensor grid, depends on the 3 dB beam width of the antenna pattern. Based on the results of a preliminary simulation, Figure 4.8(a) depicts the relationship between the antenna 3 dB beam width and the number of sensors required for perfect recovery of the pattern main beam and first side lobes. Figure 4.8(b) shows the relationship between the 3 dB beam width and the separation between the sensors. This extension is planned in the future and is not yet implemented at FORTE and, therefore, its evaluation is not considered in this thesis.



(a) Number of required sensors as function of the antenna 3 dB beam width.



(b) Position of the sensors as function of the antenna 3 dB beam width.

Figure 4.8: Number of required sensors and their positions as function of the antenna 3 dB beam width. Mounting the sensors using these parameters will enable the reconstruction of the main beam and the first side lobes of a phased array antenna while being On-The-Move. However, this extension is not yet implemented at FORTE.

4.3 Transmit Mute Measurements

In order to be compliant with the regulations, it is compulsory that any SOTM terminal is armed with the mute functionality. This functionality inhibits transmissions when either of the two following conditions is met:

- The antenna de-pointing exceeds the regulatory threshold, e.g., 0.4° for EUTEL-SAT. This information must be delivered by the Antenna Control Unit (ACU).
- The modem loses synchronization of the out-route¹.

The SOTM terminal switches off the transmit signal either using the ACU or using the modem. The delay time before the signal is switched off or attenuated when the antenna de-pointing exceeds the regulatory threshold is measured. For example, the regulations of the Federal Communications Commission (FCC) and of the Global VSAT Forum (GVF) specifies that the transmit mute delay should not exceed 100 milliseconds if the de-pointing exceeds 0.5° . The ACU must not switch on the transmit signal again unless the de-pointing is reduced to 0.2° or less. The accurate measurement of the antenna de-pointing, as illustrated in Section 4.2, ensures the accurate evaluation of the transmit mute functionality of SOTM terminals.

4.4 Data Traffic Measurements

Monitoring the data traffic flow is important to evaluate the overall performance of the SOTM terminal also including the modem. The SOTM modem should be able to adapt

¹An example out-route is the signal propagation path from the hub station through the space segment (the satellite) until the SOTM terminal.

the modulation and coding schemes depending on the channel status and on the network topology. Different network topologies, e.g., star and mesh topologies can be applied in the test. The data traffic flow is evaluated at the different nodes in the network. At FORTE, the data traffic can be evaluated with respect to all relevant parameters (Doppler, shadowing, motion, etc.) at once or separately for a selected parameter.

Chapter 5

Proposed Motion Profiles

This chapter presents one of the main achievements of this work: motion profiles proposed for standard testing of Satellite Communications On-The-Move (SOTM) terminals. An essential part of the performance tests, described in Chapter 4, depends on the proper choice of the motion profile. In [1], the data sheets of 100 SOTM terminals were investigated including the most popular and widely deployed ones nowadays. Out of this representative sample group, only 8% mentioned the motion profile used to test the terminal. For the remaining 92%, either no motion track is specified or no information about testing is mentioned at all. This complicates the comparison of SOTM terminals from the different vendors. An objectively compared poor performing SOTM terminal may outperform a good one simply because of the choice of a motion profile that leads to an unfair comparison. Therefore, to standardize motion profiles is important to provide a fair judgment and comparison of SOTM terminals. A framework to select representative motion profiles and propose them as a standard is one of the major contributions of this thesis.

Motion profiles are defined, in this thesis, for the land mobile and the maritime environments. An extension including the aeronautical and the train environments is planned for the future. In Section 5.1, the campaigns carried out to measure the motion dynamics are presented. Sections 5.2 and 5.3 discuss the analysis and classification of the measurement data. In Section 5.4, the process of profile selection is introduced. The complete profile definition process is applied to the measurements in the land mobile and the maritime environment and the proposed profiles are presented in Section 5.5. The profiles were published in [4]. Section 5.7 presents the inclusion of the proposed motion profiles in the GVF-105 standard recommendations.

Four steps have been considered in order to develop the motion profiles:

1. **Measurement of the motion dynamics.**
2. **Statistical analysis:** The complete manifold of measurements has been segmented. A measurement segment is defined as the motion dynamics, e.g., angular positions or rates, over a certain period of time. Statistical measures like the

mean and the variance have been then extracted from each measurement segment.

3. **Measurement classification:** The measurements were classified in two classes based on the extracted statistics. The classes have been labeled, namely, Class A and Class B.
4. **Profile selection:** A representative motion profile for each class has been selected and proposed as a standard motion profile for the corresponding class.

In the following, each of the four steps is described in more detail.

5.1 Measurement of the Motion Dynamics

In the context of an ESA project [11], multiple measurement campaigns were performed in the land mobile and maritime environments. The measurement campaigns were carefully planned in order to:

- Cover the largest possible variety of measurement scenarios in each environment. A measurement scenario is specified by its environment type, its terrain type, and its platform type.
 - Environment type: land mobile or maritime.
 - Terrain type: for each environment, different terrain types were considered. For example, off-road or highway in the land mobile environment, and storm or rough sea in the maritime environment.
 - Platform type: the platform is the vehicle which is used to measure the motion dynamics, e.g., pickup or bus in the land mobile environment, and large vessel or small rescue boat in the maritime environment.
- Include well known or reference test tracks if possible. For example, measurements were carried out at the Millbrook Proving Ground (MPG) in the UK. The tracks at the MPG include a variety of terrain types such as off-roads with deep ditches, federal ways with ramps, and special tracks with sinusoidal surfaces. An exemplary picture of an off-road vehicle in a deep ditch on a track at Millbrook is shown in Figure 5.1.

A high precision in measuring the motion dynamics was guaranteed by using an Inertial Measurement Unit (IMU) which employs fiber optic gyroscopes. The measured dynamics include angular positions, rates, and accelerations as well as translational velocities and accelerations. These parameters were measured for each of the three body axes: yaw, pitch, and roll. A measurement database was created including a total of 33 hours-long maritime and 30 hours-long land mobile measurements [51].



Figure 5.1: A measurement with an off-road vehicle in the Millbrook Proving Ground (MPG). The vehicle is in a deep ditch designed to test the dynamics in such an off-road scenario.

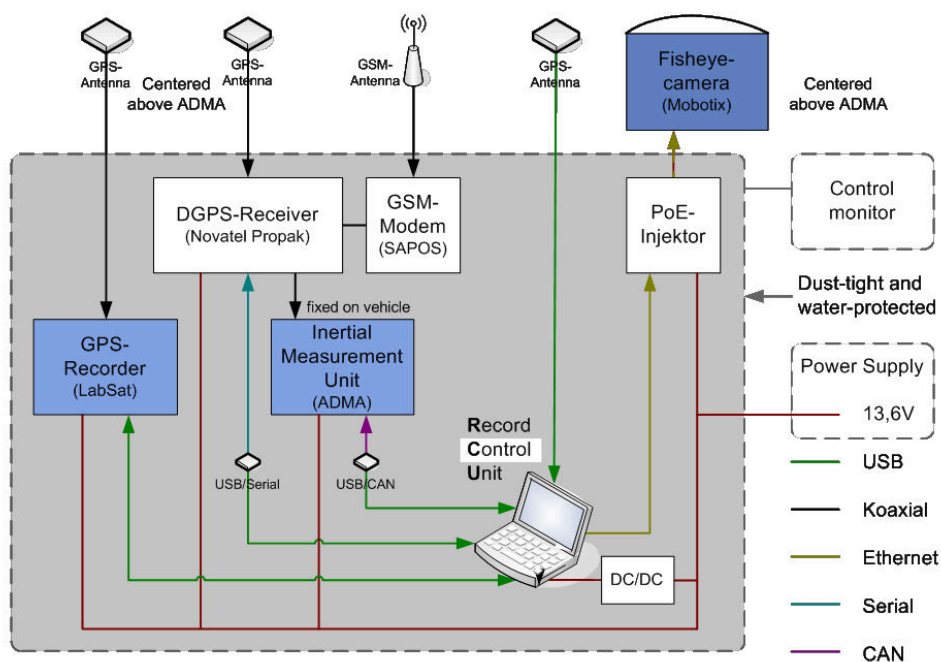


Figure 5.2: Motion dynamics measurement system.

The structure of the measurement equipment (ME) which was used to measure the motion dynamics is depicted in Figure 5.2. The components include: An Inertial Measurement Unit (IMU) based on fiber optic gyroscopes and servo-accelerometers, a (D)GPS-Receiver connected to GSM modem to obtain RTCM-correction data, a GPS antennas and a GSM antenna, A fisheye camera, a GPS-Recorder, and a Record and control unit (RCU).

5.2 Statistical Analysis

The analysis of the motion dynamics is based on statistical parameters. For each measurement segment, the minimum, maximum, mean, and standard deviation of the

measured dynamics were extracted. The Probability Density Function (PDF) and the Cumulative Distribution Function (CDF) were also calculated.

The parameter space is multidimensional. In order to facilitate the definition of the motion profiles, a single parameter should be selected. The **95% quantile of the measured angular rate vector norm** is selected. The vector norm of the angular rate of the yaw, pitch, and roll axes is calculated as in Equation 5.1.

$$Rate_{\text{norm}} = \sqrt{Rate_{\text{yaw}}^2 + Rate_{\text{pitch}}^2 + Rate_{\text{roll}}^2} \quad (5.1)$$

The 95% quantile, referred to as (Q95), is extracted from the CDF of the angular rate vector norm. This parameter was selected for the following reasons:

1. Rotational dynamics: The SOTM antenna must compensate for the vehicle rotation in yaw, pitch, and roll in order to point towards the target satellite. Therefore the rotational dynamics are more relevant when testing the performance of antenna tracking.
2. Rates: The angular rates are directly measured using gyroscopes and are good indicators for the demands of the actuation system in terms of power and speed. Moreover, the rates and the accelerations were found to be strongly correlated according to the investigations explained in Appendix B.
3. Vector norms: The norm of all axes, yaw, pitch, and roll ensures the contribution of the dynamics from all dimensions.
4. Q95 was chosen as a trade-off between Q68 or Q99: It is considered fair for terminal tests, not as loose as Q68 where important dynamics are bypassed and not too stringent as Q99 where very rare and not representative dynamics, e.g., a deep notch are included.

5.3 Measurement Classification

SOTM applications can be seen as divided in two main classes: applications in harsh conditions such as in military or in disaster scenarios, and applications in smoother motion conditions such as mobile internet backhauling. A threshold to classify the measurements according to these two classes is defined based on the distribution of the Q95 values of the angular rate vector norm as will be explained in Section 5.5 in detail.

5.4 Profile Selection

A representative motion profile is selected for each class. The mean and the confidence interval (standard deviation) of the Q95 angular rate vector norm values of each class

were calculated and the measurement segment with the closest value to the mean is chosen as the representative motion profile of the corresponding class. The profiles are proposed as a standard to be used for testing the different types of SOTM terminals.

5.5 Applying the Procedure for Land mobile and Maritime

The four steps of the standard motion profile definition process were applied for the land mobile and the maritime environments as follows:

5.5.1 Land Mobile

Five platforms and seven terrain types were included in the land mobile measurement campaign. Table 5.1 shows how the terrain types were covered by the different platforms. For example, the bus was used only on rural, urban, and highway terrains.

Table 5.1: Platforms and terrain types used in the land mobile measurement campaign.

	Off-road	Gravel	Mixture	Rural	Urban	Federal	Highway
Pickup	x	x	x	x	x	x	x
Truck	x	x		x	x	x	x
Small van	x	x	x	x	x	x	x
Bus				x	x		x
Passenger car			x				

In Figure 5.3, the Q95 angular rate vector norm values are plotted in a scatter plot versus terrain type. Each point represents the Q95 angular rate vector norm of one measurement segment of one terrain measured with each of the given platforms represented by the different markers. The measurements collected at Millbrook are plotted using a different marker, the black diamonds.

The PDF of the Q95 angular rate vector norm values is depicted in Figure 5.4. From Figure 5.4, it can be seen that the distribution has three modes and a tail. The two measurement classes were defined based on this shape. Class A that represents harsh terrains and off-roads will include all measurements in the tail of the PDF. Class B that represents paved terrains and relaxed off-roads will include all measurements in the three modes. The separation threshold is defined at the falling edge of the third mode at $22.24^\circ/\text{s}$. This value divides 10% of the measurements to be belonging to Class A and 90% to be belonging to Class B.

The threshold level is also shown in the left sub-figure of Figure 5.3 and the two classes are also labeled.

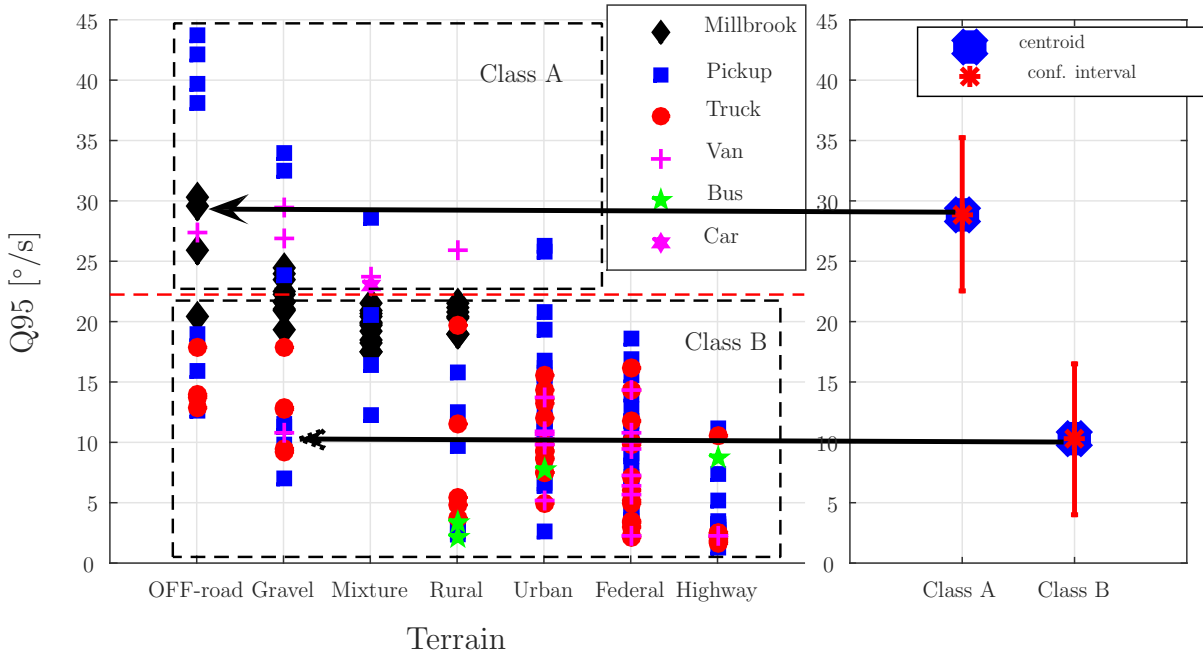


Figure 5.3: Motion profile selection process for the land mobile environment. In the left sub-figure, the Q95 values of the angular rate vector norm are shown. In the right sub-figure, the mean and confidence interval of the Q95 angular rate vector norms are depicted. The measurement closest to the mean value is selected and proposed as a standard motion profile. The Class A profile is an off-road Millbrook measurement with a pickup, while the Class B profile is a gravel dirt road measurement with a Van.

The right sub-figure of Figure 5.3, depicts the mean and the standard deviation values of all measurements in each class. The mean and the confidence interval for each class are summarized in Table 5.2.

Table 5.2: Mean and confidence interval of the Q95 angular rate vector norms for the land mobile Class A and Class B.

Parameter	Class A	Class B
Angular Rate [$^{\circ}/s$]	29 ± 6	10 ± 6

The proposed standard motion profiles selection is depicted in Figure 5.3. The black arrows point at the measurement segments which are selected for Class A and Class B. The representative profiles have a Q95 of the angular rate vector norm that is closest to the mean for each class.

5.5.1.1 Class A Motion Profile

For the land mobile Class A, the representative motion profile is an eight minutes measurement segment on a off-road at Millbrook with the landrover as the platform. Figure 5.5 shows the satellite view and the geographical location of the land mobile Class A motion profile.

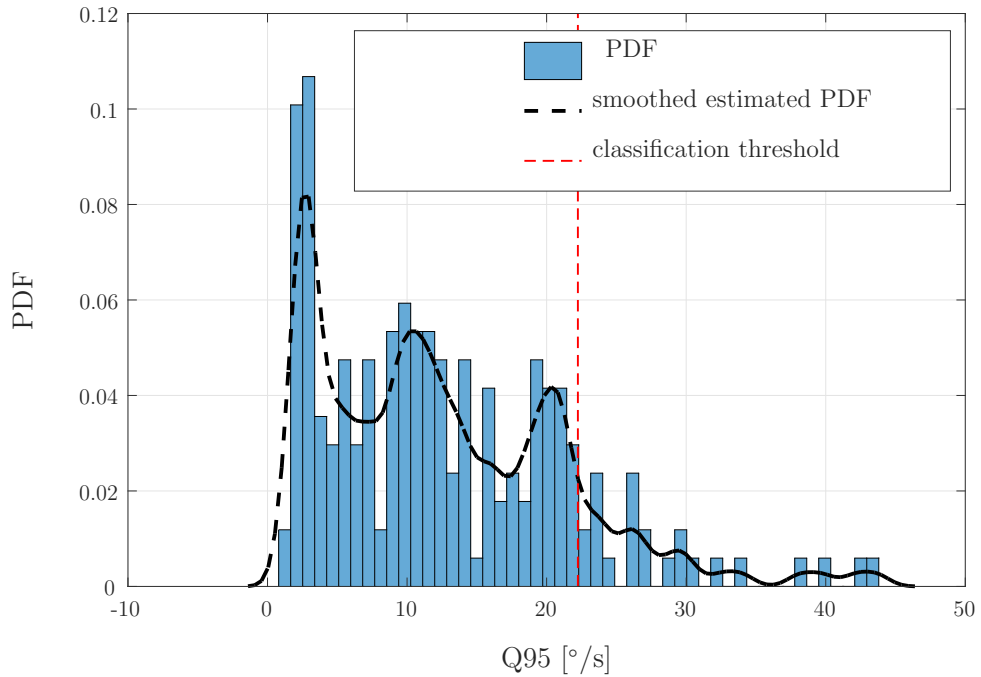


Figure 5.4: The PDF and its smoothed estimation of Q95 values of the angular rate vector norm for the land mobile environment. A threshold defined at 22.24 $^{\circ}/s$ (red dashed line) separates Class A which represents harsh terrains from Class B which represents paved terrains.

5.5.1.2 Class B Motion Profile

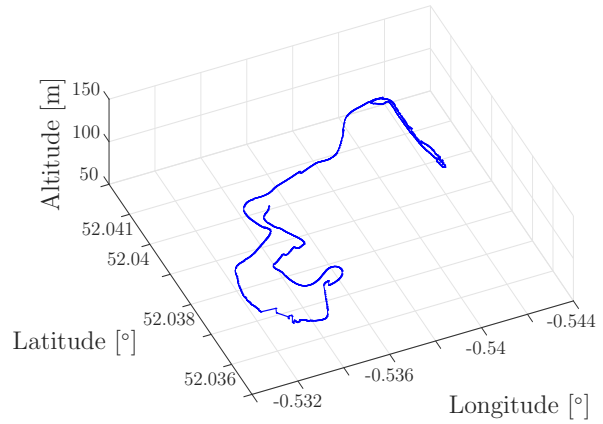
For Class B, the representative motion profile is another eight minutes segment on gravel dirt road driven with the van. Figure 5.6 shows the satellite view and the geographical location of the land mobile Class B profile.

5.5.1.3 Profile Time Series

The time series of the land mobile standard motion profiles are plotted in the following. Figure 5.7 plots the time series for the angles, Figure 5.8 for the angular rates, Figure 5.9 for the angular accelerations, and Figure 5.10 for the translational accelerations. Both profiles are having the same length (500 s).

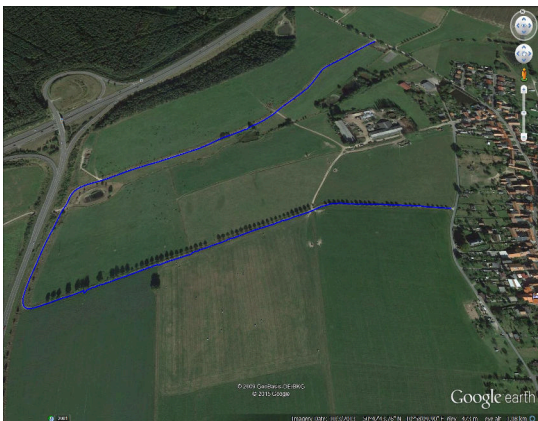


(a) The satellite view of the land mobile Class A motion profile.

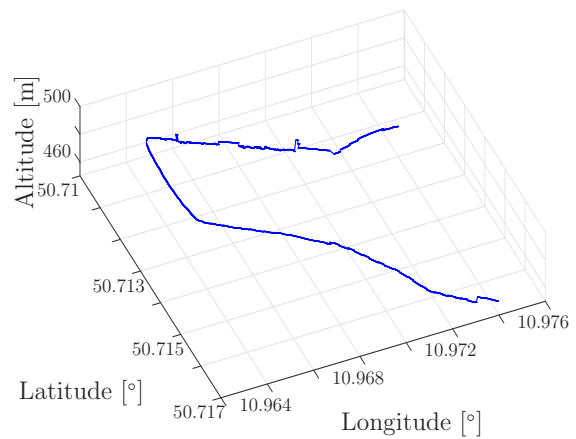


(b) The geographical location of the land mobile Class A motion profile.

Figure 5.5: The satellite view and the geographical location of the land mobile Class A motion profile.



(a) The satellite view of the land mobile Class B motion profile.



(b) The geographical location of the land mobile Class B motion profile.

Figure 5.6: The satellite view and the geographical location of the land mobile Class B motion profile.

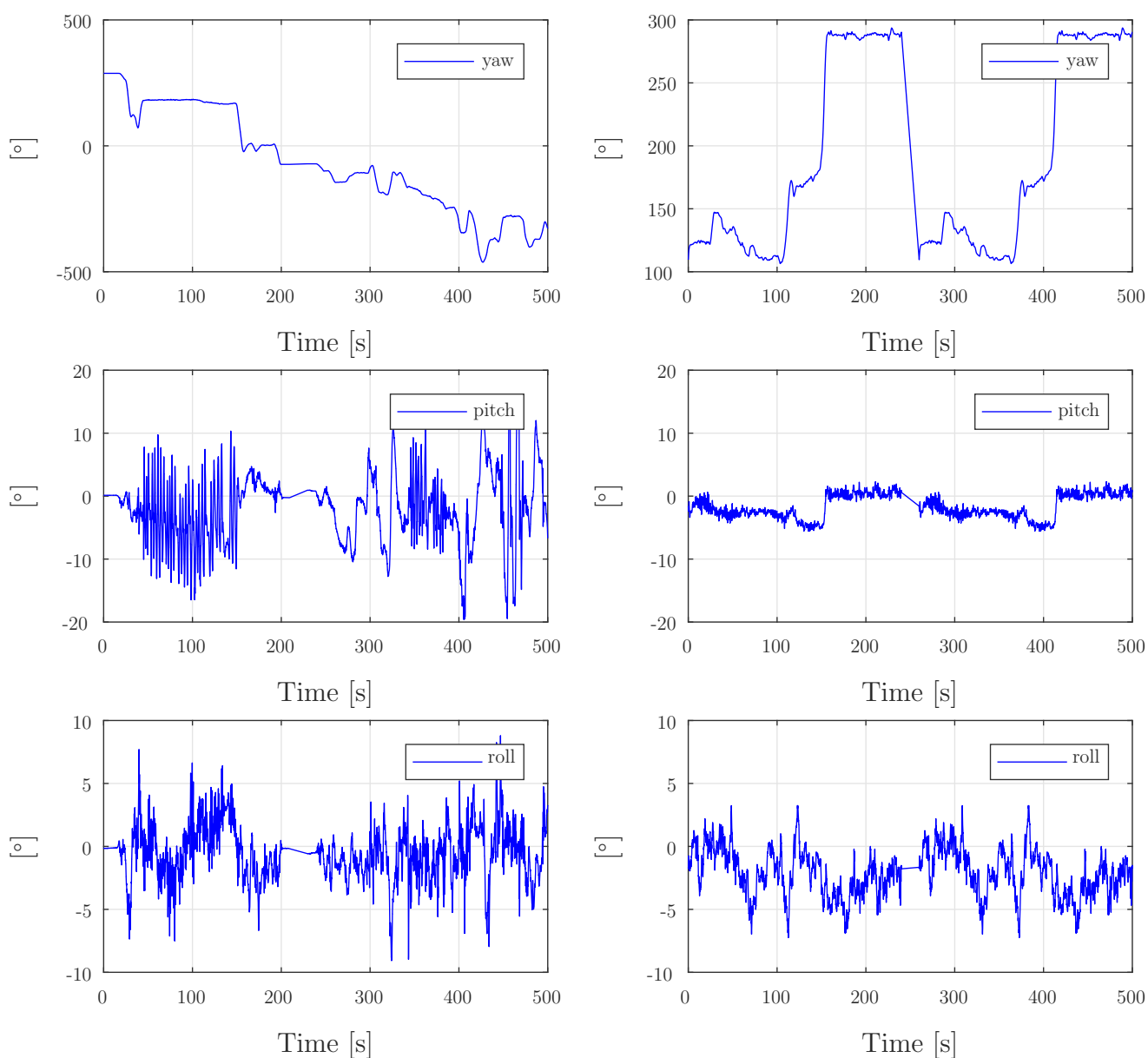


Figure 5.7: Time series of the angles of the land mobile standard motion profiles: Class A (left column) and Class B (right column).

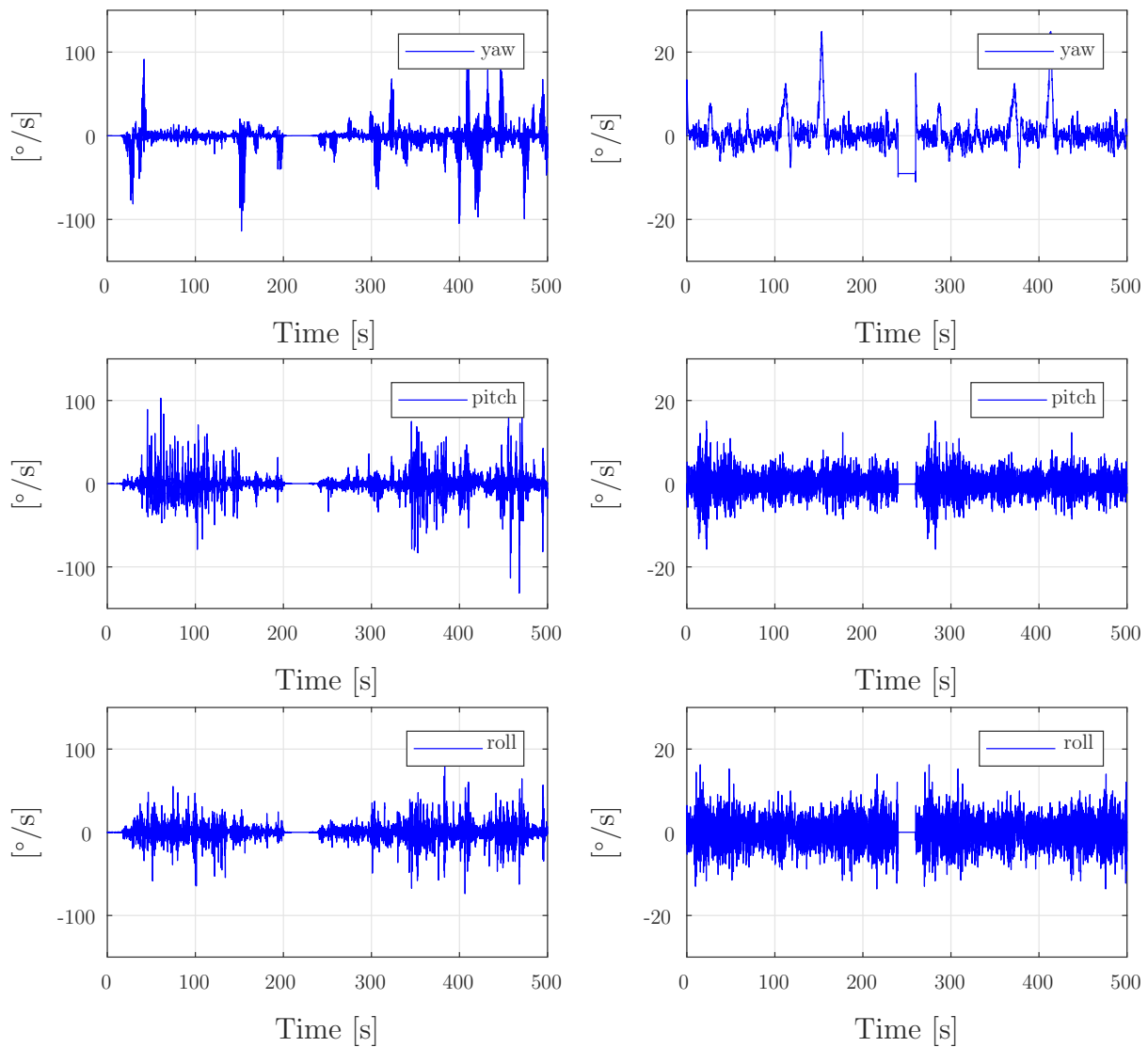


Figure 5.8: Time series of the angular rates of the land mobile standard motion profiles: Class A (left column) and Class B (right column).

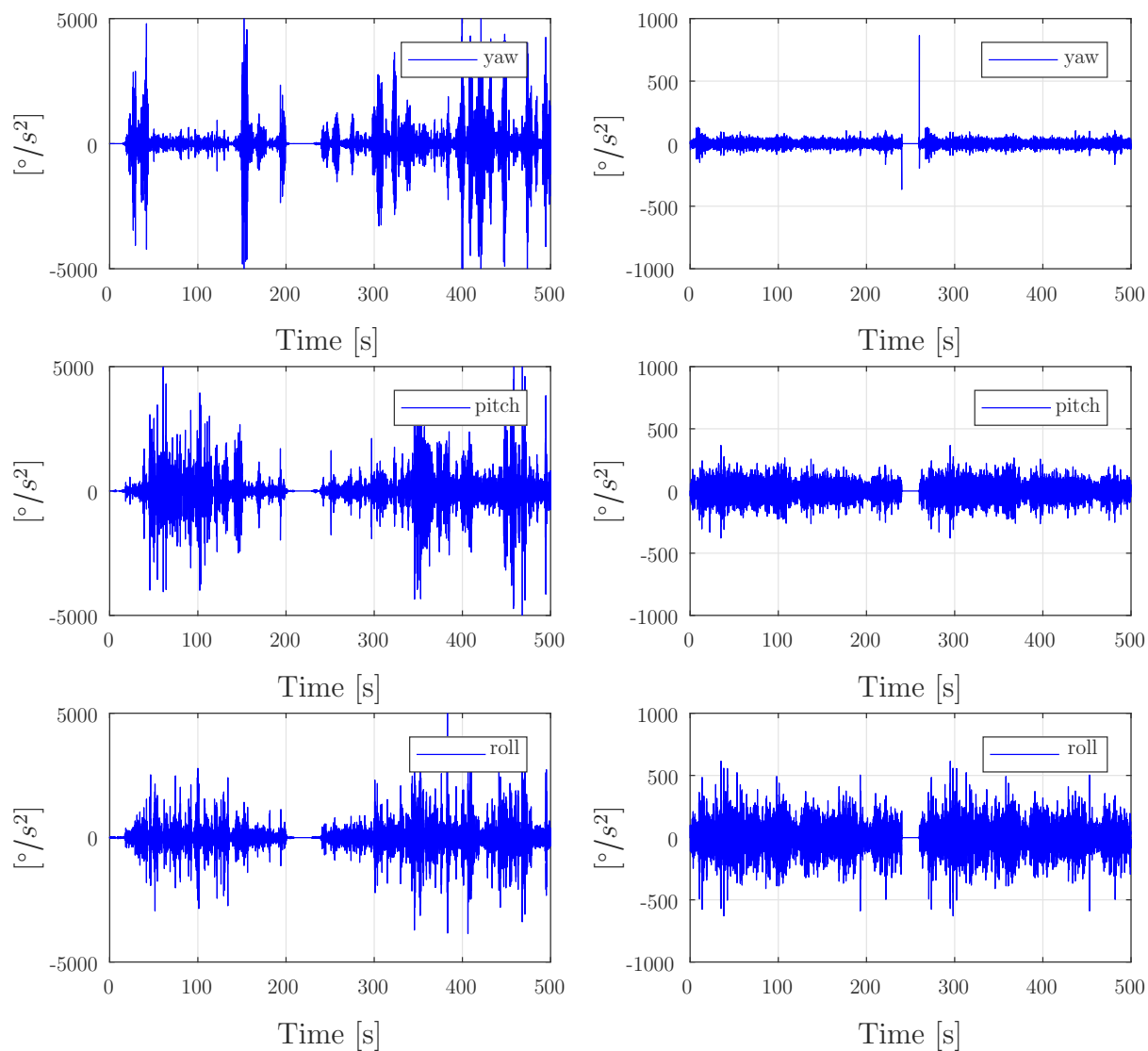


Figure 5.9: Time series of the angular accelerations of the land mobile standard motion profiles: Class A (left column) and Class B (right column).

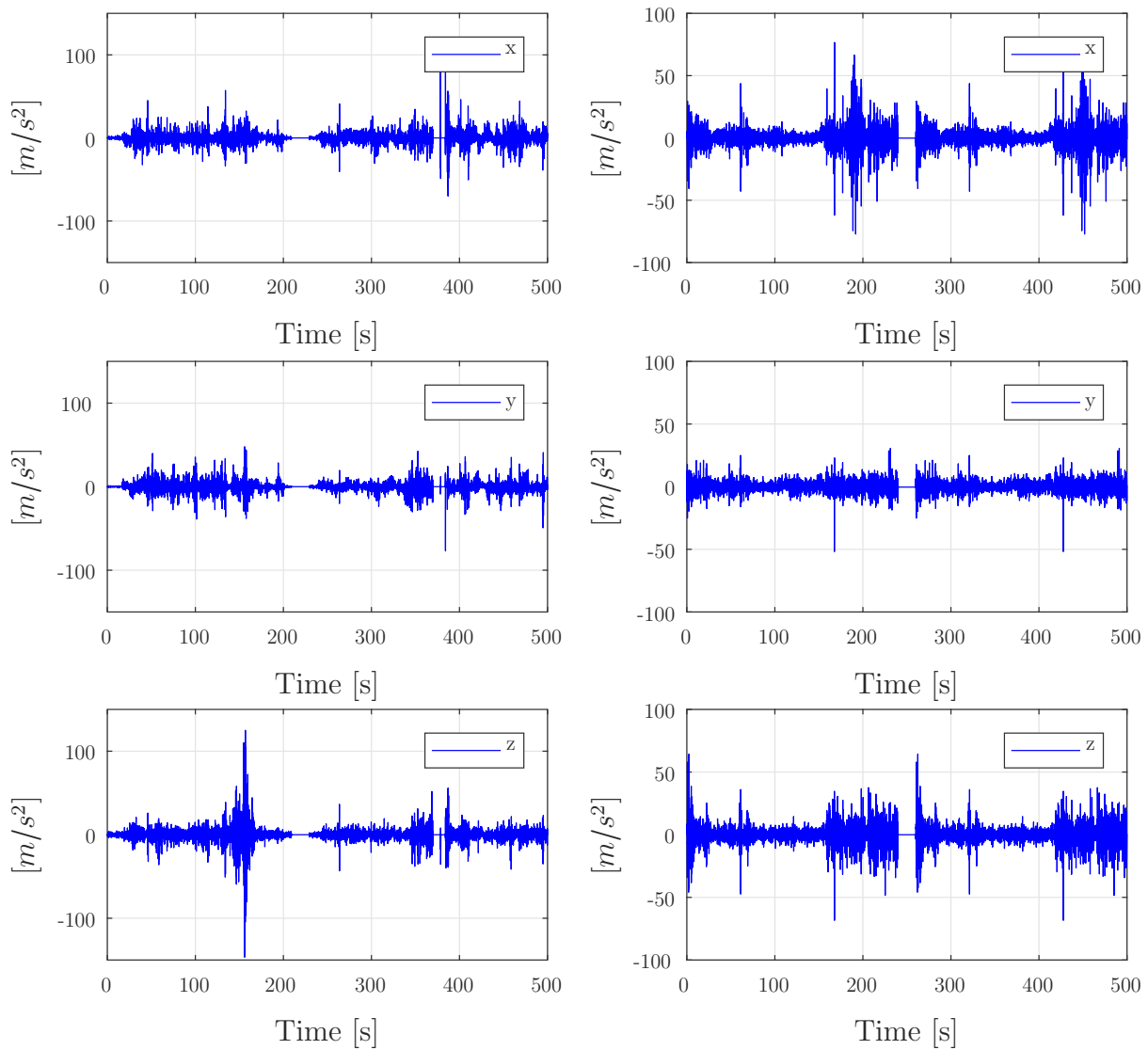


Figure 5.10: Time series of the translational accelerations of the land mobile standard motion profiles: Class A (left column) and Class B (right column).

5.5.2 Maritime

Three vessel types and five different sea conditions were included in the maritime measurement campaign. Table 5.3 shows how the sea conditions were covered by the different vessel types. For example, the small vessel was used only in light, moderate, and rough sea conditions.

Table 5.3: Vessel sizes and sea conditions used in the maritime measurement campaign.

	Light (0-2 Bft ¹)	Moderate (3-5 Bft)	Rough (6-9 Bft)	Storm (9-11 Bft)	Hurricane (≥ 12 Bft)
large-size (>100 m)	x	x	x	x	x
medium-size (20-100 m)		x	x		
small vessel (<20 m)	x	x	x		

The Q95 angular rate vector norm values for the maritime environment are plotted in the left sub-figure of Figure 5.11.

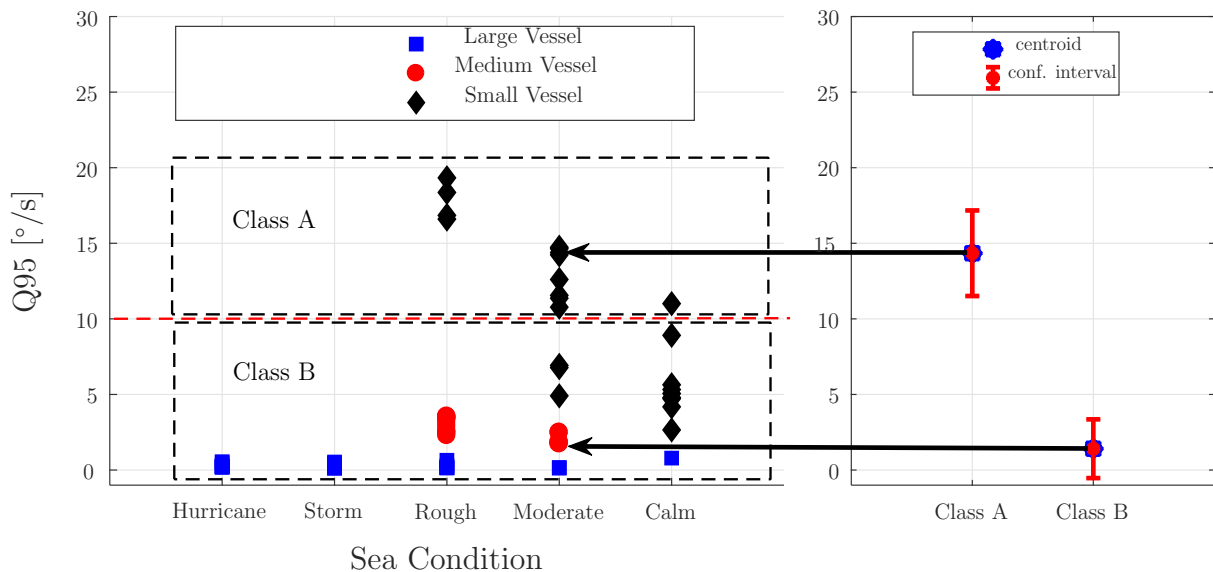


Figure 5.11: Motion profile selection process for the maritime environment. In the left sub-figure, the Q95 values of the angular rate vector norm are shown. In the right sub-figure, the mean and confidence interval of the Q95 angular rate vector norms are depicted. The measurement closest to the mean value is selected as the proposed standard motion profile. The Class A profile is a measurement with a small rescue boat in moderate sea conditions. The Class B best representative is found to be a segment with a medium size vessel in moderate sea condition, however it was not selected as the proposed standard profile. The proposed standard profile for Class B is selected as a measurement with the same rescue boat as in Class A but in calm sea conditions.

The PDF of the Q95 angular rate vector norm values is depicted in Figure 5.12. A

¹Bft: Beaufort

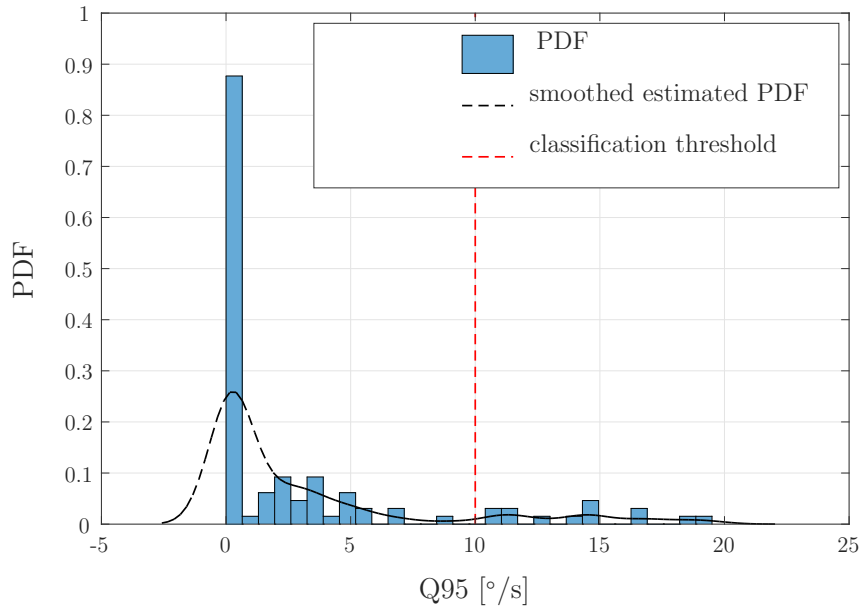


Figure 5.12: The PDF and its smoothed estimation of Q95 values of the angular rate vector norm for the maritime environment. A threshold defined at $10^\circ/\text{s}$ (red dashed line) separates Class A which represents rough sea conditions from Class B which represents calm seas.

classification threshold is defined to separate the first mode of the PDF and the tail. The threshold is set at $10^\circ/\text{s}$ to keep the same percentages, as in the land mobile environment, for Class A and Class B. Class A includes 10% of all maritime measurements and Class B includes 90%.

The right sub-figure of Figure 5.11, depicts the mean and the standard deviation values of all measurements in each class. The statistics of the two classes are summarized in Table 5.4.

Table 5.4: Mean and confidence interval of the Q95 angular rate vector norms for the maritime Class A and Class B.

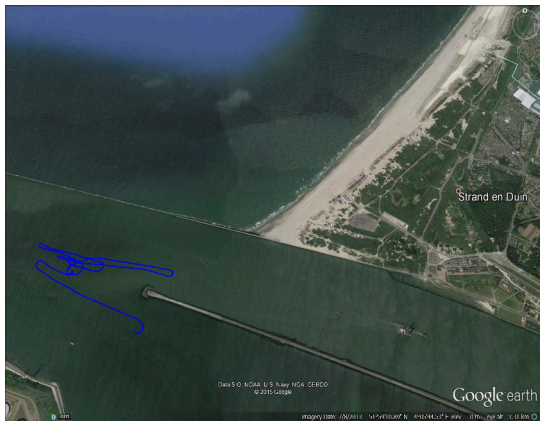
Parameter	Class A	Class B
Angular Rate [$^\circ/\text{s}$]	14 ± 3	1.5 ± 2

5.5.2.1 Class A Motion Profile

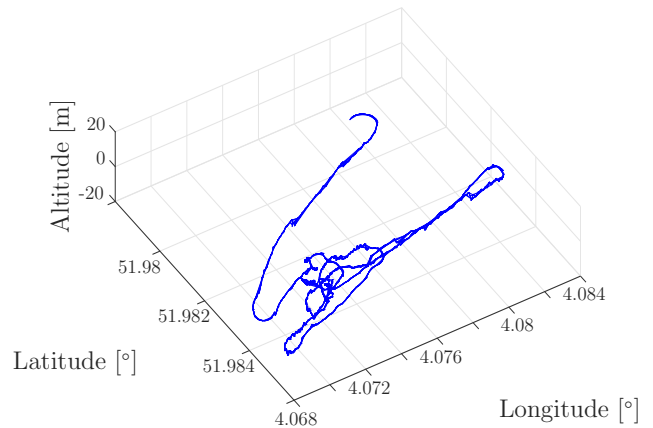
From Figure 5.11, the Class A proposed standard motion profile is selected as a 15 minutes measurement segment in moderate sea conditions with a rescue boat from the Royal Netherlands Sea Rescue Institution (KNRM). Figure 5.13 shows the satellite view and the geographical location of the maritime Class A motion profile.

5.5.2.2 Class B Motion Profile

For Class B, the black arrow in Figure 5.11 points to a measurement with a medium size vessel in moderate sea conditions. However, in the maritime environment the dynamics depend strongly on the vessel size. As seen in the left sub-figure of 5.11, a large vessel in



(a) The satellite view of the maritime Class A motion profile.

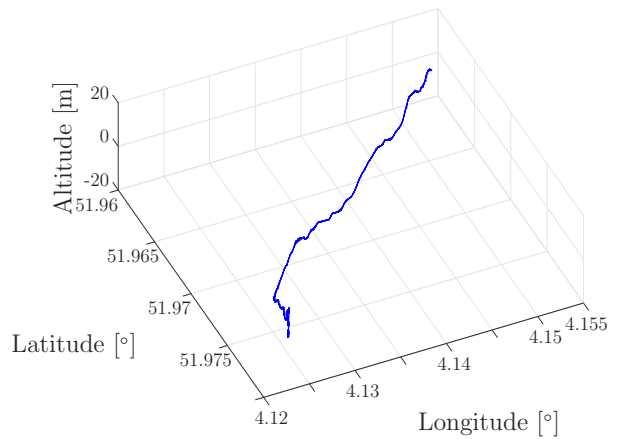


(b) The geographical location of the maritime Class A motion profile.

Figure 5.13: The satellite view and the geographical location of the maritime Class A motion profile.



(a) The satellite view of the maritime Class B motion profile.



(b) The geographical location of the maritime Class B motion profile.

Figure 5.14: The satellite view and the geographical location of the maritime Class B motion profile.

a hurricane shows lower dynamics than a small vessel in calm sea. Therefore, in order to neglect the effect of the vessel size when comparing the profiles of Class A and Class B, a measurement segment with the same rescue boat as in the Class A profile was selected for Class B. The Class B representative motion profile is selected as the measurement segment with the rescue boat which is the closest to the mean value of the class. A 15 minutes rescue boat measurement in calm sea conditions is the best fit. Figure 5.14 shows the satellite view and the geographical location of the land mobile Class B profile.

5.5.2.3 Profile Time Series

The time series of the maritime standard motion profiles are plotted in the following. Figure 5.15 plots the time series for the angles, Figure 5.16 for the angular rates, Fi-

Figure 5.17 for the angular accelerations, and Figure 5.18 for the translational accelerations. Both profiles are having the same length (900 s).

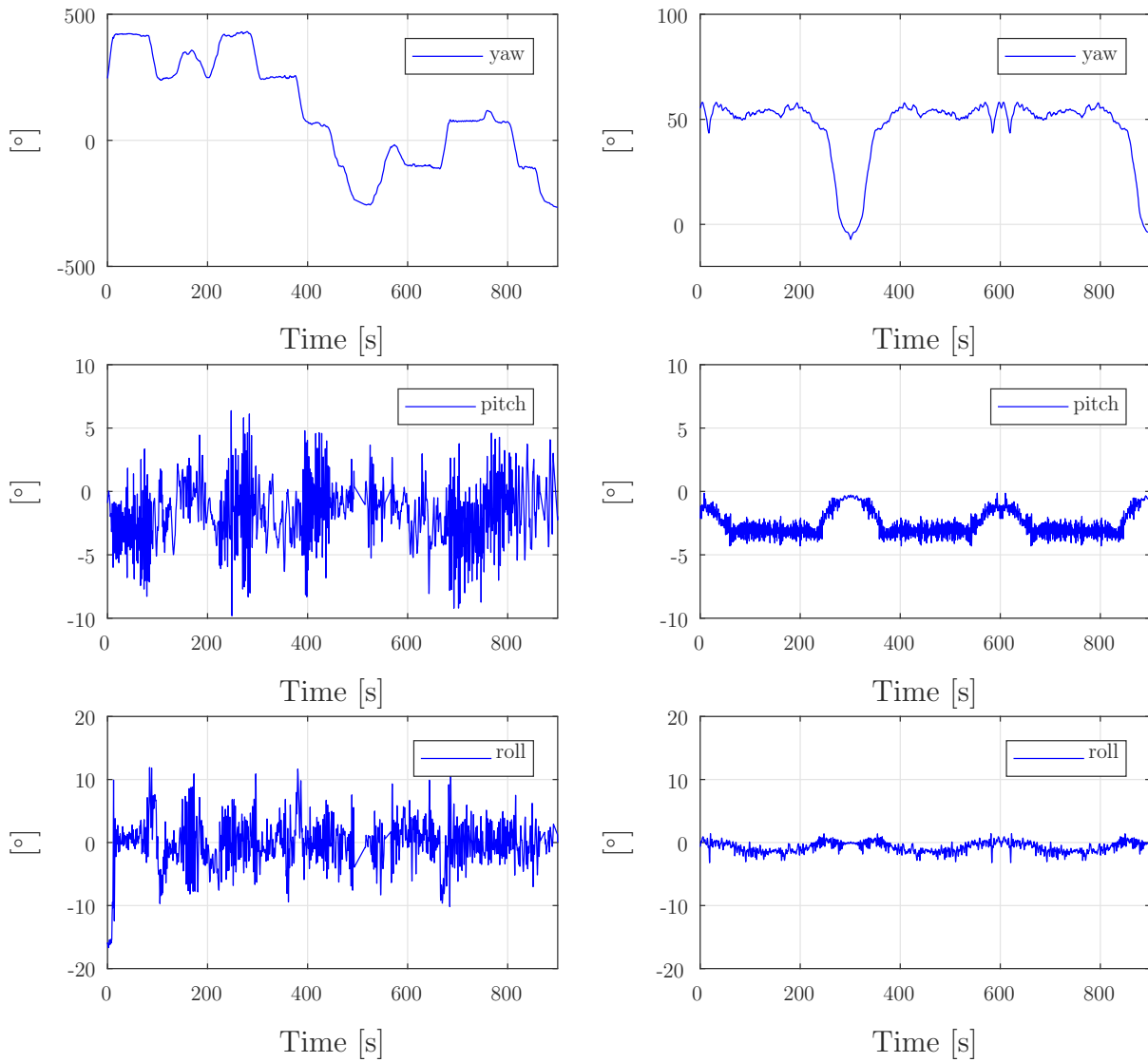


Figure 5.15: Time series of the angles of the maritime standard motion profiles: Class A (left column) and Class B (right column).

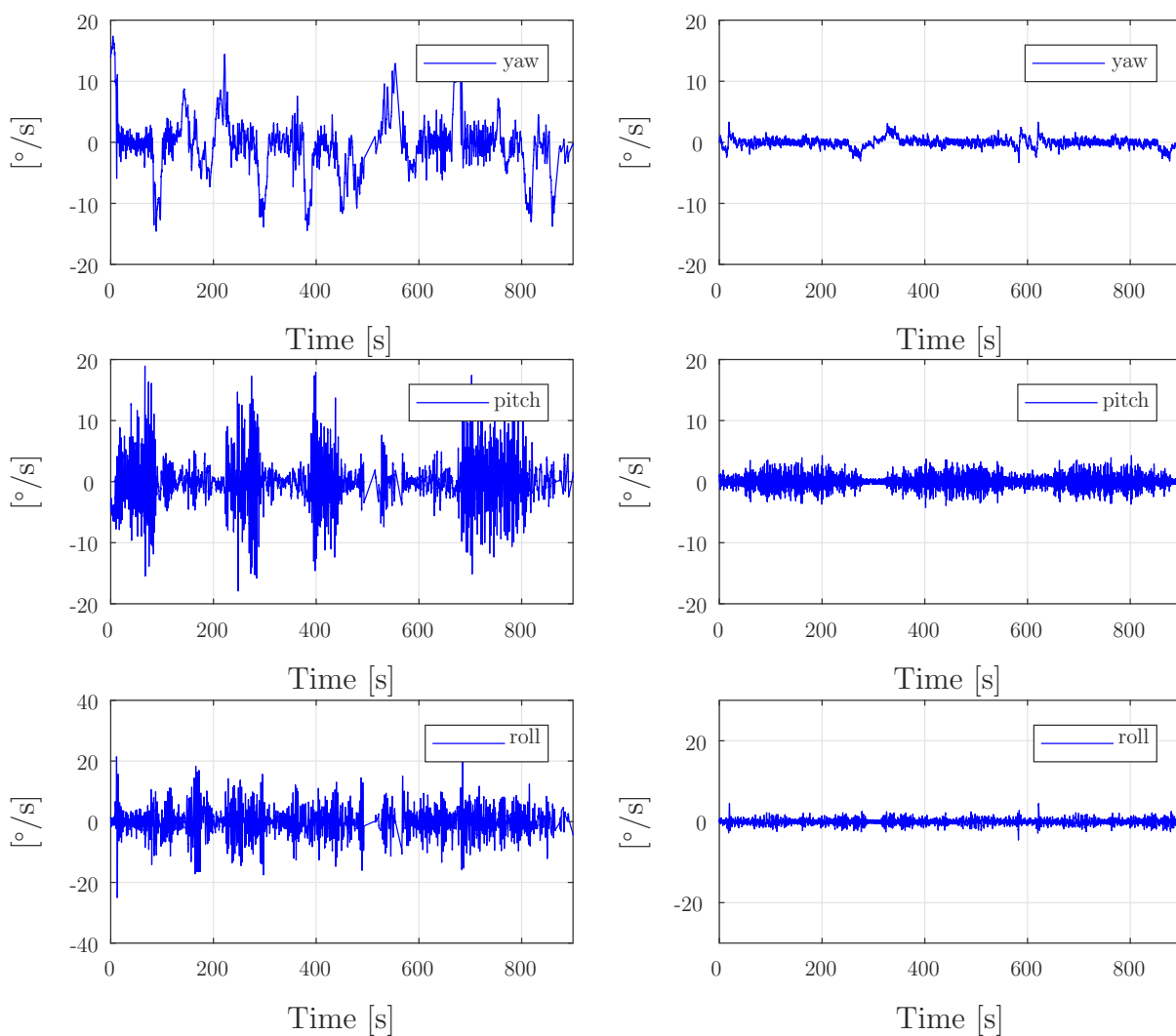


Figure 5.16: Time series of the angular rates of the maritime standard motion profiles: Class A (left column) and Class B (right column).

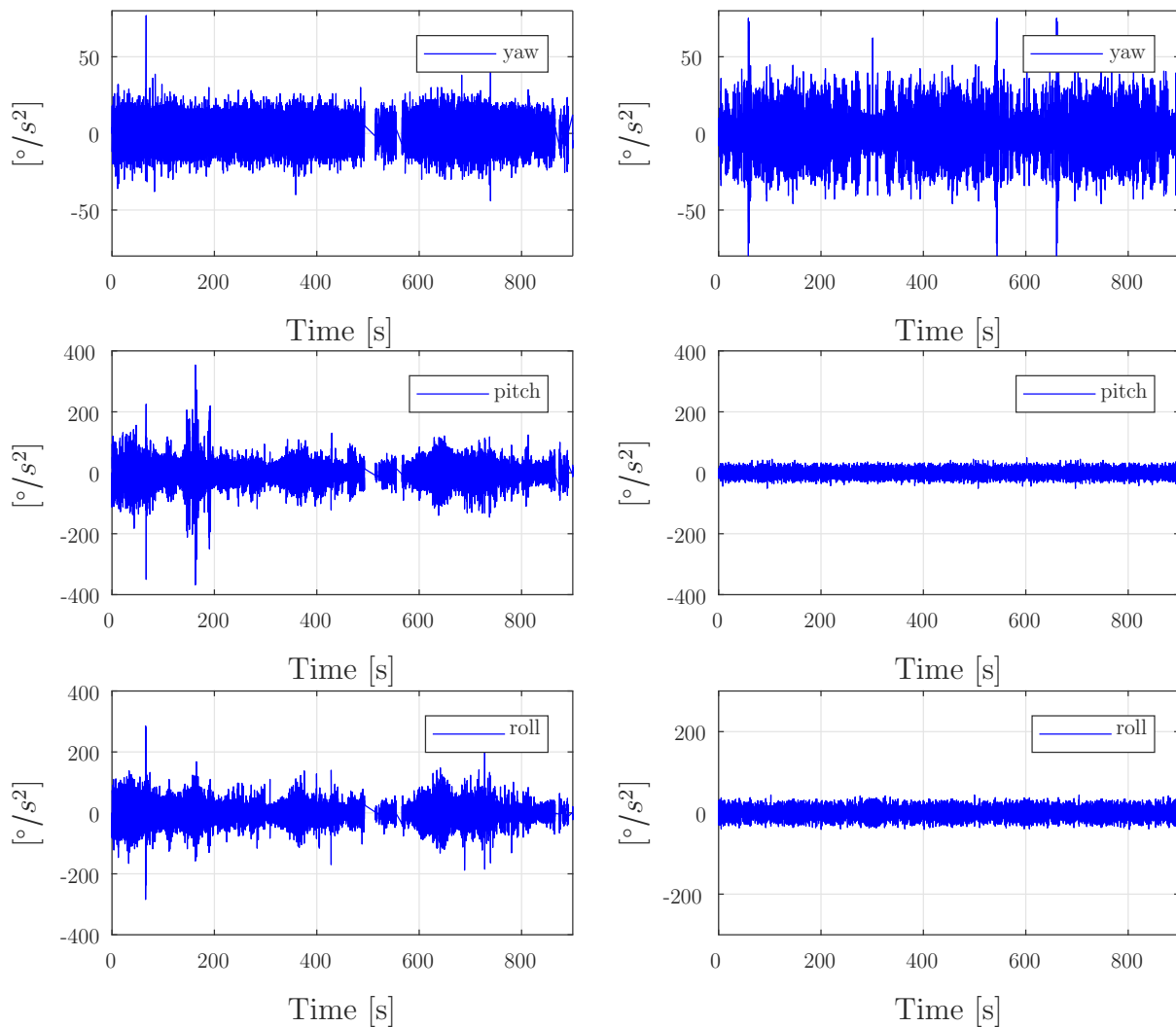


Figure 5.17: Time series of the angular accelerations of the maritime standard motion profiles: Class A (left column) and Class B (right column).

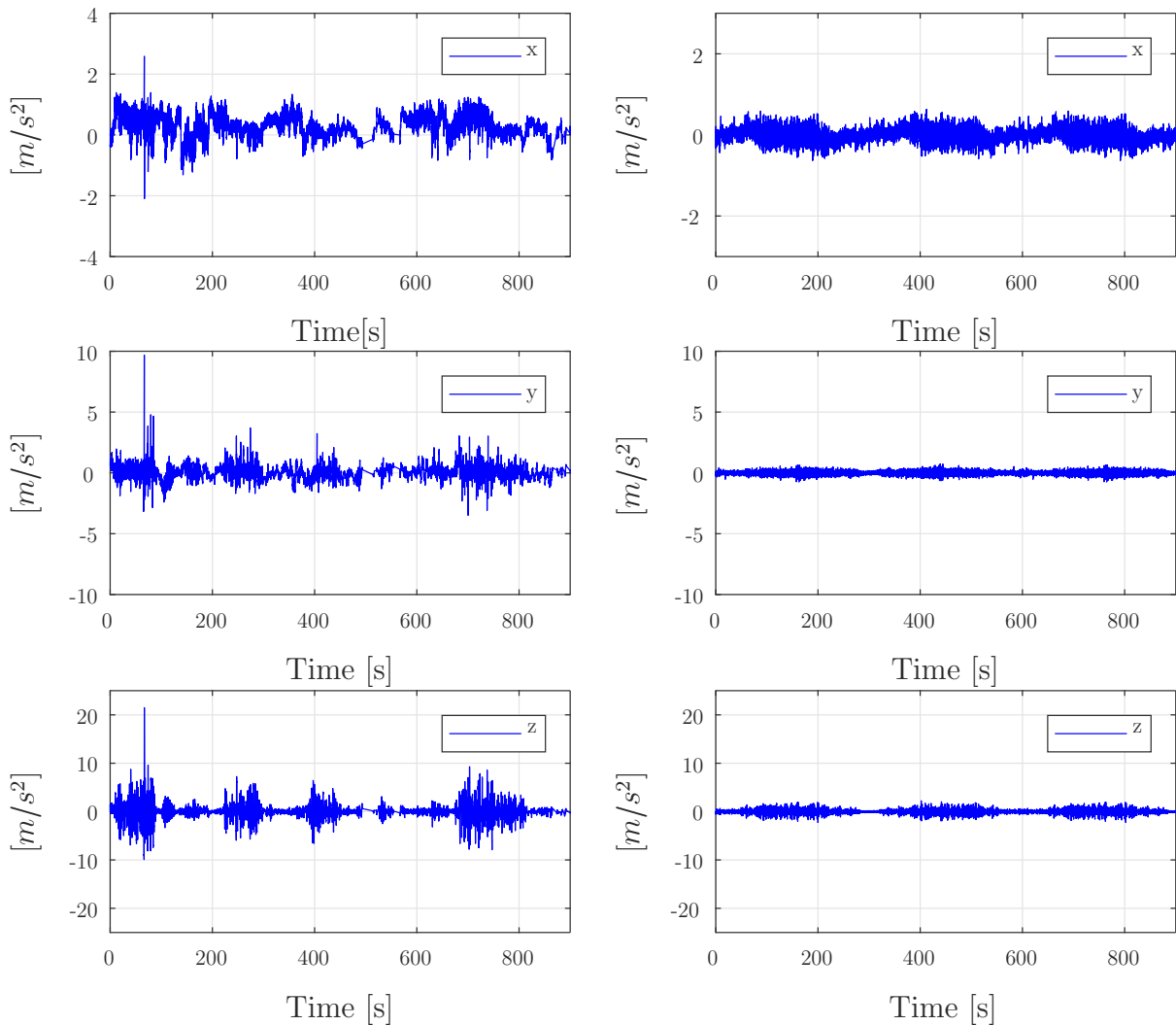


Figure 5.18: Time series of the translational accelerations of the maritime standard motion profiles: Class A (left column) and Class B (right column).

5.6 Land mobile, Maritime, and Churchville B

Figure 5.19 depicts the CDF of the angular rate vector norm for the Class A and Class B representative motion profiles of the land mobile and the maritime environments. The CDF of the angular rate vector norm for the Churchville B motion track is plotted in the same figure for the sake of comparison. The dynamics of the Churchville B track are very close to the dynamics of the land mobile Class B representative motion profile.

It can be seen from Figure 5.19 that the land mobile Class A represents the upper bound of the motion dynamics and the maritime Class B represents the lower bound.

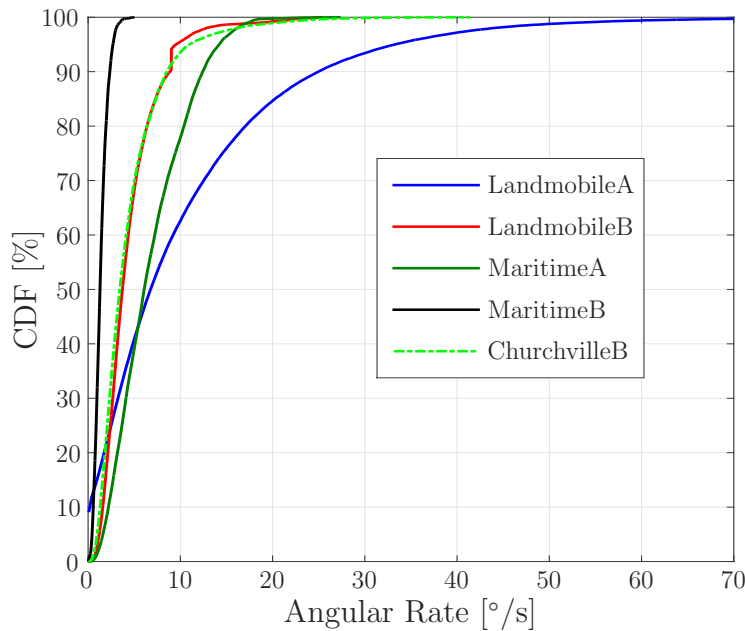


Figure 5.19: The CDF of the angular rate vector norms for the motion profiles of Class A and Class B of the land mobile and the maritime environments. The CDF of the angular rate vector norm for the Churchville B motion track is also plotted.

5.7 Standard Motion Profiles in GVF-105

The proposed motion profiles were added to the terminal testing recommendations “GVF-105” document. It is stated as a recommendation that a SOTM terminal is to be tested using the proposed profiles in either:

- A laboratory environment where the dynamics and the actual time series of the motion profiles from Class A and Class B can be replayed and the tracking performance can be measured, or
- A free field: In this case, it has to be ensured that at least the statistics of the test track match the statistics of the selected representative motion profiles for the corresponding environment and class. It also has to be ensured that an accurate IMU is used to record the dynamics of the motion profile during the test such that the dynamics can be compared.

Chapter 6

Proposed Shadowing Profiles

This chapter presents one of the main achievements of this work: shadowing profiles proposed for standard testing of Satellite Communication On-The-Move (SOTM) terminals. Section 6.1 presents the definition of the environment types which were considered for the profile definitions. In Section 6.2, the adopted image post processing algorithm is introduced. Sections 6.3 and 6.4 present the process of shadowing profile extraction. The shadowing profile is extracted from the image profile of a certain environment for a specific geographical location and for a specific satellite longitudinal position. A standard shadowing profile from any type of environment can be combined with any motion profile in order to have flexible conditions for SOTM testing. This is the scope of Section 6.5.

Satellite communications are based on Line-of-Sight radio frequency transmission. The channel between the SOTM terminal and the target satellite is often referred to as the Land Mobile to Satellite (LMS) channel. The Line-of-Sight (LOS) and Non-Line-of-Sight (NLOS) conditions of the LMS channel depend on the environment around the SOTM terminal and on the pointing direction to the satellite. The LOS and NLOS effects (also called shadowing effects) need to be considered when the SOTM terminal is tested.

LMS channel characterization, so far, depends on statistical modeling or on RF measurements. The statistical channel models, e.g., those proposed in [52–54], derive the time series of the channel states using parameters driven from statistical distributions. For the Ku-/Ka-band frequencies that are relevant for the scope of this thesis, there exist no statistical model in the literature which is able to model the LMS channel at these high frequencies for any satellite position and any environment scenario. There exist some models based on RF measurements at Ku-/Ka-bands, e.g., [55–59], however, they are only valid for limited positions of satellites and limited number of environments. The characteristics of the Ku-/Ka-band satellite channel (11-40 GHz) are similar to those of the optical channel. Multipath components are irrelevant and can be neglected since SOTM applications usually use directive antennas [60]. With respect to the shadowing, the Ku-/Ka-band LMS channel can be treated as a frequency-flat ON/OFF channel.

Based on this observation, we propose standard shadowing profiles in this section based on the processing of optical images.

The proposed standard shadowing profiles offer a unique reference or a benchmark for SOTM terminal testing and comparison. They can be used in any laboratory which employs channel emulators. If the terminal is tested in a field test instead, it is recommended that the shadowing profile from the field test track statistically matches the developed shadowing profiles presented in this section. This maintains a fair basis to test and compare different SOTM terminals.

In order to define the shadowing profiles, four steps are involved. These are:

1. Image capturing and environment definition.
2. Image post processing: classification of the images into LOS or NLOS.
3. Shadowing profile extraction: profile extraction from the processed images at a certain angular position.
4. Selection of proposed standard shadowing profiles: one shadowing profile for each environment is selected as a representative shadowing profile.

In the following, these steps are presented in detail.

6.1 Image Capturing and Environment Definition

In addition to the measurement of the motion dynamics described in Section 5.1, a fisheye camera pointing towards the sky was mounted on the rooftop of the vehicles. A sequence of images of the upper hemisphere were captured at a rate of 5 frames per second along a specific motion profile. We denote this sequence as “*image profile*”. As an example, Figure 6.1(a) shows a single snapshot of a hemispheric image profile in an urban scenario.

The image profiles were classified into seven different environment types as the following:

1. Forest: heavy tree shadowed environment. The total duration of measurements in the forest is approximately one hour.
2. Urban: three or more story buildings with narrow streets is typical for urban scenarios in Germany where the majority of measurement data was collected. Vegetation is a minority. In the urban environment, about six hours of measurements were carried out.
3. Suburban: one or two story buildings with wider streets and more vegetation compared to the urban scenarios. Six hours of measurement data was collected in the suburban environment.

4. Light tree shadowed: typical for federal roads between small cities where vegetation is distributed lightly on the sides of the road. Approximately seven hours of measurements were collected in the light tree shadowed environment.
5. Highway: with two or three lanes per direction with no lamp posts, some objects like windmills and with complete blockage in tunnels and under bridges. On highways, nine hours of measurements were collected.
6. Open: mostly Line-Of-Sight with rare randomly distributed obstacles. In open environments, approximately five hours of measurements were collected.
7. Train: there were no train measurements performed in the campaign. However, the high speed train tracks are mainly in open fields and with a small percentage of tunnels and bridges. In Germany tunnels sum up to about 10% of the whole high speed train tracks [61]. Using this percentage, we selected parts of the highway track image profiles and considered them as representative for the train environment. Approximately two hours of measurements were considered to represent the train environment.



(a) An exemplary hemispheric image from an urban environment.



(b) An overlay consisting of the original and the binary categorization into *sky* and *obstruction*.

Figure 6.1: The original hemispheric image (left) and the result of the image classification (right).

6.2 Image Post Processing

A classification algorithm segregates the image into regions with LOS and NLOS [62]. The algorithm filters the sun spot and the clouds in order to exclude their effects. Figure 6.1(b) shows the two classes for the same snapshot depicted in Figure 6.1(a). Red represents NLOS or obstruction while blue represents LOS or sky.

For a better representation of azimuth and elevation angle pairs, the image is transformed into a rectangular landscape panoramic monochrome format. The new angular grid has a resolution of one degree in both, azimuth and elevation. This transformation is followed by a circular rotation in azimuth to account for heading compensation. The image is rotated by the vehicles heading, such that the resulting image will have the geographical north at 0° in azimuth. Figure 6.2, shows the heading compensated monochrome panoramic image for the same snapshot which is depicted in Figure 6.1(a).

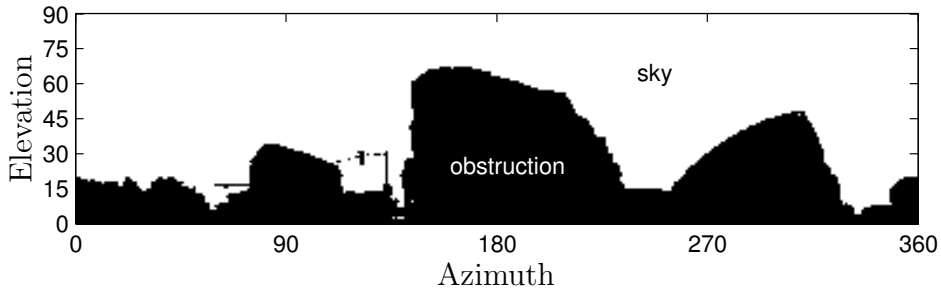


Figure 6.2: The resulting monochrome panoramic image with north direction at 0° in azimuth. Black represents obstruction or NLOS and white represents sky or LOS.

6.3 Shadowing Profile Extraction

Knowing the geographical location, i.e. the longitude and latitude of the vehicle at a specific time, the location (azimuth and elevation) of a specific satellite, given its orbital longitudinal position, can be determined. Based on the obtained azimuth and elevation angle pair, the reception state of the satellite can be extracted from the panoramic image. The shadowing profile related to one motion profile can be generated by extracting the LOS information from the sequence of images in the corresponding image profile. Figure 6.3 shows an exemplary monochrome panoramic image profile with azimuth, elevation, and time. Figure 6.4 depicts the shadowing profile corresponding to the land mobile Class A proposed standard motion profile if the EUTELSAT 10A satellite located at 10° East is considered. The profile consists of two shadowing levels, “ON” for no shadowing (LOS) and “OFF” for obstruction (NLOS). The percentage of LOS for the land mobile class A corresponding shadowing profile is approximately 94%.

Using this image-based method, shadowing profiles for different satellite positions can be obtained. In a field test, in contrast, this is not possible unless the complete measurement is repeated for each satellite position or if multiple antennas are involved in the measurement, each pointing towards a different satellite.

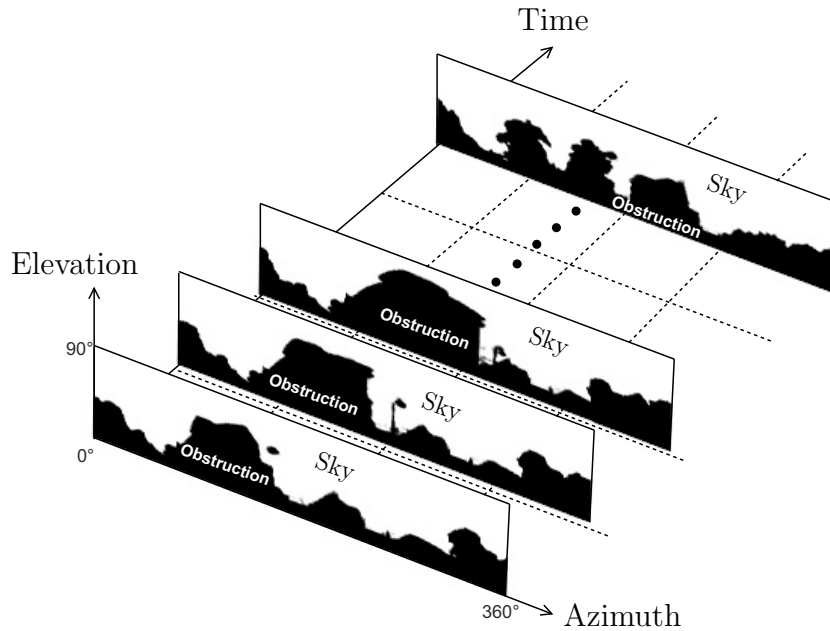


Figure 6.3: An exemplary panoramic image profile showing the LOS and NLOS reception states for each azimuth and elevation angle pair at each time instance. The image capturing rate defines the number of images in the whole duration of the profile.

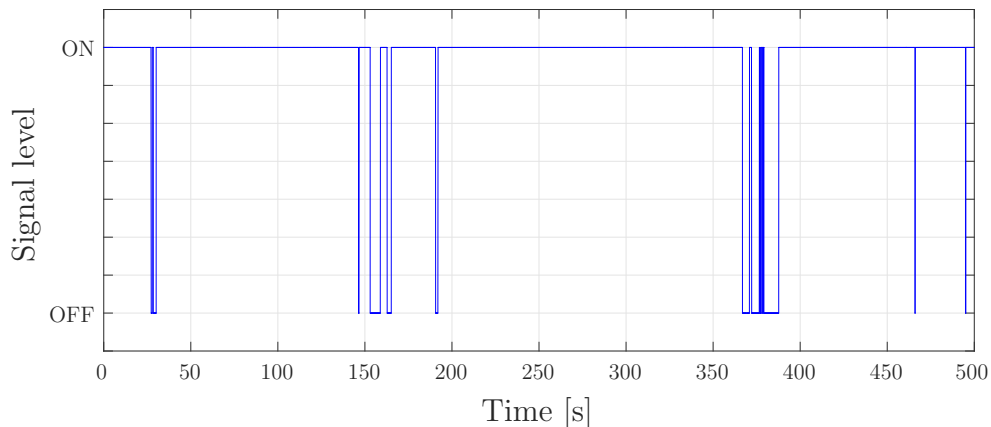


Figure 6.4: The shadowing profile extracted from the images captured at the Class A motion profile for the EUTELSAT 10 A satellite. ON represents no shadowing (LOS) and OFF represents obstruction (NLOS). Approximately 94% of the profile is covered by LOS.

6.4 Definition of Standard Shadowing Profiles

To select and define the shadowing profiles, we consider the **percentage of LOS in the shadowing profile**. For each azimuth and elevation angle pair in every image profile, a shadowing profile (cf. Figure 6.4) is extracted and the percentage of LOS is calculated along time dimension. For the sake of simplicity, the dimensions are further reduced by averaging the LOS percentage over all azimuth angles. This results in the mean LOS percentage versus elevation and is denoted the **LOS-elevation contour**. Figure 6.5 depicts the LOS-elevation contours calculated for the forest environment where five image profiles were collected.

Additionally, the mean of all LOS-elevation contours is calculated for each environment. The resulting mean is denoted as the **environment mean LOS-elevation**

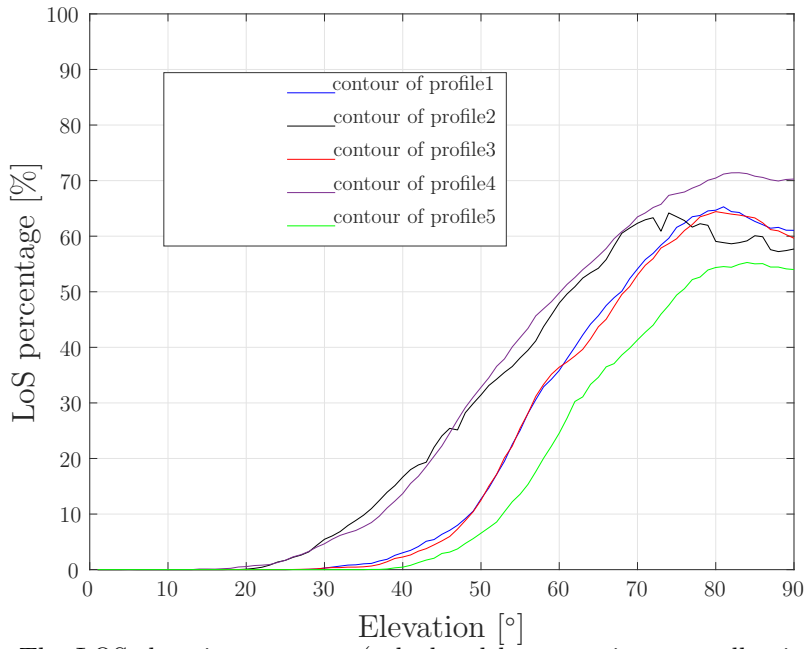


Figure 6.5: The LOS-elevation contours (calculated by averaging over all azimuth angles) for each image profile in the forest environment.

contour and is depicted for each of the defined environments in Figure 6.6.

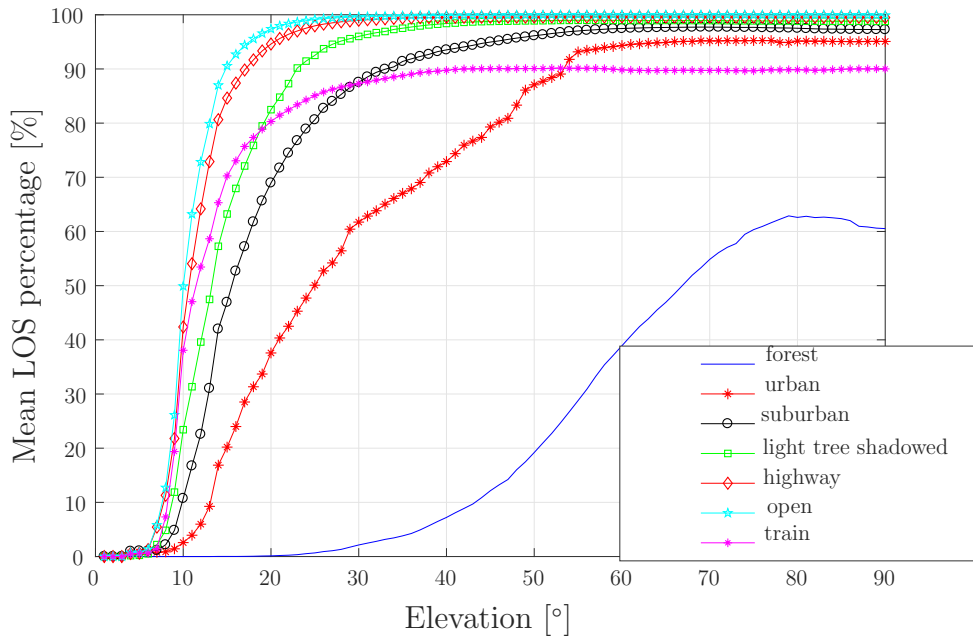


Figure 6.6: The Environment mean LOS-elevation contours for the seven defined environments.

In a next step, the Root-Mean-Square Deviation (RMSD) between the individual LOS-elevation contours (cf. Figure 6.5) and the corresponding environment mean LOS-elevation contour (cf. Figure 6.6) is calculated. For each environment, the image profile with the lowest RMSD is selected as the proposed standard image profile. For a specific satellite location, the proposed standard shadowing profile is then extracted from the standard image profile.

Figure 6.7 summarizes the process to define the proposed standard shadowing profiles.

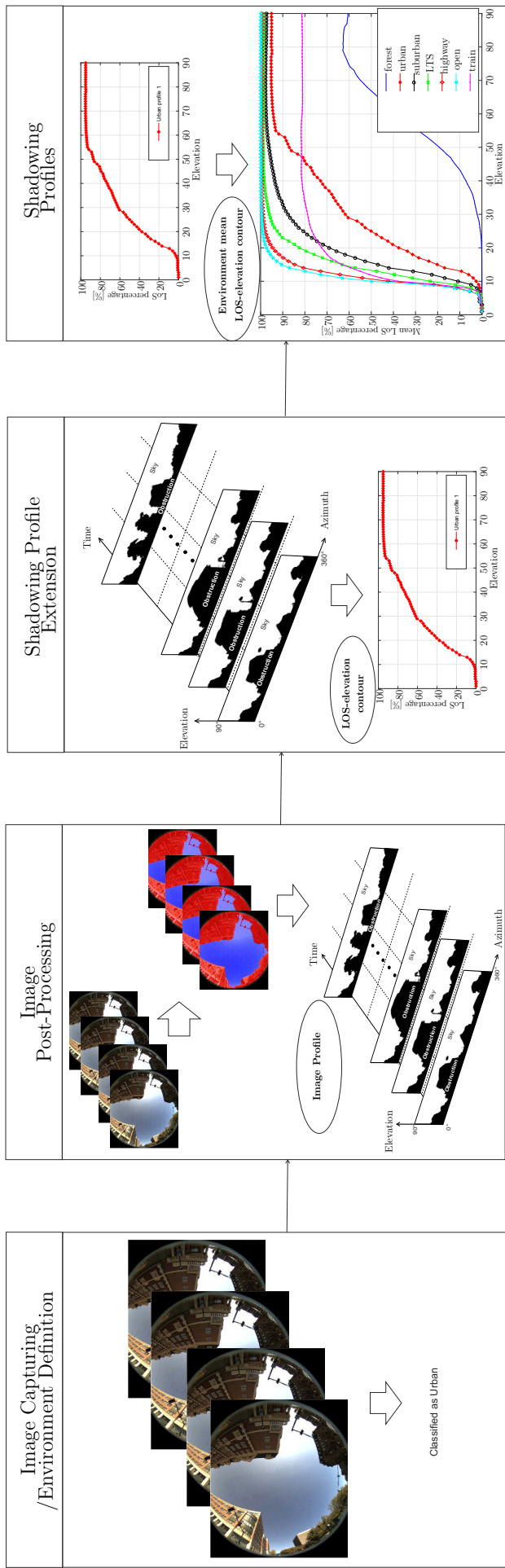


Figure 6.7: A block diagram summarizing the process to define the proposed standard shadowing profiles. A shadowing profile is defined with respect to a specific satellite location.

6.5 Combining Motion and Shadowing Profiles for Testing

In a SOTM terminal test scenario, the shadowing profile should always be synchronized to the corresponding motion profile. However, the combination of a shadowing profile from one geographical location with a motion profile from a different geographical location is needed for a SOTM terminal test in a laboratory environment, such as FORTE. This is important in order to test the performance of the SOTM terminals with different combinations of motion and shadowing. Here, three main challenges exist:

1. The heading in the image profile does not match the heading in the new motion profile, which is from a different location.
2. The image profile and the new motion profile may not have the same length in time.
3. The speed of the vehicle while capturing the image profiles does not match the speed of the vehicle at the motion profile.

The definition of the motion profiles (cf. Section 5.2) is based on the vector norm of the angular rates. In order to investigate if the heading mismatch between the image and the motion profiles need to be compensated or can be neglected, the correlation between the gradient of the heading, and the gradient of the roll and pitch angles was investigated. If the correlation is low, the evolution of the heading in the image profile is considered independent of the evolution of the dynamics in the motion profile and no heading compensation is required.

Figure 6.8 plots the correlation coefficient for all motion profiles described in Chapter 5.

From Figure 6.8, it can be seen that the correlation coefficient does not exceed 0.25. Hence, the heading from the image profile does not need to match the heading in the motion profile. In other words, the image profile can be used with its original heading to extract the shadowing profile at any geographical location on earth.

In order to overcome the second challenge, which is to match the length of the image profile to the length of the motion profile, two cases need to be considered:

1. The image profile is longer than the motion profile: we choose the part of the image profile which yields a shadowing profile having a LOS percentage which is closest to the one expected from Figure 6.6 for the corresponding satellite elevation.
2. The image profile is shorter than the motion profile: we flip and repeat the image profile multiple times, and fill the last segment with the part of the image profile which guarantees the closest LOS percentage to the one expected from Figure 6.6 for the corresponding satellite elevation.

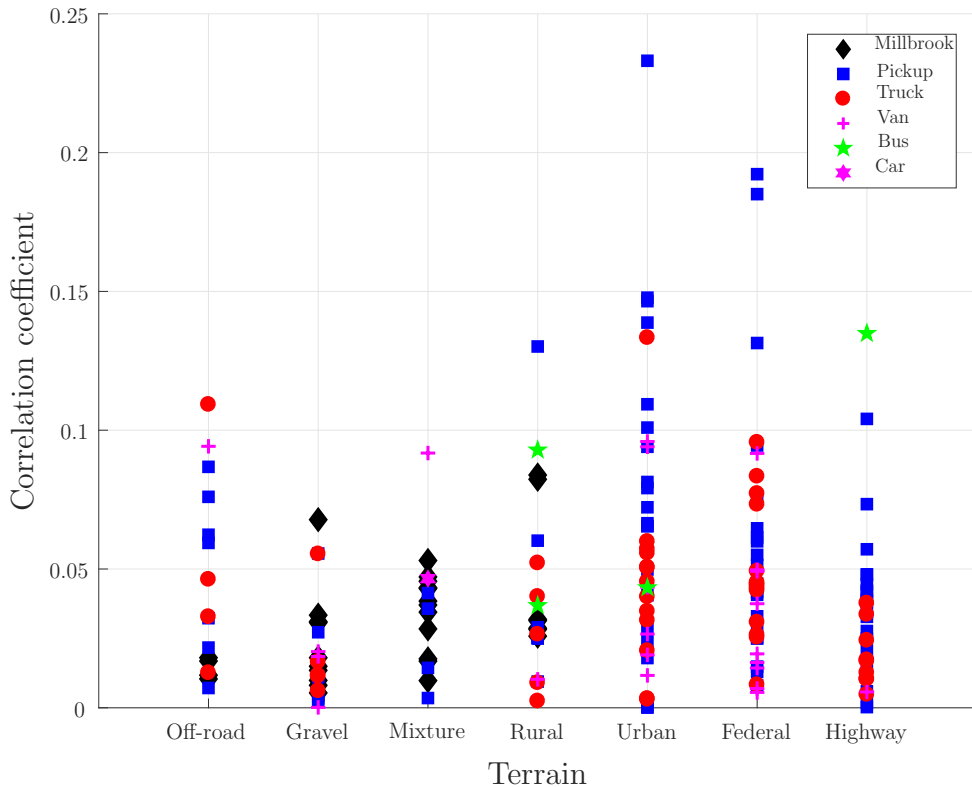


Figure 6.8: The correlation coefficient between the derivative of the heading and the angular rate vector norm.

The third challenge, which is the different speeds of the vehicle at the shadowing and motion profiles, can be overcome by stretching or shrinking the LOS/NLOS states in the shadowing profile. For instance, if the average speed at the motion profile is double the average speed at the shadowing profile, the shadowing profile will be down-sampled by rate of one-half. Afterwards, the new down-sampled profile will be repeated twice in order to keep the same original length and LOS/NLOS statistics. For the sake of simplicity, we assume that the motion profiles and the image profiles are driven at the same speed for the rest of the analysis.

The proposed standard shadowing profiles for the defined seven environments extracted at the geographical location of the land mobile class A motion profile for the EUTELSAT 10A satellite are depicted in Figure 6.9.

Generally, the motion of the vehicle causes Doppler, i.e. frequency shifts inside the band of operation occur. Investigations of Doppler effects are not considered in this thesis. In measurements performed at FORTE, we experienced that the effect of Doppler on the overall performance of the SOTM terminal is marginal compared to the effect of the motion or of the shadowing. It is more challenging for the modem to mitigate the effect of signal blockages than to handle frequency shifts caused by the Doppler effect. Moreover, other impairments e.g., the atmospheric losses, the rain attenuation, the Faraday rotation effect, etc. are not considered in this thesis.

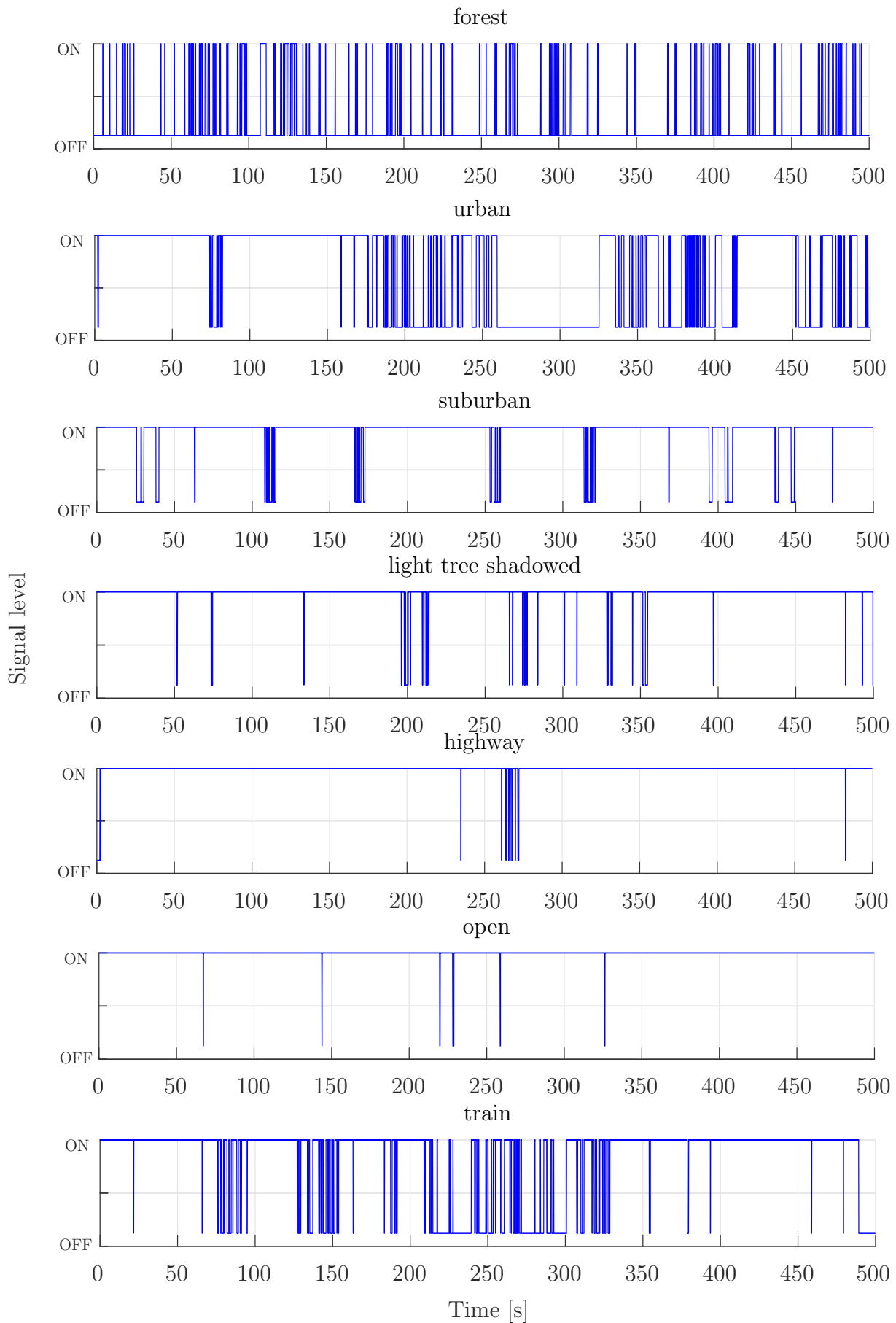


Figure 6.9: The proposed standard shadowing profiles for the different environments assuming the geographical location of the land mobile class A motion profile and the EUTELSAT 10A satellite located at 10° East.

Chapter 7

Measurement Results

In this chapter, the results of a tested Ka-band Satellite Communication On-The-Move (SOTM) antenna at the Fraunhofer Facility for Over-the-air Research and Testing (FORTE) are presented. The test was performed according to the methodology proposed in Chapter 4 and the motion profiles proposed in Chapter 5 were applied. The test was performed in compliance with the GVF-105 type approval recommendations defined by the Global VSAT Forum (GVF). As the GVF-105 recommendations do not specify operational limits, the specifications ESOG-120 [50] and the EESS-502 [63] from EUTELSAT were applied additionally. Section 7.1 presents the measurement scenario and the antenna under test. In Section 7.2, parts of the measurement results are introduced. The conformance of the radiation pattern with the SOTM standards, the antenna de-pointing, the Adjacent Satellite Interference (ASI), and other parameters are measured.

7.1 The Measurement Scenario

The antenna under test and its tracking unit were developed in the context of the project KASYMOSA (Ka-Band Systems for Mobile Satellite Communications)¹. This project aimed to develop and validate new technologies and algorithms for mobile satellite communications in the Ka-band. The developed antenna has a dish with a diameter of 60 cm and operates in the Ka-band (≈ 30 GHz uplink and ≈ 20 GHz downlink). A mechanical two-axis tracking unit is attached to the antenna in order to track in azimuth and elevation [64].

An attached Inertial Measurement Unit (IMU) measures the orientation of the SOTM terminal. The heading information is estimated with the help of GPS. A phase discriminator gives an initial indication of the pointing error by evaluation of the received beacon from the satellite. Finally, the collected data are fed into a control algorithm based on kalman filtering in order to perform successful satellite tracking.

¹The project KASYMOSA was supported by the German Aerospace Center (DLR)

A picture of the antenna mounted on the motion emulator at FORTE is shown in Figure 7.1.

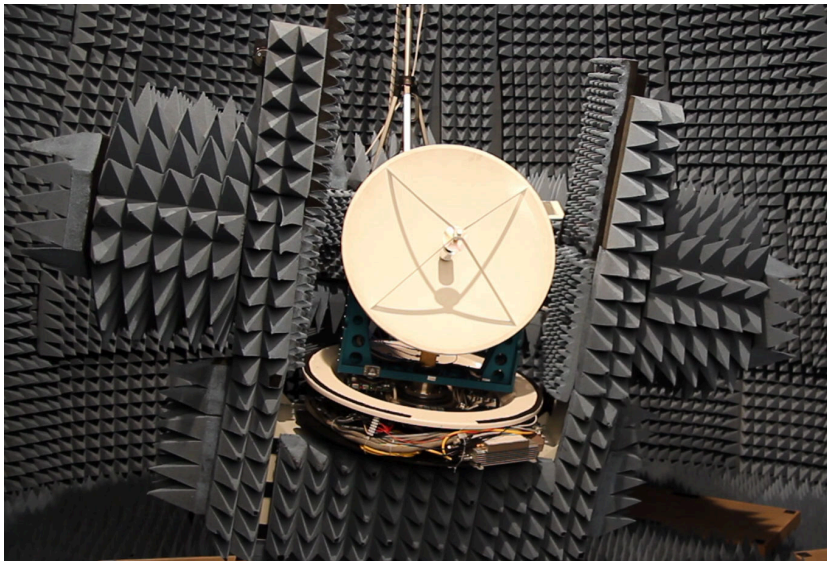


Figure 7.1: The antenna under test while being mounted on the motion emulator and tested at the Fraunhofer Facility for Over-the-air Research and Testing (FORTE).

The measurements were conducted under clear sky conditions. Furthermore, the atmospheric losses, the rain attenuation, the Faraday rotation effect, etc. were considered negligible and were not emulated in this test.

7.2 An Excerpt of the SOTM Type Approval Results

The tests performed at FORTE include:

- **Antenna Characteristics:** This includes the measurements of antenna transmit and receive gains, and patterns at the different required frequencies, polarizations, elevation pre-tilts, and radome orientations.
- **Dynamic Tests:** This includes the measurements while the antenna is moving on standard motion profiles. Antenna de-pointing, cross polarization discrimination (XPD), Adjacent Satellite Interference (ASI) are measured.

7.2.1 Antenna Characteristics

7.2.1.1 Gain Measurements

The antenna gain is measured as a first step. This measurement is performed directly at the feed port of the antenna. During the measurements, a single tone is transmitted by the antenna under test and the power level at the receive antenna at the antenna tower is

recorded. The antenna gain (in main beam direction) is finally obtained by comparison with a reference antenna with known gain. Repeating this for multiple frequencies and both polarizations (LHCP and RHCP) results in the main beam antenna gain provided in Figure 7.2.

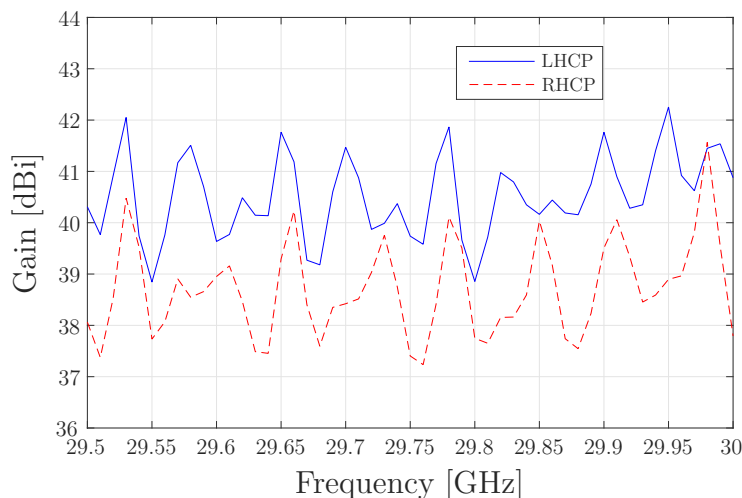


Figure 7.2: The transmit co-polarized gain of the antenna under test v.s. frequency for both polarizations LHCP and RHCP.

7.2.1.2 Radiation Pattern Measurements

The motion emulator is used to move the antenna in order to measure its patterns in the transmit and receive frequency bands. The EUTELSAT specifications [50] require measuring the antenna gain patterns at multiple antenna elevation pre-tilt angles. Hence, at least two elevations need to be measured: 0° and one angle between 30° and 35° . The specifications also require measuring the patterns at the center frequency and two other frequency points one in the lower half and one in the upper half of the transmit frequency band. For example, for the Ka-band uplink, the frequencies 29.5, 29.75, and 30 GHz need to be considered. A further requirement is to measure the pattern while having multiple radome rotations: 0° , 90° , 150° , and 270° . This makes the measurement manifold multidimensional. For the sake of brevity, we only render an excerpt of the results in this section.

The EUTELSAT specifications require that the antenna gain pattern at the transmit frequency bands has to be in conformance with the ' $29 - 25 \log(\theta)$ ' mask. The measured radiation pattern is plotted along with the mask and the conformance is investigated. In Figure 7.3, the mask overshoots are plotted for a single measurement scenario. The mask overshoot is the difference between the gain pattern and the regulatory mask. The colors of the plot represent an overshoot/no-overshoot schema. Green and black represent no overshoot, while yellow and red represent regions with overshoots. The depicted measurement is at an uplink frequency of 29.5 GHz, LHCP polarization and an antenna elevation of 30° while the radome was put off.

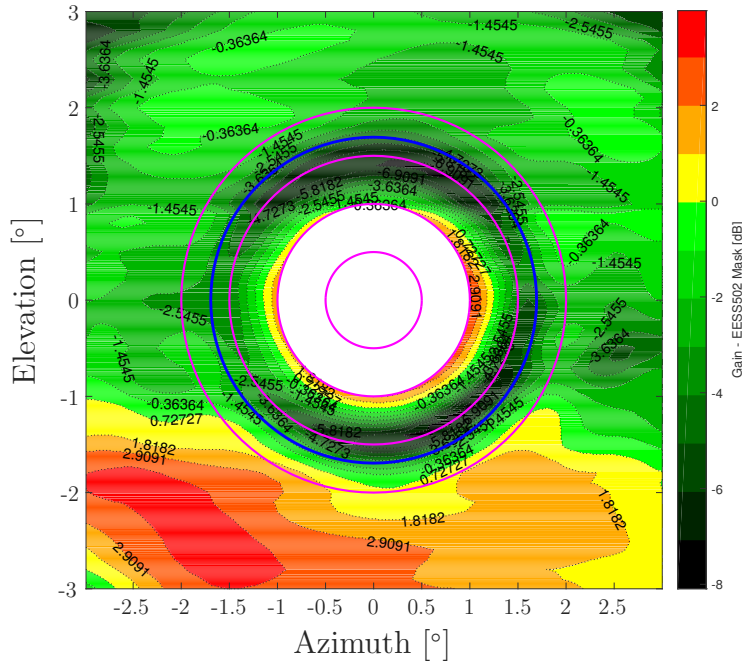


Figure 7.3: Transmit co-polar raster scan - $'29-25 \log(\theta)'$ overshoots from 1° for antenna elevation 30° , frequency 29.5 GHz, and LHCP polarization.

According to the specifications, the plot starts at 1° deviation from the main beam direction. Hence the inner circle is not measured. The magenta circles highlight contours with 0.5° angular difference, whereas the blue circle represents the α angle specified by EUTELSAT. $\alpha = 1^\circ$ or $100\lambda/D$ whichever is greater, where D is the antenna diameter and λ is the carrier wavelength.

Cross Polarization Discrimination (XPD) is a measure on how well the two orthogonal polarizations are decoupled. It describes the ability of an antenna to maintain the purity of a certain polarization. Figure 7.4 depicts an XPD raster scan with the -0.5 dB and the -1 dB templates defined by EUTELSAT. These templates represent the locations where the co-polarized gain level is reduced by 0.5 dB and 1 dB compared to its maximum.

The radiation patterns are not measured only as raster scans but also as cuts along the principle angular planes (azimuth and elevation). The EUTELSAT specifications require the full angular span of $\pm 180^\circ$ in azimuth and a smaller span (e.g., $\pm 30^\circ$) in elevation to be covered. When the radiation pattern is measured with a pre-elevation tilt different from 0° , the azimuthal span of $\pm 180^\circ$ using the motion emulator at FORTE can not be achieved. For example, at an elevation pre-tilt of 30° , the maximum span is limited to $\pm 160^\circ$. Figure 7.5 shows the transmit gain pattern of the antenna under test versus azimuth. The measurement was taken for an uplink frequency of 29.5 GHz, LHCP polarization, antenna elevation of 30° , and a radome rotation of 270° . For a better display, only the zoomed range of $\pm 10^\circ$ is depicted.

Additionally, in Figure 7.5, the $'29-25 \log(\theta)'$ mask is plotted. The same mask but shifted upwards with 3 dB for the angular range between α and 9.2° , and with 6 dB

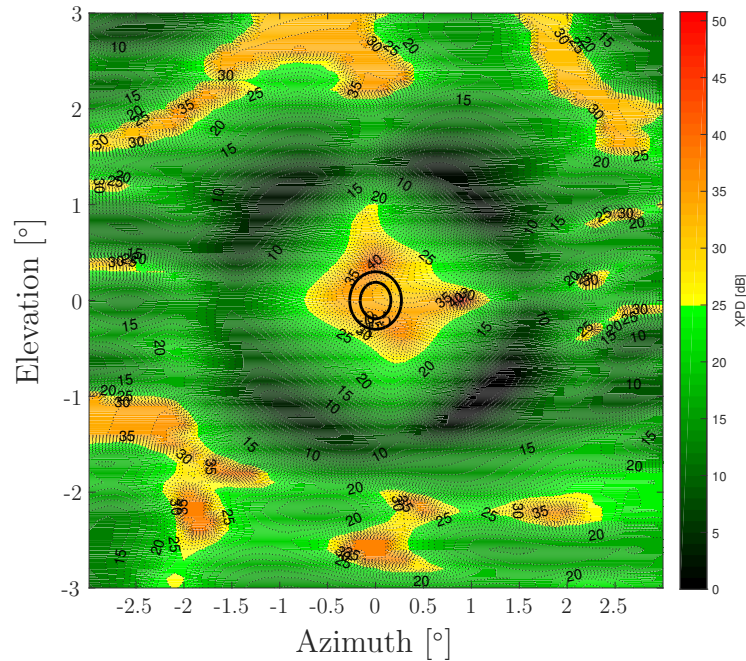


Figure 7.4: Transmit XPD raster scan with the -0.5 dB and -1 dB templates for antenna elevation 30°, frequency 29.5 GHz, and LHCP polarization.

for the angular range beyond 9.2° is also depicted. These relaxed masks are defined in the specifications of EUTELSAT to provide an extra margin for smaller antennas. The cross-polar pattern and the cross-polar mask (defined in the angular range α to 9.2°) are also plotted in Figure 7.5. The positions where the measured patterns violate the regulatory masks can be easily found by inspecting Figure 7.5.

Table 7.1 summarizes the main outcome of the mask conformance test in Figure 7.5. The F-Factors are listed as well. They are defined by EUTELSAT as the maximum value of the mask overshoots of the regulatory mask for different angular ranges.

7.2.2 Dynamic Tests

In the dynamic tests, the performance of the SOTM terminal are evaluated while being on-the-move. The terminal is mounted on the motion emulator which replays a motion profile. As described in Section 4.2, the antenna de-pointing is measured along the motion profile. Moreover, the XPD and the ASI are measured as well.

Figure 7.6, shows the evolution of the XPD when the terminal is tested with the maritime Class A proposed standard motion profile. The XPD has an average of 24 dB and a standard deviation of 0.7 dB.

ASI is measured for three satellite positions specified by EUTELSAT: 1.18°, 2.36°, and 3.53°. The power normalized to the line of sight level received at the target satellite at 0° is plotted in Figure 7.7 for adjacent satellite positions of $\pm 1.18^\circ$ as an example. The figure shows that, in the worst case, the adjacent satellite at +1.18° receives a power level 11 dB below the power level received when the SOTM antenna exactly points towards

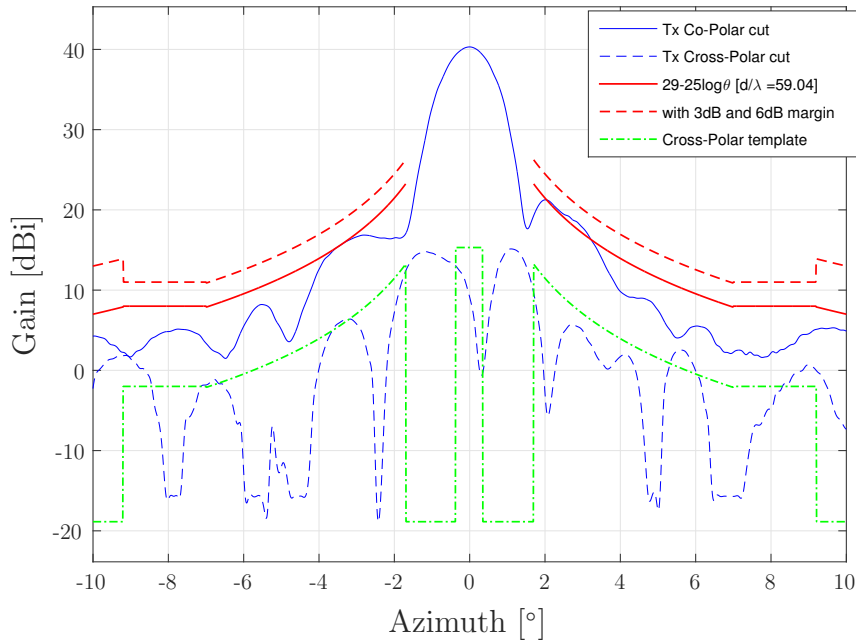


Figure 7.5: Transmit azimuth plane cut for antenna elevation 30° , frequency 29.5 GHz, RHCP polarization, and radome rotation 270° . A zoomed angular range of $\pm 10^\circ$ is depicted for the sake of a better display.

the target satellite. In the best case the level is more than 19 dB lower.

Figure 7.8(a) shows the time evolution of the antenna de-pointing along azimuth and elevation for the maritime Class A proposed standard motion profile. According to EUTELSATs specifications, the antenna de-pointing must not exceed 0.4° under all circumstances. As seen from Figure 7.8(a), the antenna de-pointing does not exceed 0.4° in any case. Therefore the antenna is compliant with EUTELSATs specifications. Figure 7.9(b) shows the Cumulative Distribution Function (CDF) of the de-pointing estimation results in Figure 7.8(a). It can be seen that the antenna de-pointing, in azimuth as well as in elevation, does not exceed 0.4° in any case.

If the antenna is tested using the land mobile Class A proposed standard motion

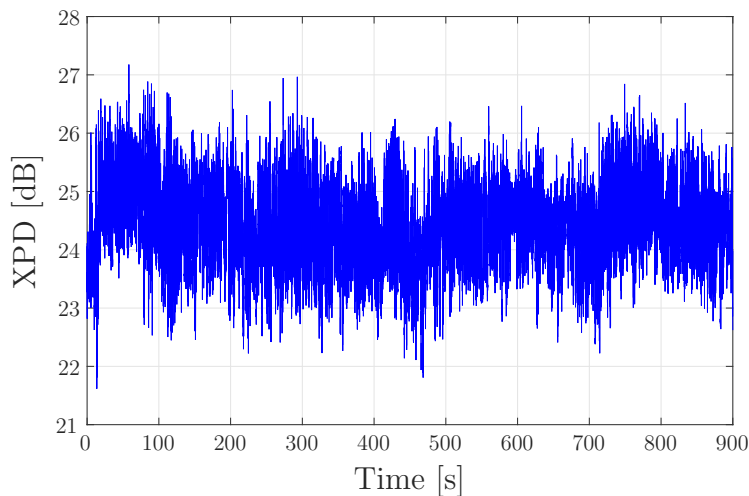
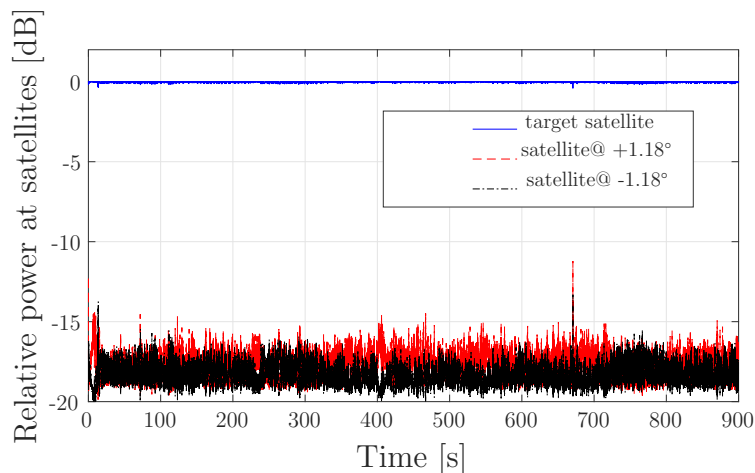


Figure 7.6: Cross-polarization discrimination (XPDP) of the SOTM antenna under test when tested on the maritime Class A proposed standard motion profile.

Table 7.1: Summary of the measured values of the transmit co-polar azimuth plane cut for for antenna elevation 30° , frequency 29.5 GHz, LHCP polarization, and radome rotation 270° .

Parameter	Value
Frequency [GHz]	29.5
Gain [dBi]	40.31
Max -1 dB Contour XPD [dB]	40.15
% over mask [%]	5.9
α [°]	1.69
Max CoPol Overshoot [dB]	0.86
Angle of Max CoPol Overshoot [deg]	2.85
Max XPol Overshoot [dB]	3.86
Angle of Max XPol Overshoot [deg]	-9.12
Max out of specs [dB]	
$\alpha^\circ : 9.2^\circ$	0.86
$9.2^\circ : 10^\circ$	0
F-Factors [dB]	
$0.5^\circ : 10^\circ$	0.86
$1^\circ : 10^\circ$	0.86
$1.5^\circ : 10^\circ$	0.86
$2^\circ : 10^\circ$	0.86
$2.5^\circ : 10^\circ$	0.86
$\alpha^\circ : 10^\circ$	0.86

profile, the de-pointing estimation results depicted in Figure 7.9(a) are obtained. The antenna de-pointing exceeds 0.4° in azimuth as well as in elevation. This antenna is not equipped with the transmit mute functionality. For this reason, it transmits although the de-pointing exceeds 0.4° . From Figure 7.9(a), it is obvious that the antenna does not fulfill the requirement of EUTELSAT for the land mobile Class A motion profile. However, by investigating the statistics of the de-pointing estimation results, the decision for the antenna to be approved or not can drastically change. Figure 7.9(b) shows the CDF of the de-pointing estimation results in Figure 7.9(a). It can be seen that the antenna de-pointing exceeds 0.4° only in 0.34% of the time in azimuth direction and

**Figure 7.7:** Adjacent Satellite Interference (ASI) at satellite positions $\pm 1.18^\circ$ of the SOTM antenna under test when tested on the maritime Class A proposed standard motion profile. The ASI is presented as normalized power levels relative to the line of sight value at the target satellite.

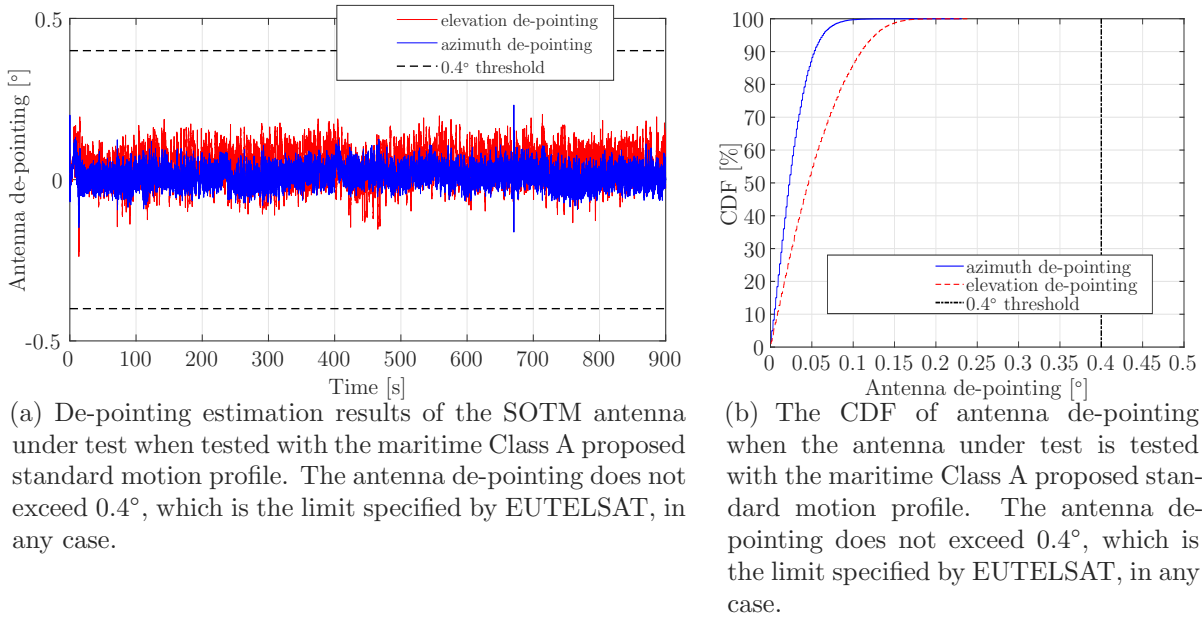


Figure 7.8: Antenna de-pointing estimation time sequence and CDF for the maritime Class A proposed standard motion profile.

in 1.5% of the time in elevation direction. This is approximately 1.7 seconds and 7.5 seconds in the 500 seconds long land mobile Class A motion profile. This fact might change the decision of the operator and the antenna might be approved for the land mobile environment as well.

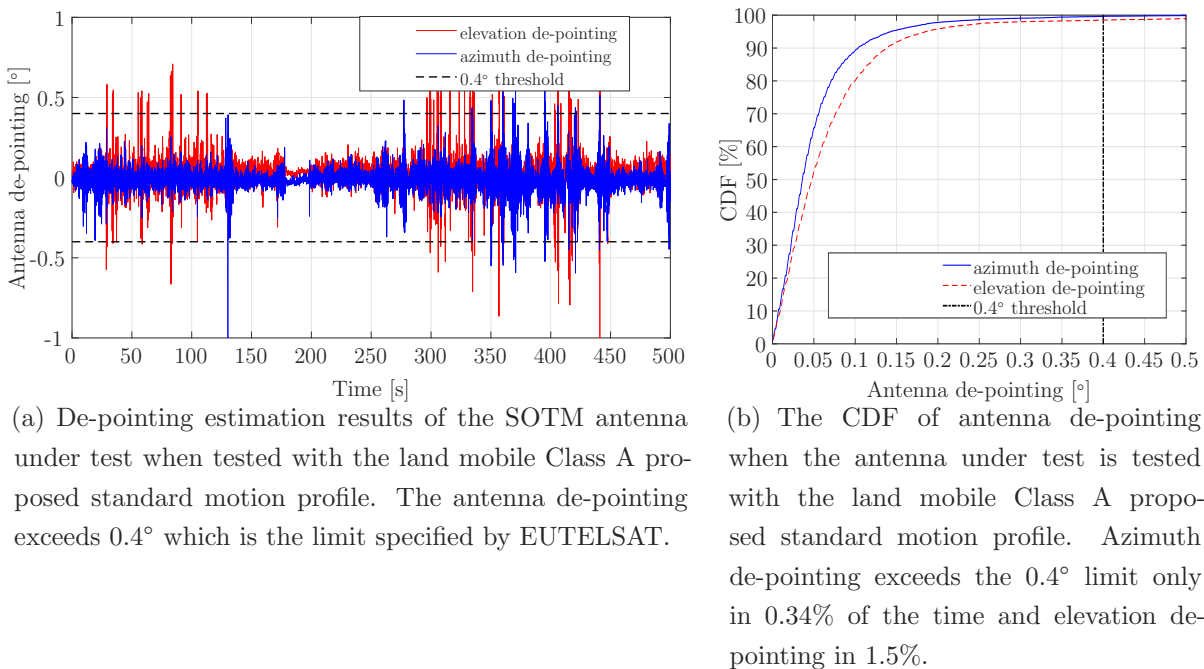
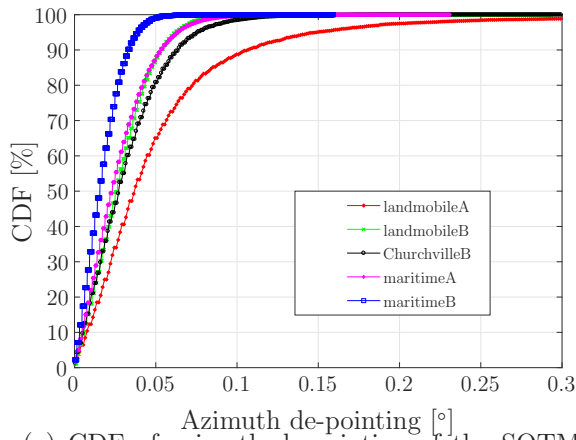


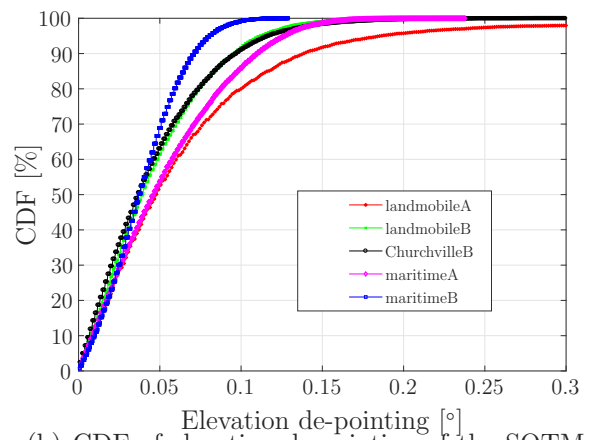
Figure 7.9: Antenna de-pointing estimation time sequence and CDF for the land mobile Class A proposed standard motion profile.

The CDFs of antenna de-pointing are plotted for the different motion profiles in Figure 7.10(a) and Figure 7.10(b) for azimuth and elevation, respectively. The proposed standard motion profiles for the land mobile and the maritime environments as well as

for the Churchville B motion track are included. It can be seen from Figure 7.10 that the maritime Class B motion profile is the easiest for the antenna to track and the land mobile Class A motion profile is the most challenging. This matches the findings in Chapter 5.



(a) CDF of azimuth de-pointing of the SOTM antenna under test when tested on different motion profiles.



(b) CDF of elevation de-pointing of the SOTM antenna under test when tested on different motion profiles.

Figure 7.10: CDF of the de-pointing estimation of the SOTM antenna under test when tested on different motion profiles. The results of the well-known Churchville B motion track are also presented.

Chapter 8

Concluding Remarks and Possible Future Extensions

In this thesis, state-of-the-art Satellite Communication On-The-Move (SOTM) standards and existing type approval procedures were reviewed and compared. This was followed by an investigation of the capabilities of the existing environments used for SOTM testing. In a laboratory environment, the SOTM terminal is tested in conditions similar to those found in the field of operation, yet without the involvement of operational satellites. As an example of a laboratory environment for SOTM testing, the framework of testing SOTM terminals at the Fraunhofer Facility for Over-the-air Research and Testing (FORTE) [65] was presented. SOTM performance metrics, like antenna de-pointing and Adjacent Satellite Interference (ASI) can be tested at FORTE. In this thesis, a comprehensive methodology to test the performance of SOTM terminal employing parabolic antennas was introduced. A solution for testing terminal which incorporate phased arrays was proposed based on future extension of FORTE. As a major contribution of this thesis, motion profiles were developed and are proposed to be used as a standard for SOTM testing. The proposed standard motion profiles were developed for the land mobile and the maritime environments. Profiles for other environments, such as, aeronautical and high speed railways are to considered in future extensions. Standard motion profiles offer a fair basis to compare the performance of different terminals. The major satellite operators in the GVF-MRA working group showed an interest to support the deployment of the proposed profiles widely in their SOTM testing recommendations. As a result, the SOTM testing procedures of the Global VSAT Forum (GVF-105) were updated by adding the definition process of the proposed standard motion profiles. It is highly recommended that the satellite operators widely start to apply the GVF-105 test recommendations along with the GVF-SOMAP requirements and consider them in their type approvals. This will lead to an enhancement of the whole SOTM value chain through a unified type approval procedure and a unique set of regulatory limits to which all members can easily refer. Standard shadowing profiles were also proposed and developed for the land mobile environment based on an image processing approach.

The definition of the proposed motion and shadowing profiles in addition to the repeatability which is guaranteed at the testing laboratories offer a comprehensive environment to test the performance of the SOTM terminal with respect to the test methodology proposed in this thesis. In an example test scenario, a Ka-band SOTM terminal with a 60cm dish antenna was tested at FORTE. The recommendations in the GVF-101 and GVF-105 documents along with the specifications of EUTELSAT were applied in the test. An excerpt of the results was presented to demonstrate how good the antenna is in accordance with the specifications. The results help to show the points of strength and weakness of the terminal and help the designers in its development process.

Appendices

Appendix A

Coordinate Transformations at the Fraunhofer Facility for Over-the-air Research and Testing (FORTE)

At the Fraunhofer Facility of Over-the-air Research and Testing (FORTE):

- If the Satellite Communication On-The-Move (SOTM) antenna under test is tilted in its local coordinate frame to reach a certain required pre-tilt and
- If the radiation pattern is to be measured by moving the motion emulator.

A coordinate frame transformation is required in order to represent the measurements in the correct pattern frame.

With an initial pre-tilt, Figure A.1 shows the trace when the motion emulator is moved to measure the azimuth cut. The coordinate frame mismatch leads to measure an arc instead of the correct azimuth footprint.

The following coordinate frame transformation will lead to the correct trace of pattern measurements when the elevation pre-tilt is performed with the antenna. The transformation is generalized to account for pattern measurements along azimuth, elevation, and skew.

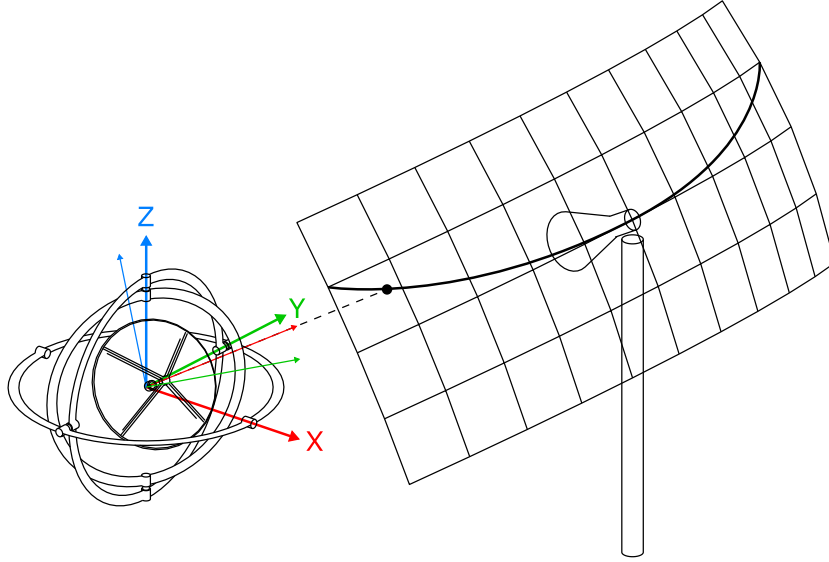


Figure A.1: The SOTM antenna has an initial pre-tilt in elevation. A simple movement of the motion emulator about its z-axis will not yield the correct azimuth cut and therefore a coordinate frame transformation is required.

Coordinate Frame Transformations Considering the setting in Figure 4.2, we assume R to be the matrix used to describe the rotation performed for the pattern measurement. For the sake of completeness, R accounts for the elevation and the skew angles of the probe antenna on the tower.

$$R = R_Y(\text{ToW}_{\text{pitch}}) \cdot R_X(\text{ToW}_{\text{roll}}) \cdot R_X(\text{Pat}_{\text{az}}) \cdot R_Y(\text{Pat}_{\text{el}}) \cdot R_Z(\text{Pat}_{\text{sk}}) \cdot R_Y(-\text{Pretilt}) \quad (\text{A.1})$$

with

- | | |
|----------------------------------|---|
| R | The resulting rotation for patten measurements |
| $R_Y(\text{ToW}_{\text{pitch}})$ | Local rotation of the elevation of the antenna on the tower. At FORTE (c.f. Figure 4.2), this is about -16.2° because the antenna has to point down to the motion emulator |
| $R_X(\text{ToW}_{\text{roll}})$ | Local rotation of the polarization skew of the antenna on the tower |
| $R_Y(-\text{Pretilt})$ | SOTM antenna pre-tilt in elevation. The negative sign is to account for the right-hand coordinated frame convention assumed |
| $R_X(\text{Pat}_{\text{sk}})$ | Local rotation of the wanted pattern in polarization |
| $R_Y(\text{Pat}_{\text{el}})$ | Local rotation of the wanted pattern in elevation |
| $R_Z(\text{Pat}_{\text{az}})$ | Local rotation of the wanted pattern in azimuth |

The local rotations are all simple angle-axis rotations in the right-hand coordinate

frame shown in Figure A.1.

$$R_X(\theta) = \begin{bmatrix} 1 & 0 & 0 \\ 0 & \cos(\theta) & -\sin(\theta) \\ 0 & \sin(\theta) & \cos(\theta) \end{bmatrix} \quad (\text{A.2})$$

$$R_Y(\theta) = \begin{bmatrix} \cos(\theta) & 0 & \sin(\theta) \\ 0 & 1 & 0 \\ -\sin(\theta) & 0 & \cos(\theta) \end{bmatrix} \quad (\text{A.3})$$

$$R_Z(\theta) = \begin{bmatrix} \cos(\theta) & -\sin(\theta) & 0 \\ \sin(\theta) & \cos(\theta) & 0 \\ 0 & 0 & 1 \end{bmatrix} \quad (\text{A.4})$$

$$(\text{A.5})$$

The motion emulator at FORTE has an outer-middle-inner axis structure (c.f. Figure A.2). X is the outer axis, Y is the middle axis, and Z is the inner axis. A rotation about the outer axis (X) will influence the orientation of the middle (Y) and inner (Z) axes. A rotation about Y will not influence the orientation of X but will influence that of Z and a rotation about Z will neither affect the orientation of Y nor X .

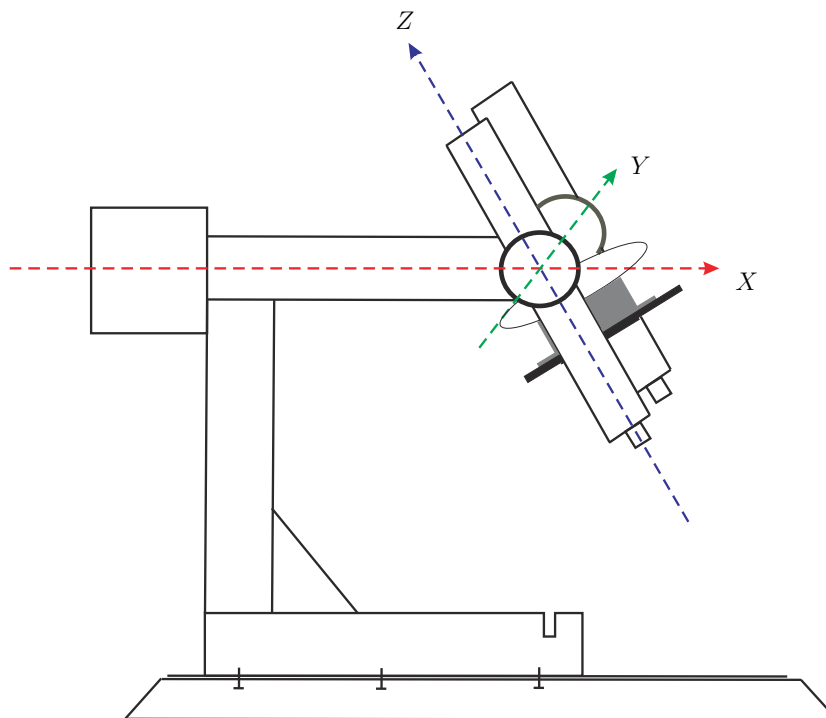


Figure A.2: An abstraction of the motion emulator showing its structure.

The order of intrinsic rotations (rotations about the local rotated axes) of the motion emulator axes which lead to the required position of the object which is mounted on its turn table is as follows:

1. Rotation α about X followed by,
2. Rotation β about Y followed by,
3. Rotation γ about Z .

In order that the motion emulator at the coordinate system origin can execute the rotation R , the three angles α , β , γ have to be calculated. The rotation matrix which describes the rotation using the motion emulator is written as follows:

$$R_{\text{MoEm}} = R_X(\alpha) \cdot R_Y(\beta) \cdot R_Z(\gamma) \quad (\text{A.6})$$

$$R_{\text{MoEm}} = \begin{bmatrix} \cos \beta \cos \gamma & -\cos \beta \sin \gamma & \sin \beta \\ \cos \alpha \sin \gamma + \sin \alpha \sin \beta \cos \gamma & \cos \alpha \cos \gamma - \sin \alpha \sin \beta \sin \gamma & -\sin \alpha \cos \beta \\ \sin \alpha \sin \gamma - \cos \alpha \sin \beta \cos \gamma & \sin \alpha \cos \gamma + \cos \alpha \sin \beta \sin \gamma & \cos \alpha \cos \beta \end{bmatrix} \quad (\text{A.7})$$

If the local rotations above are based on the same coordinate system as the motion emulator, then the following holds

$$R_{\text{MoEm}} \stackrel{!}{=} R \quad (\text{A.8})$$

Equation A.8 can be decomposed to get the angles α , β , γ . One possible solution is

$$\alpha = -\text{atan2}(R_{2,3}, R_{3,3}) \quad (\text{A.9})$$

$$\beta = \text{asin}(R_{1,3}) \quad (\text{A.10})$$

$$\gamma = -\text{atan2}(R_{1,2}, R_{1,1}). \quad (\text{A.11})$$

With

$R_{i,j}$ the element at row i and column j of the rotation matrix R .

Because

$$R_{\text{MoEm}} = \begin{bmatrix} \cos \beta \cos \gamma & -\cos \beta \sin \gamma & \sin \beta \\ \cos \alpha \sin \gamma + \sin \alpha \sin \beta \cos \gamma & \cos \alpha \cos \gamma - \sin \alpha \sin \beta \sin \gamma & -\sin \alpha \cos \beta \\ \sin \alpha \sin \gamma - \cos \alpha \sin \beta \cos \gamma & \sin \alpha \cos \gamma + \cos \alpha \sin \beta \sin \gamma & \cos \alpha \cos \beta \end{bmatrix} \quad (\text{A.12})$$

So the angles can be extracted as shown below.

$$\alpha = -\text{atan2}(-\sin \alpha \cos \beta, \cos \alpha \cos \beta) \quad (\text{A.13})$$

$$= -\text{atan2}(-\sin \alpha, \cos \alpha) \text{ for } -\pi \dots + \pi \quad (\text{A.14})$$

$$(\text{A.15})$$

$$\beta = \text{asin}(\sin \beta) \text{ for } -\pi/2 \dots + \pi/2 \quad (\text{A.16})$$

$$(\text{A.17})$$

$$\gamma = -\text{atan2}(-\cos \beta \sin \gamma, \cos \beta \cos \gamma) \quad (\text{A.18})$$

$$= -\text{atan2}(-\sin \gamma, \cos \gamma) \text{ for } -\pi \dots + \pi \quad (\text{A.19})$$

This solution provides the angles of the motion emulator needed to achieve any antenna pattern angles give a certain antenna elevation pre-tilt.

This mathematical frame work is valid to describe only antennas with fixed beam patterns. For electrically steerable antennas and phased arrays the pattern changes with respect to the steering direction. Measuring the radiation pattern by moving the antenna will be infeasible due to the large number of patterns to be considered. In Chapter 4, another solution is proposed to evaluate the performance of SOTM terminals which employ phased arrays.

Appendix B

Analysis of the Angular Rate and Acceleration Correlations

In the campaigns carried out to measure the motion dynamics as described in Chapter 5, the angular rates were directly measured using gyroscopes. The accelerations are derived from the rates after filtering.

In Chapter 5, the **95% quantile of the measured angular rate vector norm** was selected to define the motion profiles. In order to validate this selection, the correlations between the angular rates, angular accelerations, and translational acceleration are investigated. The correlations between the angular rate vector norm and the angular rate on each individual axis are also calculated.

The **GGobi** data visualization system [66] was used in the analysis and visualization of the correlation between the different rate and acceleration parameters. In the following the analysis is shown for the land mobile as well as the maritime environments.

B.1 Land Mobile

Figure B.1 shows the auto- and the cross-correlation between the angular rate vector norm and angular rate of the individual axes: Yaw, Pitch, and Roll.

On the diagonal, the auto-correlation is plotted. The two colors represent the two classes: Violet for Class A and Yellow for Class B. From the auto-correlation plots it can be seen that the classification criteria is valid not only for the vector norm but also for the sub-axes as there is a clear separation between the two classes in almost all plots. There are outliers in some cases but with a few occurrences. The off-diagonals show the cross-correlation between the different axes. It can be seen that the angular rate vector norm is correlated with the angular rate along the different axes. The points on the off-diagonals are to a large extent confined in an anti-diagonal line. This high correlation shows that the vector norm is a good choice as a basis for profile selection.

Figure B.2 shows the correlation between the angular rate vector norm, the angular acceleration vector norm and the translational acceleration vector norm. It can be seen

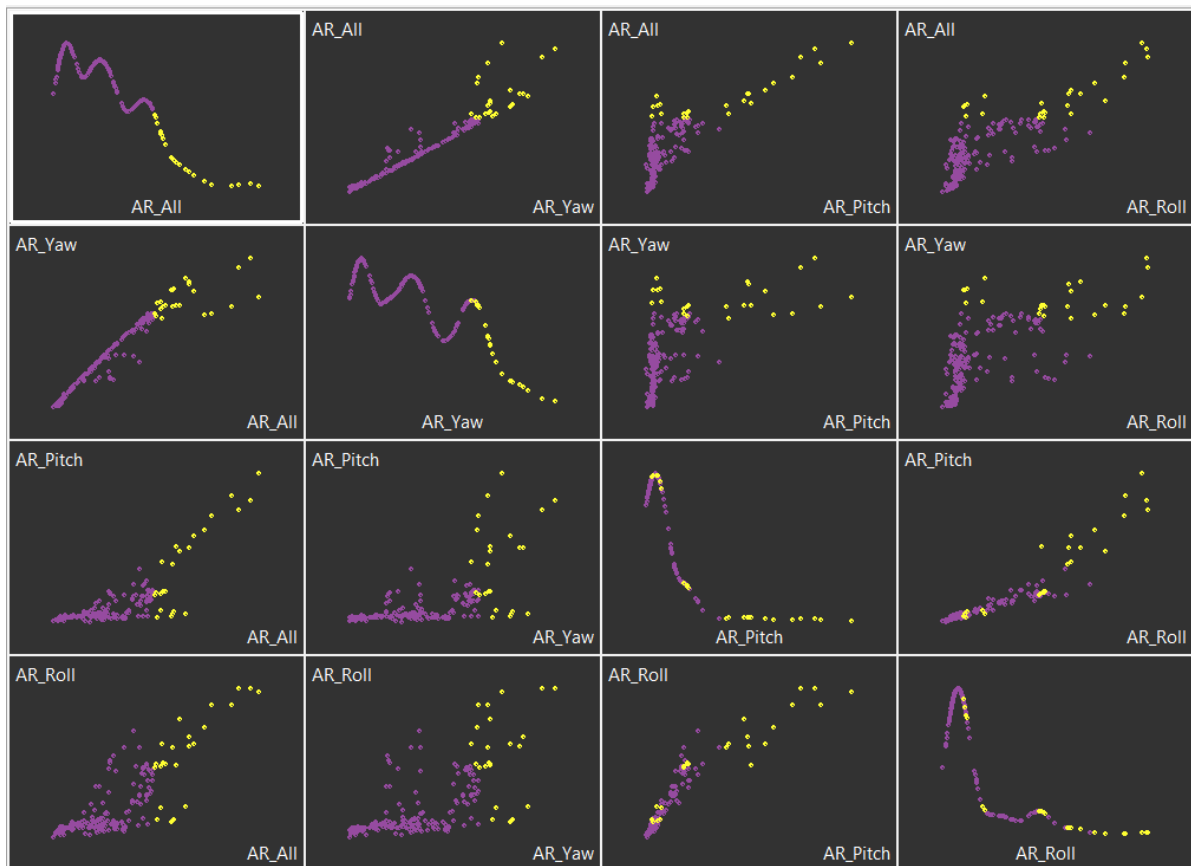


Figure B.1: Correlation plots of the Q95 values of the angular rate along the individual axes and the angular rate vector norm for the land mobile environment. The auto-correlation plots are on the diagonal and the cross-correlation plots are on the off-diagonals. AR stands for Angular Rate.

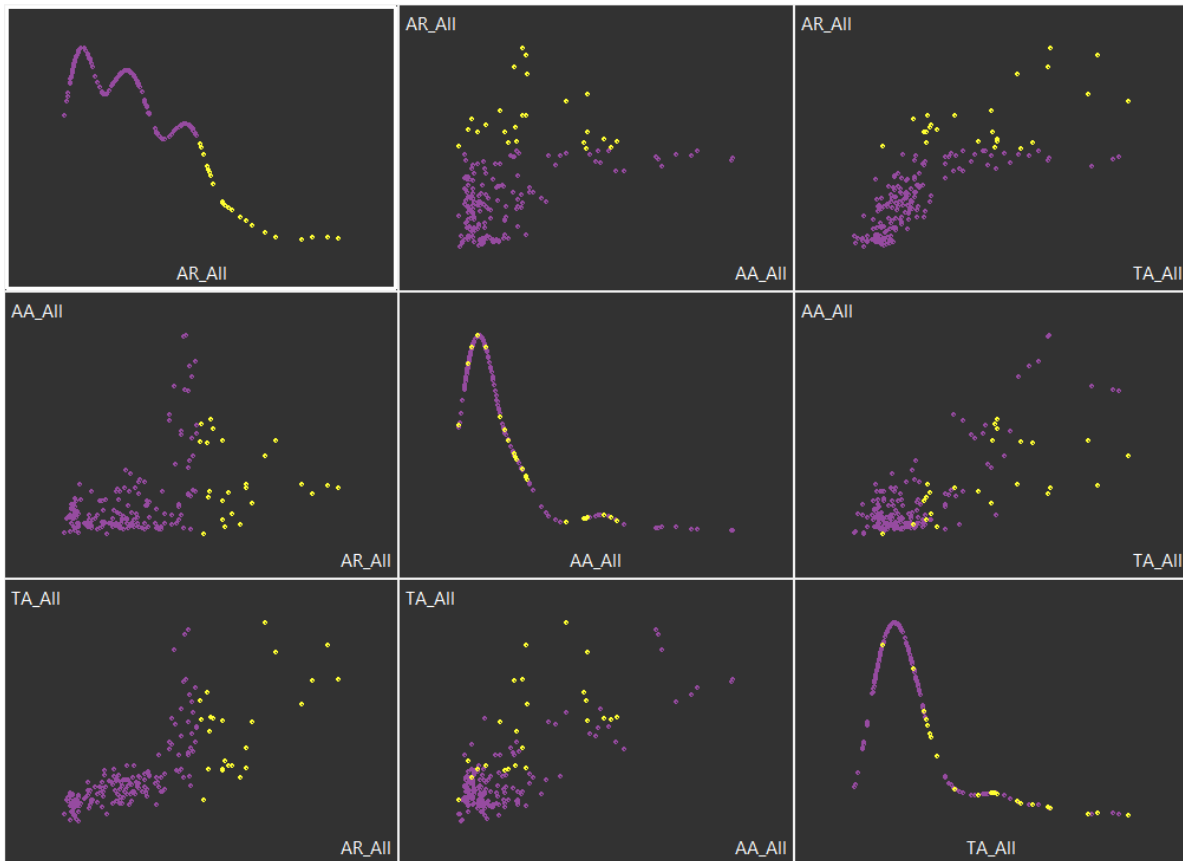


Figure B.2: Correlation plots of the Q95 values of the vector norm of the angular rate, the angular acceleration, and the translational acceleration for the land mobile environment. The auto-correlation plots are on the diagonal and the cross-correlation plots are on the off-diagonals. AR stands for Angular Rate, AA for Angular Acceleration, and TA for Translational Acceleration.

from the off-diagonals that in each plot, all the measurement segments lie on a diagonal line. Therefore, the three parameters are to a large extent correlated with few outliers. This confirms that the angular rate can be selected as a representative parameter for profile selection.

B.2 Maritime

Figure B.3 shows the auto- and the cross-correlation between the angular rate vector norm and angular rate of the individual axes: Yaw, Pitch, and Roll.

On the diagonal, the auto-correlation is plotted. The two colors represent the two classes: Violet for Class A and Yellow for Class B. From the auto-correlation plots it can be seen that the classification criteria is valid not only for the vector norm but also for the sub-axes as there is a clear separation between the two classes in almost all plots. There are outliers in some cases but with a few occurrences. The off-diagonals show the cross-correlation between the different axes. It can be seen that the angular rate vector norm is correlated with the angular rate along the different axes. The points on the off-diagonals are to a large extent confined in an anti-diagonal line. This high correlation shows that the vector norm is a good choice as a basis for profile selection.

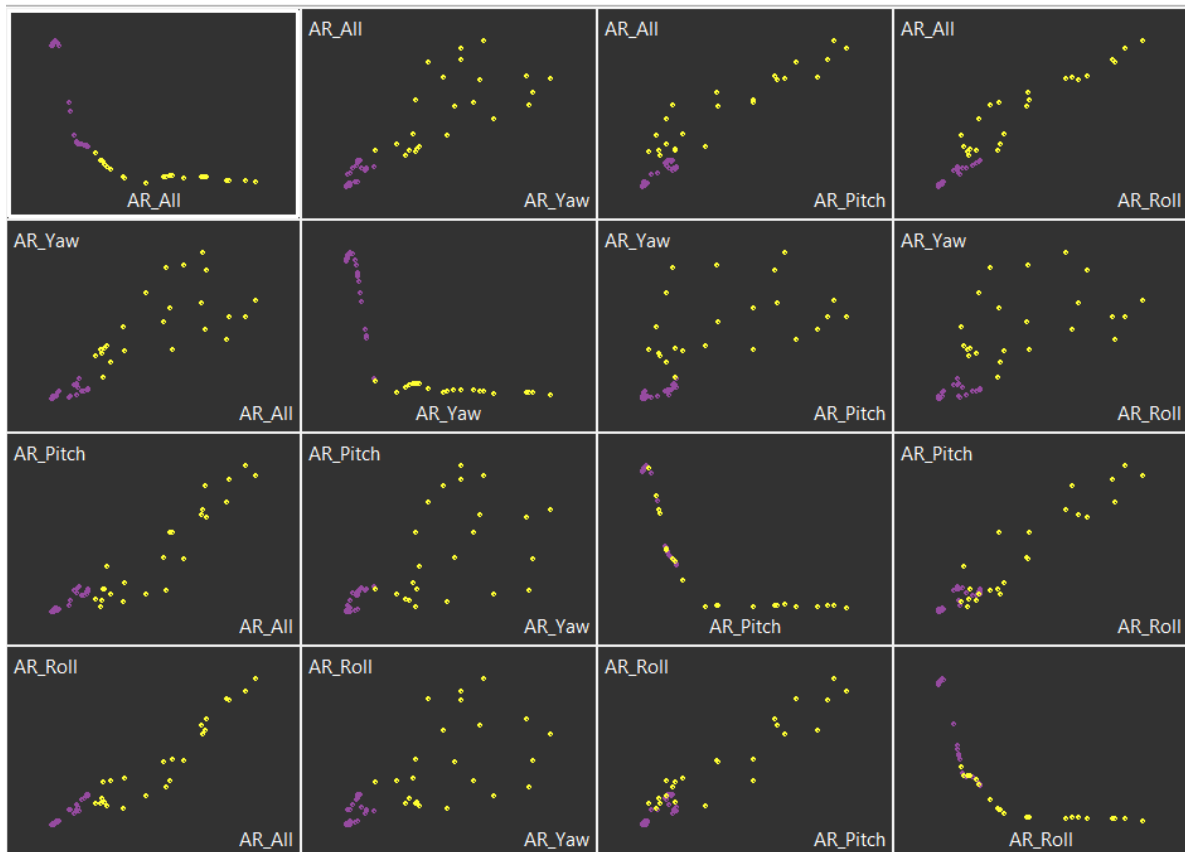


Figure B.3: Correlation plots of the Q95 values of the angular rate along the individual axes and the angular rate vector norm for the maritime environment. The auto-correlation plots are on the diagonal and the cross-correlation plots are on the off-diagonals. AR stands for Angular Rate.

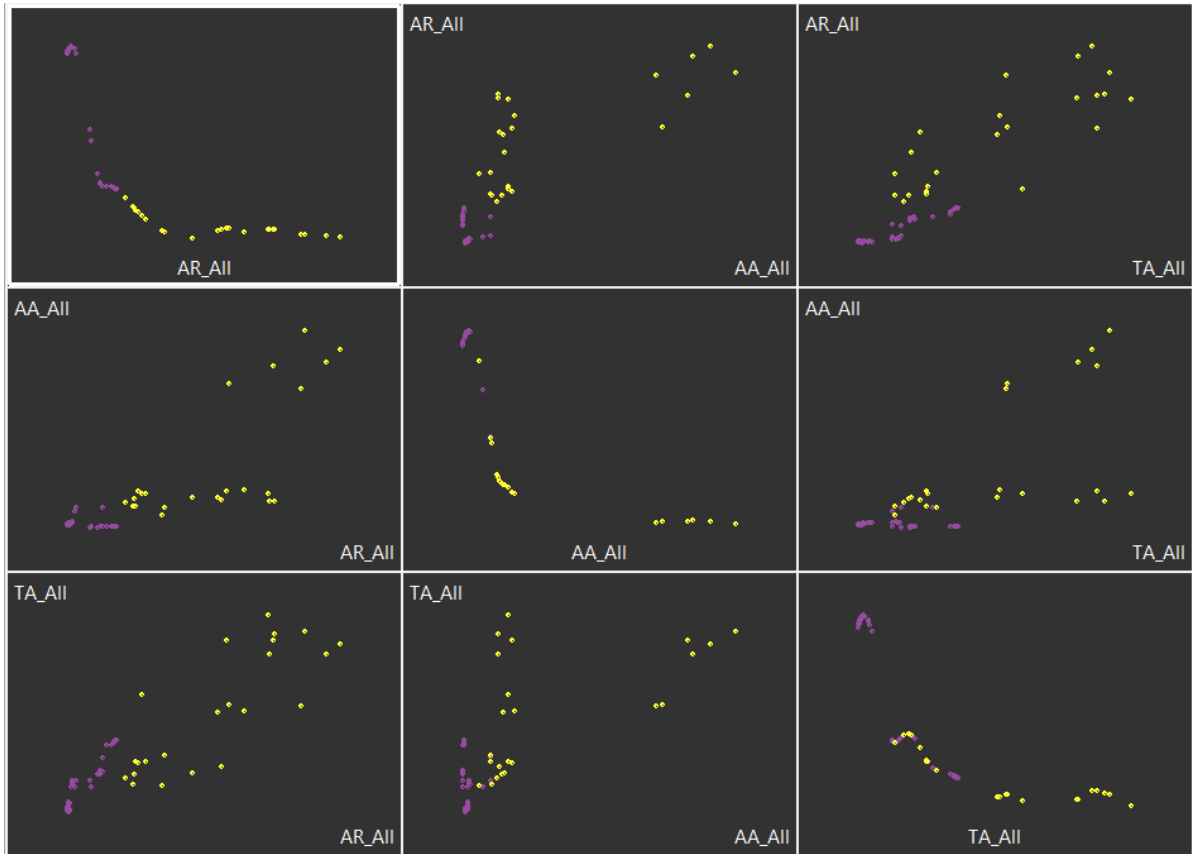


Figure B.4: Correlation plots of the Q95 values of the vector norm of the angular rate, the angular acceleration, and the translational acceleration for the maritime environment. The auto-correlation plots are on the diagonal and the cross-correlation plots are on the off-diagonals. AR stands for Angular Rate, AA for Angular Acceleration, and TA for Translational Acceleration.

Figure B.4 shows the correlation between the angular rate vector norm, the angular acceleration vector norm and the translational acceleration vector norm. It can be seen from the off-diagonals that in each plot, all the measurement segments lie on a diagonal line. Therefore, the three parameters are to a large extent correlated with few outliers. This confirms that the angular rate can be selected as a representative parameter for profile selection.

Appendix C

Wave Polarization and its Measurement Methods

Polarization is a measure for the orientation of the electric field vector (\mathbf{E}) with respect to the direction of wave propagation. It is convenient to consider linear and circular polarization as special cases of elliptical polarization. Figure C.1 graphically illustrates the three types of wave polarization.

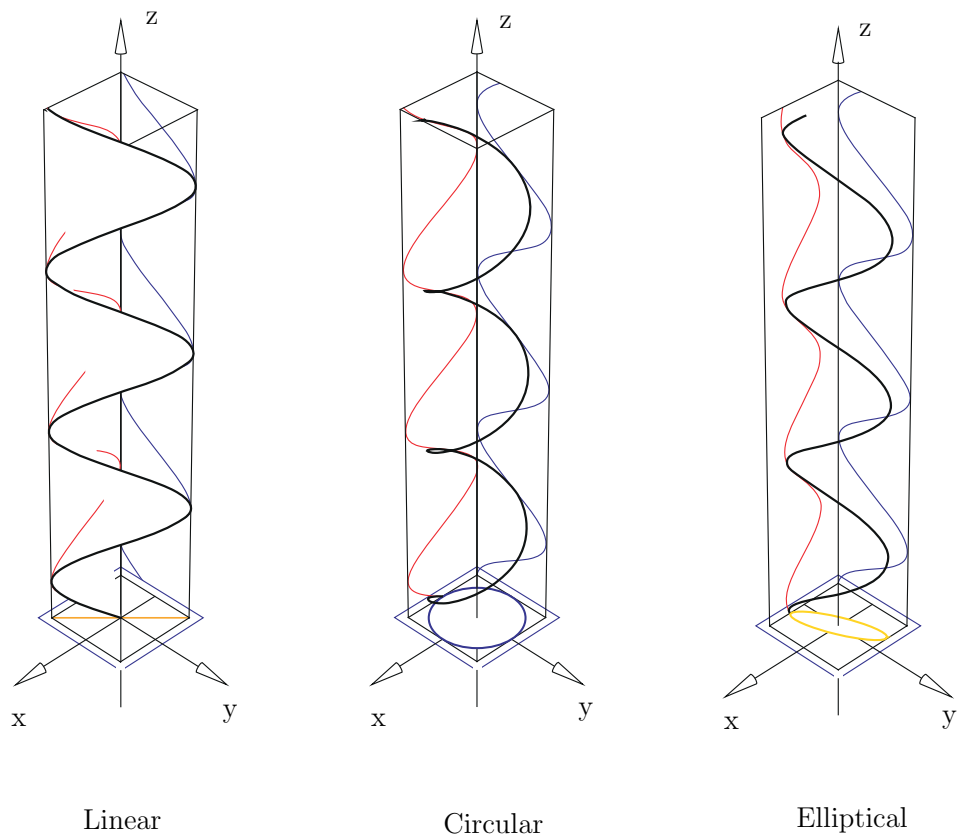


Figure C.1: Linear, circular and elliptical polarization. Figure courtesy of [61].

An elliptically polarized wave may be considered as the resultant of two orthogonal

linearly polarized waves at the same frequency described in Equations C.1 and C.2.

$$E_h = \Im \dot{E}_h = E_1 \cdot \Im e^{j(\omega t - \beta z)} = E_1 \cdot \sin(\omega t - \beta z) \quad (\text{C.1})$$

$$E_v = \Im \dot{E}_v = E_2 \cdot \Im e^{j(\omega t - \beta z + \delta)} = E_2 \cdot \sin(\omega t - \beta z + \delta) \quad (\text{C.2})$$

where:

- $\Im x$ is the imaginary component of x .
- E_1 is the amplitude of the horizontally polarized wave, E_2 is the amplitude of the vertically polarized wave and δ is the relative phase by which E_v leads E_h (the horizontally polarized wave is taken as the reference for phase).

From Equations C.1 and C.2, the generalized polarization ellipse can be depicted as in Figure C.2:

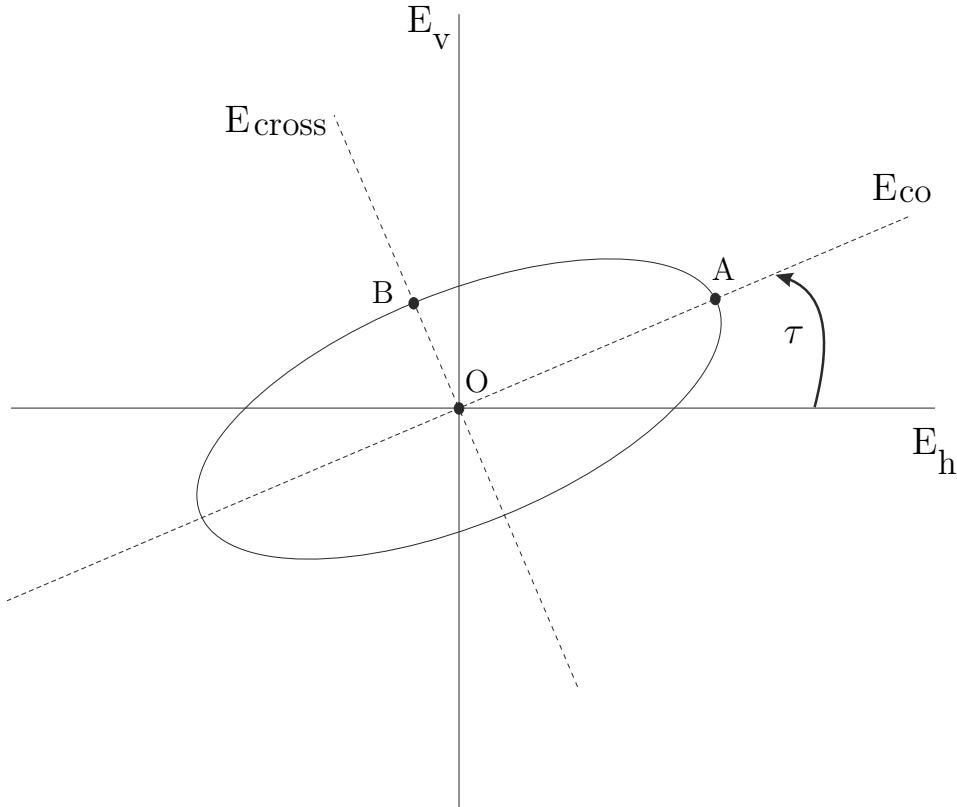


Figure C.2: Polarization ellipse.

τ is the tilt angle of the semimajor axis of the polarization ellipse. (τ) is calculated using Equation (C.3).

$$\tau = \frac{1}{2} \arctan \frac{2E_h E_v \cos \delta}{E_h^2 - E_v^2} \quad (\text{C.3})$$

C.1 Polarization Measurements

Antennas are not perfect in transmitting single polarizations. If the antenna is designed to transmit linear horizontally polarized wave, there is a vertically polarized component transmitted simultaneously. The *Cross Polarization Discrimination (XPD)*, is a measure of how accurate the antenna can maintain the purity between the co-polarized and the cross-polarized signal components. In order to fully investigate the polarization state of an Electromagnetic (EM) wave transmitted by an antenna, the following methods are considered:

- **Polarization Pattern Method** in which the polarization pattern is measured by rotating a linearly polarized antenna in front of the incoming wave. An auxiliary measurement is required to determine the sense of rotation.
- **Linear Component Method** in which the amplitudes (E_h and E_v) are measured by two orthogonal linearly polarized antennas. The relative phase difference (δ) needs to be also measured (Equation C.3).
- **Circular component method** in which the amplitudes are measured by two orthogonal circularly polarized antennas. The relative phase difference (δ') needs to be also measured.
- **Multiple Component Method** in which the amplitudes of two orthogonal linearly polarized antennas are measured. Moreover, the amplitude of a single linearly polarized antennas tilted 45° as well as of a single circularly polarized antenna are also measured. No phase information is measured.

Appendix D

Satellite Communication On-The-Move (SOTM) Test Facilities

Table D.1, lists the major state-of-the-art environments and laboratories which have the capabilities to test either the complete Satellite Communication On-The-Move (SOTM) terminal or only parts of it.

Table D.1: State-of-the-art facilities which offer services related to testing SOTM terminals.

Facility	Location	Description
Fraunhofer FORTE	Ilmenau, Germany	Test facility designed specifically for conducting all aspects of SOTM terminals qualification measurements using repeatable dynamic motion profiles
Aberdeen Proving Ground (APG)	Aberdeen MD, USA	Location for renowned Churchville test track. Provides extensive capabilities to conduct outdoor SOTM terminal measurements. Capabilities extend well beyond those required for tracking accuracy terminal evaluations
Qinetiq Funtington (formerly ASWRE)	Bosham UK	Extensive antenna pattern test facilities using far-field outdoor range as well as indoor anechoic chamber. Measurement test capability HF through 60 GHz
Combitech	Arboga, Sweden	Large outdoor range. Suitable for testing heavier antenna terminals for satellite bands through Ku-band
Raytheon	Multiple locations in USA. Antenna test facilities located in Waltham MA and El Segundo CA.	Multiple ranges comprising anechoic chambers (far-field configuration), near-field and compact antenna test facilities. Measurement capabilities cover all satellite frequency bands up to 110 GHz

Table D.1: Continued

Facility	Location	Description
Catapult Satellite	UK (Various locations)	Equipped with comprehensive microwave test facilities including outdoor antenna pattern ranges
European Space Agency (ESA)	Europe	Large compact range providing quiet zone measuring $\approx 1.2m \times 1m \times 1m$. Range uses dual reflector antenna arrangement and supports AUT loads up to 100 Kg. Operational frequency range ≈ 4 GHz - 250 GHz
ProBrand International	Locations in the USA and UK	Operates large compact range located in Atlanta. Facility extensively used for VSAT measurements in Ku and Ka-band frequencies. Supports AUT loads up to ≈ 45 Kg (100lb). Five axis positioner (Roll manual off-set El Az and floor slide.) Measurement frequency range covers ≈ 2 GHz through 40 GHz
Rhode and Schwarz	Memmingen, Germany	Advanced anechoic test facility for radiation pattern and other antenna measurements covering a frequency range of ≈ 200 MHz through 40 GHz. The 8-axis positioning hardware supports loads up to 200 Kg
Cobham	Chevely, UK	Operates spherical near-Field range covering frequency range of ≈ 0.4 to 30 GHz
Naval Research Laboratory	Wash DC. , USA	Multiple anechoic chambers including compact ranges covering majority of satellite bands of interest. One large chamber is equipped with a a motion table
General Dynamics Satcom Technologies and North Carolina	Texas locations, USA	Multiple outdoor far-field test ranges covering satellite frequency bands through 30 GHz. Texas facility used ground based satellite emulators for evaluating tracking accuracy
EADS Astrium	Munich, Germany	Spherical and near-Field test facilities covering frequency range from ≈ 1 GHz through 40 GHz. Beam pointing accuracy up to 0.01° . Supports heavy loads up to 5000 Kg
France Telecom	La Turbie Site, France	Far-field outdoor range (path length 1450 m) covering operational frequency range 0.5 GHz to 50 GHz. Angular accuracy of 0.02°
Technical University of Denmark. (DTU-ESA Facility)	Copenhagen, Denmark	Facility equipped with large anechoic chamber to handle test articles up to 6 m diameter. Operational frequency range up to 40 GHz. Maximum AUT weight limit is ≈ 250 Kg

Table D.1: Continued

Facility	Location	Description
Canadian Space Agency	Ottawa, Ontario, Canada	Multiple RF test facilities. The Antenna Test Facilities comprise the Antenna Test Facility 1 (6x6), Antenna Test Facility 2 (12x12), cylindrical near-field facility, spherical near-field facility and the rooftop antenna range. Spherical and cylindrical near-field radiation patterns are acquired indoors and with subsequent data processing, far-field antenna characteristics are derived. Frequency coverage up to 50 GHz
AvL Technologies	Ashville, NC USA	Fully equipped facility for recording antenna patterns for all satellite bands of interest through Ka-band
BTP Systems	Ludlow, MA., USA	Indoor test facilities comprising a compact antenna range and near-field antenna range covering frequencies up to 50 GHz. Facility has been involved in qualification of SOTM terminals for airborne and maritime applications
Aerospace Testing Facilities in India	Bangalore and Hyderabad, India	DRDO-Planar Near Field ranges with operational frequency to 18 GHz. Perform customary antenna radiation pattern and XPD measurements. EICL - Compact antenna test range with capability to test antennas up to 2.4 m through Ku-band
Boeing Electronic Testing Services	Multiple locations, USA	Boeing Electronics offers a variety of antenna testing services utilizing small and large compact ranges and near-field ranges. The company also provides outdoor far-field test range services. Most upper frequency test capabilities attain frequencies of 50 GHz and 100 GHz for limited applications

Bibliography

Own Publications

- [1] Mostafa Alazab, Florian Raschke, and Markus Landmann. Standard Definition for SOTM Terminals. An ESA ARTES 1 project. Technical Report Final, European Space Agency ESA/ESTEC, 2016.
- [2] Mostafa Alazab, Giovanni Del Galdo, Wolfgang Felber, Albert Heuberger, Mario Lorenz, Florian Raschke, Gregor Siegert, and Markus Landmann. Satcom on the Move (SOTM) Terminals Evaluation under Realistic Conditions. In *Vehicular Technology Conference (VTC Spring), 2013 IEEE 77th*, pages 1–5, June 2013.
- [3] Mostafa Alazab, Marie Rieche, Giovanni Del Galdo, Wolfgang Felber, Florian Raschke, Gregor Siegert, and Markus Landmann. On-Earth Performance Evaluation of SatCom On-the-Move (SOTM) Terminals. In *MILCOM 2013 - 2013 IEEE Military Communications Conference*, pages 634–640, November 2013.
- [4] Mostafa Alazab Elkhoully, Jonas König, Niklas Beuster, Florian Raschke, Alexander Ihlow, Colin Robinson, Raul Orus-Perez, Fritz Schurig, Albert Heuberger, Markus Landmann, and Giovanni Del Galdo. Standardized Testing Conditions for Satellite Communications On-The-Move (SOTM) Terminals. In *International Journal of Satellite Communications and Networking*, Accepted for publication, June 2018.
- [5] Markus Mehnert, Mostafa Alazab, Alexander Ihlow, Albert Heuberger, and Kurt Blau. Noise Measurements for Mobile Satellite Applications. In *11th Workshop on Digital Broadcasting (WSDB)*, Erlangen, Germany, 2010.
- [6] Mostafa Alazab, Wolfgang Felber, Giovanni Del Galdo, Albert Heuberger, Mario Lorenz, Markus Mehnert, Florian Raschke, Gregor Siegert, and Markus Landmann. Pointing accuracy evaluation of SOTM terminals under realistic conditions. In *34rd ESA Antenna Workshop on Challenges for Space Antenna Systems*, ESTEC, Noordwijk, The Netherlands, October 2012.
- [7] Gregor Siegert, Wolfgang Felber, Florian Raschke, Mostafa Alazab, and Markus Landmann. Advances of far field test range for SatCom On-the-Move terminals. In *7th Advanced Satellite Multimedia Systems Conference and the 13th Signal Processing for Space Communications Workshop (ASMS/SPSC)*, Livorno, Italy, September 2014.
- [8] Mostafa Alazab, Marie Rieche, Markus Landmann, and Giovanni Del Galdo. Realistic emulation of the operational environment for SatCom On-The-Move (SOTM)

terminals. In *2013 IEEE-APS Topical Conference on Antennas and Propagation in Wireless Communications (APWC)*, pages 1115–1118, September 2013.

- [9] Mostafa Alazab, Giovanni Del Galdo, Wolfgang Felber, Florian Raschke, Gregor Siegert, and Markus Landmann. Comparison of SOTM Antenna Pointing Accuracy Estimation Methods. ESA, September 2013.
- [10] Mostafa Alazab, Giovanni Del Galdo, Wolfgang Felber, Florian Raschke, Gregor Siegert, and Markus Landmann. Performance Comparison of Antenna De-pointing Estimation Methods for SOTM Terminal Testing. In *31st AIAA International Communications Satellite Systems Conference (ICSSC)*, Florence, Italy, October 2013.
- [11] Mostafa Alazab, Florian Raschke, and Markus Landmann. Mobile Tracking Needs, Contract Change Notice 2. An ESA ARTES 5.1 Project Extension. Technical Report Final, European Space Agency ESA/ESTEC, 2016.

References by Other Authors

- [12] Arthur C. Clarke. Extra-terrestrial relays. 119:14–+, 04 2013.
- [13] The US Inflation Calculator. The us inflation calculator. <https://www.usinflationcalculator.com/>. [Online; last edited 12-June-2018].
- [14] T. Pratt, C.W. Bostian, and J.E. Allnutt. *Satellite Communications*. Wiley, 2002.
- [15] Satellite Signals. List of satellites in geostationary orbit. Available at <http://www.satsig.net/sslist.htm>. [Online; last edited 08-April-2018].
- [16] Jing Zhu and S. Roy. Improving link layer performance on satellite channels with shadowing via delayed two-copy selective repeat arq. *IEEE Journal on Selected Areas in Communications*, 22(3):472–481, April 2004.
- [17] M. Rawlins. Preventing Harmful Interference to Satellite Systems. EUTEL-SAT Communications. Available at <https://www.itu.int/en/ITU-R/space/workshops/2013-interference-geneva/presentations/Mark%20Rawlins%20-Eutelsat.pdf>, June 2013.
- [18] Federal Communications Commission (FCC). Vehicle-mounted earth stations (VMES)). Technical Report FCC25p226, FCC, 2010.
- [19] The European Telecommunications Standards Institute (ETSI). Harmonized en for vehicle-mounted earth stations (vmes) operating in the 14/12 ghz frequency bands covering essential requirements under article 3.2 of the r&tte directive. Technical Report ETSI EN 302 977 v 1.1.2 Satellite, Earth Stations and Systems (SES), ETSI, 2008.
- [20] The Noun Project. Satellite systems icons. Available at <https://thenounproject.com>.
- [21] D. Roddy. *Satellite Communications, Fourth Edition*. Professional Engineering. McGraw-Hill Education, 2006.

- [22] A. Kleusberg and P.J.G. Teunissen. *GPS for Geodesy*. Environmental science. Springer Berlin Heidelberg, 1998.
- [23] L.J. Ippolito. *Satellite Communications Systems Engineering: Atmospheric Effects, Satellite Link Design and System Performance*. Wiley, 2017.
- [24] G. Maral, M. Bousquet, and Z. Sun. *Satellite Communications Systems: Systems, Techniques and Technology*. Wiley Series in Communication and Distributed Systems. Wiley, 2011.
- [25] International Telecommunication Union. Radiation Diagrams for Use as Design Objectives for Antennas of Earth Stations Operating with Geostationary Satellites. Technical Report RECOMMENDATION ITU-R S.580-6, ITU, 2004.
- [26] R. Dybdal. *Communication Satellite Antennas: System Architecture, Technology, and Evaluation*. Communication engineering. McGraw-Hill, 2009.
- [27] I.T. Union. *Handbook on Satellite Communications*. Wiley, 2002.
- [28] S. Tirró. *Satellite Communication Systems Design*. Springer US, 1993.
- [29] Louis J. Ippolito. *Radiowave Propagation in Satellite Communications*, volume 1. Springer, 01 1986.
- [30] Constantine A. Balanis. *Antenna Theory: Analysis and Design*. Wiley-Interscience, 2005.
- [31] International Telecommunication Union. Attenuation by atmospheric gases. Technical Report P Series Radiowave propagation, ITU, 2016.
- [32] EPAK. Epak dsi6 - kompakte und leichtgewichtige maritime satelliten-antenne für internetzugang auf dem meer. <http://www.epak.de/de/maritime-sat-systeme/vsat-antennen/internet-auf-dem-boot-dsi6>.
- [33] KYMETA. Kywaytm terminal. <https://www.kymetacorp.com/kymeta-products/#productMtenna>.
- [34] Wiki media Commons. Goonhilly satellite earth station receiver. <https://commons.wikimedia.org/wiki/File:Goonhilly2.jpg>. [Online; 2003].
- [35] The Aerial Man. Satellite dish. <https://theaerialman.co.uk/satellite-dish-installers-bristol/>. [Online; 2018].
- [36] ViaSat. Viasat-1. <https://www.viasat.com/viasat-1-launch>.
- [37] International Telecommunication Union. Regulation of Global Broadband Satellite Communications. Technical Report GSR Advanced Copy, ITU, 2011.
- [38] D. Minoli. *Innovations in Satellite Communications and Satellite Technology: The Industry Implications of DVB-S2X, High Throughput Satellites, Ultra HD, M2M, and IP*. Wiley, 2015.
- [39] Gonzalo de Dios. High-throughput satellites technology trends. INTELSAT. Available at https://www.itu.int/en/ITU-R/seminars/rrs/RRS-17-Americas/Documents/Forum/2_Intelsat%20Gonzalo%20de%20Dios.pdf, 2017.

- [40] Advantech Wireless. A versatile broadband vsat platform. <http://www.advantechwireless.com/products/kuka-8200-series-m2m-iot-scada-ultra-compact-all-outdoor-vsats-transceiver-router/>.
- [41] PHASOR. Very low profile, electronically steered, high gain, phased array. <http://www.phasorsolutions.com/phasors-technology>.
- [42] The Global VSAT Forum (GVF). Satellite operators minimum antenna performance (somap). Technical Report Tech. Rep. SOMAP, GVF, 2017.
- [43] D. Brunnenmeyer, S. Mills, S. Patel, C. Suarez, and L. B. Kung. Ka and ku operational considerations for military satcom applications. In *MILCOM 2012 - 2012 IEEE Military Communications Conference*, pages 1–7, Oct 2012.
- [44] The European Telecommunications Standards Institute (ETSI). Harmonized en for satellite earth stations on board vessels (esvs) operating in the 11/12/14 ghz frequency bands allocated to the fixed satellite services (fss) covering essential requirements under article 3.2 of the r&tte directive. Technical Report ETSI EN 302 340 v 1.1.1, Earth Stations and Systems (SES), ETSI, 2006.
- [45] The Global VSAT Forum (GVF). Mutual recognition of performance measurement guidelines and procedures for satellite system operator type approvals. Technical Report Tech. Rep. GVF-101 Rev E, GVF, 2014.
- [46] The Global VSAT Forum (GVF). Performance and test guidelines for type approval of comms on the move mobile satellite communications terminals. Technical Report GVF, Tech. Rep. GVF-105, GVF, 2016.
- [47] P. Woodhead. Field trials of mounted battle command ka-band satcom on-the-move. *MILSAT Magazine*, January 2011.
- [48] R. Murthy. On-satellite testing of mobile communication antennas for compliance to vmes, esv, and other pointing accuracy requirements. In *2011 - MILCOM 2011 Military Communications Conference*, pages 1812–1817, Nov 2011.
- [49] H. Beljour, S. Foresta, R. Hoffmann, L. Shamblin, J. Shields, A. Stevens, C. Uhler, E. Carl, and M. Eriksson. Army satcom otm full elevation performance characterization. In *2011 - MILCOM 2011 Military Communications Conference*, pages 1964–1967, Nov 2011.
- [50] EUTELSAT. Type approval characterization procedures esog120. Technical Report Issue 6.3, vol.1, EUTELSAT, 2017.
- [51] Fraunhofer IIS. The mobile tracking needs (mtn) database. Available at <https://motiondb.iis.fraunhofer.de/cmtn/main/>.
- [52] M. S. Karaliopoulos and F. N. Pavlidou. Modelling the land mobile satellite channel: a review. *Electronics Communication Engineering Journal*, 11(5):235–248, Oct 1999.
- [53] Roberto Prieto-Cerdeira, Fernando Pérez-Fontán, Paolo Burzigotti, Ana Bolea Alamañac, and I. Sanchez-Lago. Versatile two-state land mobile satellite channel model with first application to dvb-sh analysis. *Int. J. Satellite Communications Networking*, 28:291–315, 2010.

- [54] F. P. Fontan, M. Vazquez-Castro, C. E. Cabado, J. P. Garcia, and E. Kubista. Statistical modeling of the lms channel. *IEEE Transactions on Vehicular Technology*, 50(6):1549–1567, Nov 2001.
- [55] S. Scalise, H. Ernst, and G. Harles. Measurement and modeling of the land mobile satellite channel at ku-band. *IEEE Transactions on Vehicular Technology*, 57(2):693–703, March 2008.
- [56] Erwin Kubista, Fernando Pérez-Fontán, Maria Angeles Vázquez-Castro, Sergio Buonomo, Bertram Arbesser-Rastburg, and José Pedro V. Poiares Baptista. Ka-band propagation measurements and statistics for land mobile satellite applications. *IEEE Trans. Vehicular Technology*, 49:973–983, 2000.
- [57] P. Conforto, R. Mura, L. Secondiani, and S. Scalise. Multimedia service provision in mobility: the FIFTH solutions for the railroad environment. In *Proceedings, Ischia*, 2003.
- [58] Giorgio Sciascia, Sandro Scalise, Harald Ernst, and Rodolfo Mura. STATISTICAL CHARACTERIZATION OF THE RAILROAD SATELLITE CHANNEL AT KU-BAND.
- [59] Sandro Scalise, Oliver Lücke, and Elisabet Torralbo. A Link Availability Model for the Railroad Satellite Channel. In *24th AIAA International Communications Satellite Systems Conference*, International Communications Satellite Systems Conferences (ICSSC). American Institute of Aeronautics and Astronautics, June 2006.
- [60] C. A. Hofmann, R. T. Schwarz, and A. Knopp. Sotm measurements for the characterization of the wideband mobile satellite channel at ku-band. In *SCC 2015; 10th International ITG Conference on Systems, Communications and Coding*, Feb 2015.
- [61] Wikipedia contributors. List of tunnels in germany — Wikipedia, the free encyclopedia. https://en.wikipedia.org/wiki/List_of_tunnels_in_Germany. [Online; last edited 03-January-2018].
- [62] A. Ihlow, D. Arndt, F. Topf, C. Rothaug, T. Wittenberg, and A. Heuberger. Photogrammetric satellite service prediction - correlation of rf measurements and image data. In *2011 IEEE International Symposium on Broadband Multimedia Systems and Broadcasting (BMSB)*, pages 1–6, June 2011.
- [63] EUTELSAT. Earth station minimum technical and operational requirements, standard m eess 502. Technical Report Issue 14, Rev.0, EUTELSAT, 2011.
- [64] H. Bayer, A. Krauss, R. Stephan, and M. A. Hein. A dual-band multimode monopulse tracking antenna for land-mobile satellite communications in ka-band. In *2012 6th European Conference on Antennas and Propagation (EUCAP)*, pages 2357–2361, March 2012.
- [65] Fraunhofer IIS. The Fraunhofer Facility for Over-the-air Research and Testing (FORTE). <https://www.iis.fraunhofer.de/en/profil/standorte/forte.html>.
- [66] Debby Swayne, Di Cook, Duncan Temple Lang, and Andreas Buja. Ggobi data visualization system. <http://www.ggobi.org/>. [Online; 2010].

Index

- Adjacent Satellite Interference, 5, 82
- Antenna
 - Characteristics, 82
 - De-pointing, 32, 40, 86
 - Pointing Angle, 20
 - Polarization, 22
 - Radiation Pattern, 18
 - Radiation pattern, 83
 - Tracking, 22
 - Types, 19
- C-band, 3
- Churchville B, 69
- Cloud Attenuation, 26
- Cross Polarization Discrimination, 82
- Data Traffic Measurements, 48
- Doppler Shift, 14
- Dynamic Tests, 85
- Early bird, 1
- European Telecommunications Standards Institute, 2
- Faraday Rotation, 27
- Federal Communications Commission, 2
- Fraunhofer Facility for Over-the-air Research and Testing, 39
- Free Space Path Loss, 24
- Geostationary Orbit, 13
- Geosynchronous Orbit, 13
- Global Positioning System, 13
- Global VSAT Forum, 4
- Ground Segment, 17
- GVF-105, 70
- High Earth Orbit, 13
- High Throughput Satellites, 3, 31
- Image
 - Capturing, 72
 - Post Processing, 73
- Inertial Measurement Unit, 52
- Intelsat I, 1
- International Telecommunications Union, 2
- Ka-band, 3
- Kepler's Laws, 9
- Ku-band, 3
- Land Mobile, 55
- Land Mobile to Satellite, 71
- Line-of-Sight, 71
- Link budget, 24
- Low Earth Orbit, 12
- Maritime, 63
- Medium Earth Orbit, 12
- Millbrook Proving Ground, 52
- Molniya Orbit, 13
- Motion
 - Dynamics, 51
 - Profiles, 51
- Non-Line-of-Sight, 71
- Off-axis Emissions, 32, 40
- Optimum Sensor Positions, 42
- Orbital Perturbations, 14
- Phased Arrays, 46
- Propagation Effects, 24
- Rain
 - Attenuation, 25
 - Depolarization, 25
- Range Variations, 16
- S-band, 3
- Satellite
 - Applications, 2
 - Communication On-The-Move, 4
 - Testing, 31
 - Type Approvals, 33

- Frequencies, 3
- Orbits, 12
- Services
 - Broadcast, 29
 - Fixed, 29
 - Mobile, 30
- Scintillation, 27
- Shadowing Profiles, 71
- Sidereal Day, 1
- Solar Eclipse, 15
- Space Segment, 9
- Sun Transit Outage, 16

- Transmit Cessation Time, 32, 48

- X-band, 3

Erklärung

Ich versichere, dass ich die vorliegende Arbeit ohne unzulässige Hilfe Dritter und ohne Benutzung anderer als der angegebenen Hilfsmittel angefertigt habe. Die aus anderen Quellen direkt oder indirekt übernommenen Daten und Konzepte sind unter Angabe der Quelle gekennzeichnet.

Bei der Auswahl und Auswertung folgenden Materials haben mir die nachstehend aufgeführten Personen in der jeweils beschriebenen Weise entgeltlich/unentgeltlich geholfen:

1. ...
2. ...
3. ...

Weitere Personen waren an der inhaltlich-materiellen Erstellung der vorliegenden Arbeit nicht beteiligt. Insbesondere habe ich hierfür nicht die entgeltliche Hilfe von Vermittlungs- bzw. Beratungsdiensten (Promotionsberater oder anderer Personen) in Anspruch genommen. Niemand hat von mir unmittelbar oder mittelbar geldwerte Leistungen für Arbeiten erhalten, die im Zusammenhang mit dem Inhalt der vorgelegten Dissertation stehen.

Die Arbeit wurde bisher weder im In- noch im Ausland in gleicher oder ähnlicher Form einer Prüfungsbehörde vorgelegt.

Ich bin darauf hingewiesen worden, dass die Unrichtigkeit der vorstehenden Erklärung als Täuschungsversuch bewertet wird und gemäß 7 Abs. 10 der Promotionsordnung den Abbruch des Promotionsverfahrens zur Folge hat.

Ilmenau, der 30.06.2018

Mostafa Alazab Elkhoully